Bulk Supramolecular Polymerization *via* "Weak" Hydrogen Bonds and Aromatic Interactions: Recognizing the Potential of Metal Coordination Geometry

By

Nicholas Francis Shaun Lanigan

A thesis
presented to the University of Waterloo
in fulfillment of the
thesis requirement for the degree of

Doctor of Philosophy
in
Chemistry

Waterloo, Ontario, Canada, 2019

Examining Committee Membership

The following served on the Examining Committee for this thesis. The decision of the Examining Committee is by majority vote.

External Examiner	THOMAS BAUMGARTNER Professor
Supervisor	XIAOSONG WANG Professor
Internal Member	MARIO GAUTHIER Professor
Internal Member	JEAN DUHAMEL Professor
Internal-External Member	MICHAEL TAM Professor

Author's Declaration

This thesis consists of material of which I have authored or co-authored: see Statement of Contributions included in the thesis. This is a true copy of the thesis, including any required final revisions, as accepted by my examiners.

I understand that my thesis may be made electronically available to the public.

Statement of Contributions

Part of the research work discussed in Chapter 2 and Chapter 3 was published in ACS Macro Letters, 2014, 3 (12), 1281-1285. Reproduced with permission from reference 137. Copyright 2014 American Chemical Society.

X-ray diffraction and the determination of the single crystal structures in Chapter 2 was performed Abdeljalil Assoud. The measurement of the capacitance and determination of the dielectric constant was performed in collaboration with Leon Mintz.

Abstract

Bulk supramolecular polymers offer an attractive strategy for the development of functional materials. The use of small molecule monomers is of particular interest, because they maximize the potential of a fully reversible polymer backbone. However, the use of small molecules to generate bulk supramolecular polymers has been hindered by the difficulties associated with monomer design. In particular, the tendency of small molecules to crystallize and the lack of understanding of how intermolecular interactions direct the packing of molecules in bulk, make the rational design of novel monomers challenging.

To explore the potential of metal coordination geometry, the organometallic molecule $CpFe(CO)PPh_3CO(CH_2)_5CH_3$ (FpC_6) was selected as a candidate for use as a monomer to prepare a bulk supramolecular polymer. To elucidate the packing motif and potential intermolecular interactions, crystal engineering of FpC_6 was performed. FpC_6 forms 5 different crystal structures depending on recrystallization conditions. Crystal engineering revealed that FpC_6 interacts through a variety of C—H---O interactions and aromatic embraces, which are influenced by the recrystallization conditions. Depending on recrystallization conditions, FpC_6 forms three unique one-dimensional chain structures in the crystalline material.

When the crystalline solid-state structure was disrupted by melting, FpC_6 displayed typical polymer behaviour, such as the ability to form free-standing films, and fibres could be drawn from the melt. Upon cooling, FpC_6 did not immediately recrystallize and instead formed an amorphous solid which could be molded into a variety of shapes. Powder X-ray diffraction of the amorphous solid revealed a distinctive double peak pattern. The double peak pattern matched the inter-monomer distances for a ladder chain structure (identified *via* crystal engineering) formed by cooperative C—H---O hydrogen bond and aromatic embraces.

Differential scanning calorimetry indicated that no recrystallization occurred and that FpC_6 underwent a glass transition. These results demonstrated that the C—H---O hydrogen bonds and aromatic embraces are strong enough to stabilize the chain and prevent crystallization. However, FpC_6 eventually crystallized over time, indicating that the chains were metastable. The mechanical behaviour of FpC_6 was found to be very rich and complex, as it was sensitive to temperature, ageing and thermal/measurement history. Rheological experiments indicated that aged FpC_6 demonstrates viscoelastic behaviour, potentially due to the presence of chain entanglements.

In order to improve the reproducibility of the mechanical behaviour, the influence of thermal history on FpC_6 was investigated to establish a reproducible initial state. Differential scanning calorimetry experiments revealed that the glass transition temperature of FpC_6 decreased with increasing upper heating temperature and annealing time, suggesting that the network was not at equilibrium and changed over time. Based on temperature-dependent PXRD experiments of aged FpC_6, the decrease in T_g was attributed to the de-polymerization of the supramolecular chains. Annealing FpC_6 at temperatures above the T_m indicated that the chains disassembled faster at higher temperatures. Hysteresis experiments showed that no significant polymerization occurred during subsequent cooling or reheating cycles.

FpC_x (x = 5, 8 and 10) analogues with different alkyl chain lengths were prepared to investigate the effect of alkyl chain length. Preliminary investigation revealed that the FpC_x analogues also formed bulk supramolecular polymers with the same chain structure as FpC_6. Additionally, as the alkyl chain length increased, the glass transition temperature decreased FpC_6 and its analogues are the first reported bulk supramolecular polymers formed *via*

aromatic embraces and weak hydrogen bonding and represent an opportunity for novel monomer design.

Acknowledgements

During the past several years, I have had the fortune of encountering many important and wonderful people whom must be acknowledged.

I would like to start by thanking my supervisor, Xiaosong Wang, for your endless patience, steadfast support, kindness and mentorship throughout my PhD. I am forever grateful to you, for fostering my passion for chemistry since the very beginning. I have enjoyed our discussions and I feel that I have learned so much from you about chemistry and life. Thank you for always taking the time to listen. The journey has not always been smooth and I would like to thank you for your support and never wavering faith in me when I needed it the most. Your mentorship has helped me to grow not only as a scientist, but as a person as well. Thank you for all that you have done and for all that we have accomplished.

I am very fortunate to have a committee made up of an amazing group of individuals who have always gone above and beyond. I have learned so much from all of you over the years. Without your knowledge, inspiration and kindness, I would never have made it this far. Professor Gauthier, thank you so much for your help throughout my PhD. Without access to and your help repairing the rheometer, large parts of my thesis would not have been possible. Thank you for always being available to discuss with me, as I always learn so much from you. Professor Duhamel, I truly appreciate all the help and opportunities you have given over the years. Your knowledge and expertise has been invaluable. Professor Tam, thank you for providing access to the rheometer and taking the time to help me when I needed it. I am honored and fortunate to have been taught by all of you. Thank you all for choosing to be on my committee and reading my thesis.

I have been lucky enough to work alongside and become friends with some fantastic people on campus. I would like to thank Jalil Assoud, Leon Mintz, and Rick Marta.

Jalil, I want to thank you so much for all your help throughout my PhD. Your assistance with crystallography and help with writing my papers and thesis has been invaluable. I am truly fortunate to have had the opportunity to be taught by you. You are a fantastic teacher! You have always been there to offer advice about academia and life in general. It truly means so much to me! Thank you Jalil for everything that you have done and I am truly fortunate to have a friend like you.

Leon, thank you for being a wonderful friend! I will always value our epic lunch time discussions and I truly miss them. When we first started working together, I did not realize that I would end up making an incredible friend like you. Leon, thank you for encouraging me to see thing in different ways and always being ready to listen. Thank you so much!

Rick, I am truly honored to have had the opportunity to work alongside you. You have been an excellent mentor and friend. Your work ethic and enthusiasm have been an inspiration. Thank you for teaching me so much about chemistry and life. Also, thanks so much for providing access to the DSC, which has made parts of this thesis possible.

I would like to thank all my lab mates both past and present. In particular I would like to thank Kai Cao, Nimer Murshid and Dapeng Liu. You all have taught me many skills and I have truly enjoyed all the discussion we have had.

Also, I would like to thank Cath Van Esch and the incredible network of people at the University of Waterloo who have helped keep my PhD on track.

I would like to thank my incredible family, for their unconditional love and support. I am truly fortunate to have such a fantastic family in my life. Nanny and Poppy, thank you for

all of your support, encouragement and wisdom you have given me throughout this journey. Mom and Dad, from an early age you both have always encouraged me to follow my passion and nurtured my interest in science. Thank you for all your support and encouragement. Emily, Shauna, and Ayden, thank you guys for putting up with a “grad student” brother and for all of your support. It truly means so much to me.

Lastly, I would like to thank my loving wife, Alix Priest, without whom this work would not have been possible. Alix, you have been by my side every step of the way. You have encouraged me to follow my passion and made sacrifices to enable me to do so. You have shared in the struggles and in the successes. Thank you for your love and support in the good times and the bad, which have made this journey possible.

Dedication

To my loving wife

Table of Contents

List of Figures

List of Tables

List of Schemes

List of Abbreviations

6PE	Six-fold phenyl embrace
α	Dihedral angle between ring planes
θ	Donor angle of hydrogen bond
ω	Frequency
η*	Complex viscosity
τ_b	Average lifetime of supramolecular polymer chain
a-CO	Acyl carbonyl
ATR	Attenuated total reflectance
BSP	Bulk supramolecular polymers
CCD	Charge coupled device
Cp	Cyclopentadienyl
C_d	Centroid-to-centroid distance
d	Distance between hydrogen and acceptor
D	Distance between acceptor and donor
DMA	Dynamic mechanical analysis
DP	Degree of polymerization
EF	Edge-to-face
FpC_5	$CpFe(CO)PPh_3CO(CH_2)_4CH_3$
FpC_6	$CpFe(CO)PPh_3CO(CH_2)_5CH_3$
FpC_8	$CpFe(CO)PPh_3CO(CH_2)_7CH_3$
FpC_{10}	$CpFe(CO)PPh_3CO(CH_2)_9CH_3$
FpK	Cyclopentadienyl dicarbonyliron potassium

FTIR	Fourier transform infrared
G’	Storage modulus
G’’	Loss modulus
LVR	Linear viscoelastic regime
MALDI-TOF	Matrix-assisted laser desorption ionization time of flight
M_n	Number-average molecular weight
M_w	Weight-average molecular weight
NMR	Nuclear magnetic resonance
NOE	Nuclear overhauser effect
OFF	Offset face-to-face
P4PE	Parallel four-fold phenyl embrace
Ph	Phenyl
PXRD	Powder X-ray diffraction
PPh_3	Triphenylphosphine
SAXS	Small angle X-ray scattering
SP	Supramolecular polymers
t-CO	Terminal carbonyl
T_g	Glass transition temperature
T_m	Melting temperature
THF	Tetrahydrofuran
UPy	Ureido-4-pyrimidone
WAXD	Wide angle X-ray diffraction
XRD	X-ray diffraction

Chapter 1. Introduction

1.1 Overview

The field of supramolecular polymers (polymers formed by intermolecular interactions) has progressed considerably over the years.[1-4] The initial advancement of this field occurred in 1997 with the development of a supramolecular polymer based on quadruple hydrogen bonds between monomers.[5] This bonding motif allowed the monomers to achieve a significant degree of polymerization even in semi-dilute conditions. Following this breakthrough, a wide variety of intermolecular interactions have been used to prepare many functional supramolecular polymers. Furthermore, "living" supramolecular polymerization (analogous to living polymerization) has been developed, allowing for the precise control of the degree of polymerization.[6-8] However, the majority of this progress has involved solution based systems, which often lose their polymeric behaviour upon drying. Bulk supramolecular polymers, particularly those formed by small molecule monomers, are considerably less developed. Nevertheless, bulk supramolecular polymers are an attractive route to develop functional materials that can be processed using established techniques, such as spin coating, extrusion and thermo-forming. The key challenge associated with preparing bulk supramolecular polymers from small molecules is preventing crystallization. Consequently, monomer design is very difficult, because the mobility of the monomer as well as the strength and directionality of intermolecular interactions must be carefully balanced to prevent crystallization. To facilitate monomer design, an extensive understanding of the intermolecular interactions in the solid state is required. Crystal engineering has proven to be a successful tool to understand how intermolecular interactions direct the packing of molecules in the solid state.

While challenging, crystal engineering may help to provide the insight necessary to further develop bulk supramolecular polymers from small molecules.

1.2 Introduction

Main-chain supramolecular polymers (SP) are linear arrays of molecules associating through non covalent interactions, which can be prepared either in solution or in bulk (see Figure 1-1a).[1, 3-4]

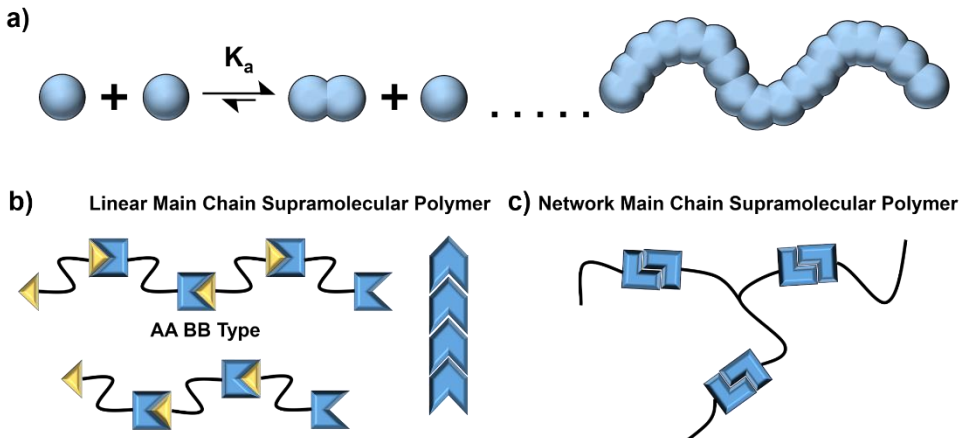

Figure 1-1 a) Schematic representation of supramolecular polymerization. Main chain SP are either linear (as seen in b) or network (as seen in c). Linear SP are formed by ditopic monomers. Ditopic monomers with self-complementary end-groups form AB type SP. Conversely, ditopic monomers with complementary end-groups form AA BB type SP. Network SP are formed by monomers with more than two associating functional groups (≥ 3).

Analogous to covalent polymers, SP possess polymeric properties derived from the presence of chains, such as viscoelasticity and a glass transition.[2] Like covalent polymers, SP can be described in terms of degree of polymerization (DP) and weight-average (M_w) or number-average (M_n) molecular weight.[2] The association of monomers through non-covalent interactions is a reversible process governed by the association constant and concentration.[2, 9] In order to obtain SP with a high DP, the equilibrium process must strongly favour the association between monomers, which requires strong intermolecular interactions.[2, 9]

Initial interest in SP arose from the study of supramolecular liquid crystals generated from the association between two non-mesogenic compounds.[10-11] Early SP had low molecular weights and did not display polymeric behaviour such as viscoelasticity and shear thinning. These early problems were caused by weak association between monomers due to insufficiently strong intermolecular interactions.[5] In 1997, Meijer *et al*. demonstrated the first supramolecular polymer with a high DP capable of forming even in semi-dilute solutions.[5] This supramolecular polymer utilized strong hydrogen bonding ($K_{dim} = 6 \times 10^7$ in chloroform) between self-complementary ureido-4-pyrimidinone (UPy) end-groups, produced by four complementary hydrogen bonds.[12-13] The resulting material displayed typical polymeric behaviour and its properties could be tuned by adjusting the temperature.[5] Thanks to considerable progress in supramolecular chemistry, a wide variety of intermolecular interactions have been harnessed to form SP in solution such as hydrogen bonding,[14-20] halogen bridging,[21] metal-metal,[22-25] metal-ligand,[26-29] and aromatic interactions,[30-33] and host guest motifs.[34-37] It is commonly observed that different interactions work cooperatively to hold the chains together.[38-39] Furthermore, a strong understanding of polymer kinetics and growth has been developed.[18, 40-48] This has led to the discovery of living supramolecular polymerization (analogous to chain growth polymerization), allowing for the preparation of monodisperse SP and precise control of DP.[6-8] Despite these impressive advances, most solution SP lose their polymeric behaviour upon drying.

1.3 Bulk Supramolecular Polymers

Bulk supramolecular polymers (BSP) refer to SP which can be formed by the association of monomers in the solid state. BSP are attractive as functional materials that can be processed using established techniques, such as spin coating, extrusion and thermo-forming.

In contrast to solution SP, BSP are much less developed, due to the difficulty in monomer design. Monomers for solution SP are easier to design because solvents can be used to moderate the intermolecular interactions and provide the mobility for the monomers to assemble. In contrast, monomers for BSP are more challenging to develop because of the following restrictive monomer requirements:[49]

(1) The monomers must have sufficient mobility to assemble in bulk.

(2) The intermolecular interactions must be sufficiently strong and directional to form and stabilize the chains.

(3) The monomers or assemblies cannot crystallize.

Developing a monomer which fulfills these requirements is challenging because by attempting to meet one requirement, another may be adversely affected.[49] For example, increasing the strength of intermolecular interactions of a monomer, may also increase its tendency to crystallize and reduce its mobility.[49] Two general approaches have been developed to design monomers for BSP.[2] One approach is the use of macromonomers.[2] Macromonomers are prepared by the functionalization of covalent oligomers with associating end-groups. The use of macromonomers first involved the functionalization of polydimethylsiloxane oligomers with self-complementary UPy end-groups.[5] Following this approach, different oligomers and end groups have been combined, resulting in a plethora of BSP.[50-60] This approach has proven very successful because the incorporation of the covalently bonded oligomer makes crystallization challenging and provides mobility to the monomer.[2]

The alternative approach is to use carefully designed small molecules. While challenging, the small-molecule approach to generating BSP is desirable, because it maximizes the potential of a fully reversible backbone. The ability to completely disassemble the main

chain into small molecules allows the processing of these materials to be easier compared to their covalent polymer counterparts.[50] In addition, the self-healing of SP from small molecules tends to be more efficient, due to the higher mobility of low molecular weight monomers.[49, 61] Lastly, the use of small-molecule monomers introduces significant order in one dimension, which has been shown to be responsible for imparting unique optical and electronic properties into certain SP.[1] There are two general categories of main chain BSP formed from small molecules, linear chains and network. The progress to date of both linear and network main chain BSP from small molecules is summarized below.

1.3.1 Linear Main Chain Bulk Supramolecular Polymers

Linear main chain BSP from small molecules (Figure 1-1b) arose from the research into supramolecular mesogens or liquid crystals.[2] Supramolecular mesogens were first prepared by mixing two different non-mesogenic monotopic molecules with complementary functional groups.[10-11] Mixtures of these molecules exhibited thermally stable liquid crystalline phases, demonstrating that complexation had occurred.[10-11] Following this work, the complexation of multitopic molecules was used to prepare supramolecular mesogens, which are considered to be the forerunners of BSP from small molecules.[62-64] It was observed that the anisotropy in liquid crystals assisted the association of the monomers into the linear assemblies increasing the DP.[65]

The first linear main chain BSP was reported by Lehn and coworkers.[66-67] This AA BB type supramolecular polymer was based on the association of the complementary non-mesogenic ditopic monomers **1** and **2** shown in Figure 1-2.[66-67]

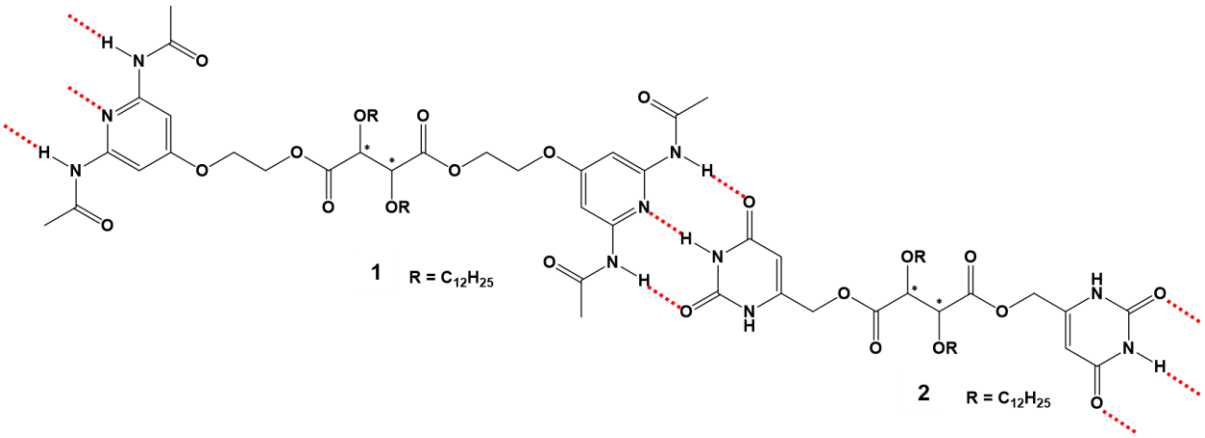

Figure 1-2 AABB type supramolecular polymer formed by compound **1** and **2**.

The 1:1 mixtures of **1** and **2** were prepared by dissolving the compounds in tetrahydrofuran (THF), and then removing the solvent by evaporation. Upon melting the resulting crystalline material, stable mesophases formed between slightly below room temperature to above 200 °C. The formation of mesophases is a direct result of complexation of the monomers through hydrogen bonding which was confirmed through Fourier transform infrared spectroscopy (FTIR). These mixtures were described as highly viscous glues that formed fibres upon spreading, which is typical polymer-like behaviour. X-ray diffraction of the mixtures indicated that they formed hexagonal columnar mesophases. This work pioneered the use of low molecular weight or small molecules for the preparation of BSP. While these mixtures were viscous and displayed liquid crystalline behaviour, the mixtures crystallized and did not undergo a glass transition.

Mixtures of non-mesogenic bispyridyls and diacids were shown by Griffin *et al.* to form BSP.[63, 68-74] Mixtures of these ditopic compounds resulted in AABB type SP.

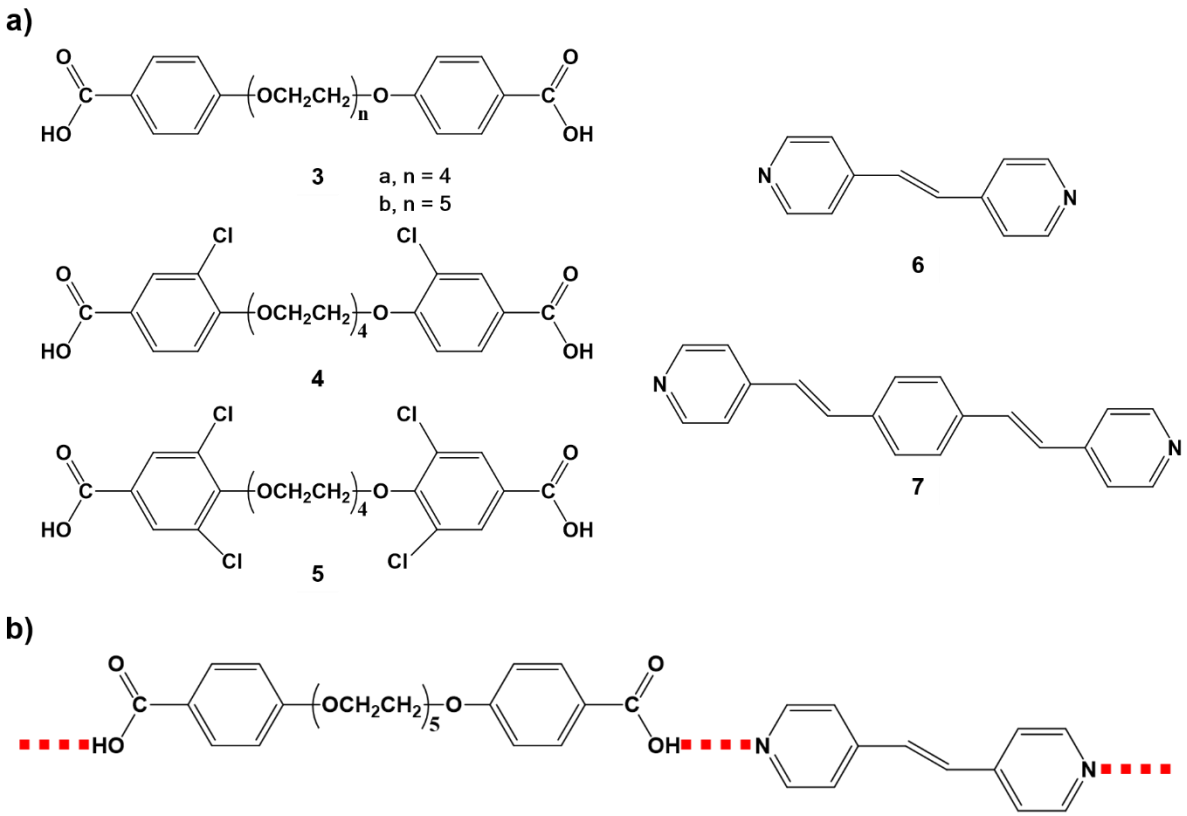

Figure 1-3 a) Ditopic diacids used as hydrogen bond donors (**3-5**) and ditopic bispyridyl used as hydrogen bond acceptors (**6-7**) b) Illustrative chain structure formed by hydrogen bonding between diacids and bispyridyl (**3b** and **6**).

For example, while individually neither compound **3** nor **6** displayed liquid crystalline behaviour, their resulting mixtures did.[68] This behaviour was attributed to the formation of supramolecular chains as shown in Figure 1-3b. Below the clearing temperature (isotropization temperature) of the liquid crystals, FTIR spectroscopy confirmed the presence of hydrogen bonding between the pyridyl groups of compound **6** and carboxylic acid groups of **3**.[68] The proposed chain structure was supported by small angle X-ray scattering (SAXS) experiments that showed a peak corresponding to the length of the repeat unit.[71] Mixtures of **3** and **6** (1:1 ratio) were characterized by differential scanning calorimetry (DSC) and were found to crystallize upon cooling, indicating that SP were formed between the melting temperature (T_m)

and the clearing temperature.[68, 71] Further DSC experiments revealed that a mixture of **3b/6** could exist as a metastable supramolecular polymer below its melting temperature; however the mixture still crystallized upon cooling.[71]

The rheological behaviour of mixtures of **3b**/**6** in different ratios was investigated.[68] It was found that as the mixtures were cooled below the isotropization temperature, there was significant increase in the storage modulus (G') (a measure of a sample's elasticity and reflective of structure).[68] As the sample was cooled further, a plateau in G' was observed. In theory, as the temperature decreases, the DP and G' should increase; however this was not observed. It was suggested that the dynamics of the hydrogen bonds were too rapid to be able to measure the elastic nature of the chains, implying that that the chains were breaking and forming too rapidly to impart polymer-like mechanical behaviour.[68]

These mixtures were prone to crystallization, because the hydrogen bonds were too weak to hold the chains together at the high temperatures, resulting in a low DP. To prevent crystallization, low temperatures were needed so that the hydrogen bonds would be strong enough to achieve a high DP and stabilize the chain.[70] To delay crystallization long enough so that a high DP could be achieved, bulk substituents were added resulting in compounds **4** and **5.** [70] The chlorine substituents significantly depressed the recrystallization temperature and made crystallization "sluggish". When more chlorine substituents were added, the more apparent these effects became. BSP prepared from mixtures of **5** and **7** were the most successful at displaying polymeric behaviour. DSC demonstrated that 1:1 mixtures of **5** and **7** did not recrystallize during cooling and a glass transition was obtained; however, these mixtures underwent cold crystallization upon reheating (Figure 1-4a).[70]

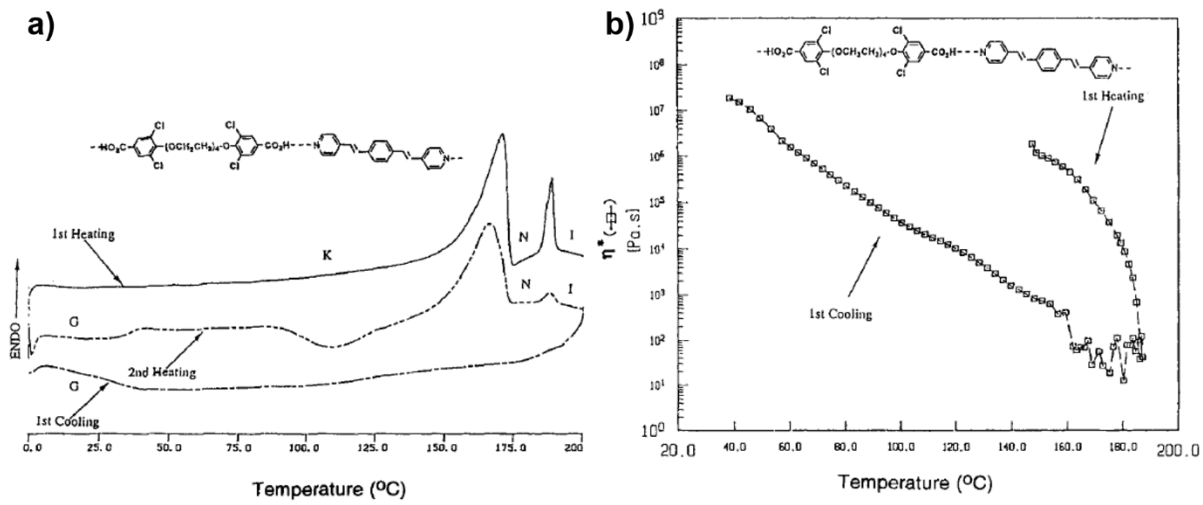

Figure 1-4 a) DSC thermogram for a 1:1 mixture of compound **5** and **7**. b) Complex viscosity as a function of temperature of a 1:1 mixture of compounds **5** and **7**. Images reproduced with permission from reference 70.

Plots of the complex viscosity (η*) vs. temperature showed a slow gradual increase in viscosity as the temperature was decreased (Figure 1-4b). This was attributed to the elongation of the supramolecular polymer chains. As the temperature was decreased the hydrogen bonds became more effective at holding the chain together.[70] Furthermore, fibres could be drawn from this mixture between 65 °C and 105 °C, indicating that the intermolecular interactions were strong enough to hold the chains together at this temperature.

Replacing the chlorine atoms in compound **5** with a methyl group also resulted in a supramolecular polymer when mixed with compound **7**.[72] Fibres were drawn from the resulting mixtures indicating the presence of supramolecular polymer chains. X-ray scattering revealed that these chains orientated during fibre formation, demonstrating the chains remained intact during shear orientation.[72] Another approach to slow crystallization was to introduce a third non-mesogenic monomer with a kink conformation mixed in various ratios.[75] While these systems displayed liquid crystalline behaviour and slow crystallization, no glass transitions were observed.[75] Additionally, random supramolecular co-polymers were generated from

mixtures of compound **3** with 3-methyladipic acid and compound 7.[73] While the monomers were non-mesogenic, the mixtures exhibited liquid crystalline behaviour demonstrating the formation of supramolecular polymer chains. Despite being random co-polymers these systems crystallized upon cooling and no glass transition was obtained, demonstrating that they were not stable.[73]

The exploration of BSP formed by mixing diacids and bispyridyls formed the basis for the future development of BSP. In particular, this work highlighted the tendency of small molecules to crystallize and illustrated the use of bulky substituents and multiple monomers to make crystallization difficult. Furthermore, this work established the need for strong intermolecular interactions to prevent crystallization and increase the integrity of the chains. In these BSP only one hydrogen bond was used to link monomers, which was ultimately unable to prevent crystallization.

A series of AA BB type SP were designed based on 1:1 mixtures between diacids (**8-9**) and azopyridine derivatives (**10-12**) as shown in Figure 1-5.[76] The BSP were prepared by melt mixing the diacids and azopyridine derivatives in a 1:1 ratio under an inert atmosphere. The resulting BSP often displayed monotropic liquid crystalline behaviour and in some cases vitrified upon cooling.[76] In general, an increase in the length of a mesogen resulted in a concomitant increase in phase transition temperature. As the flexibility of the spacer was increased, the phase transition temperatures decreased.[76]

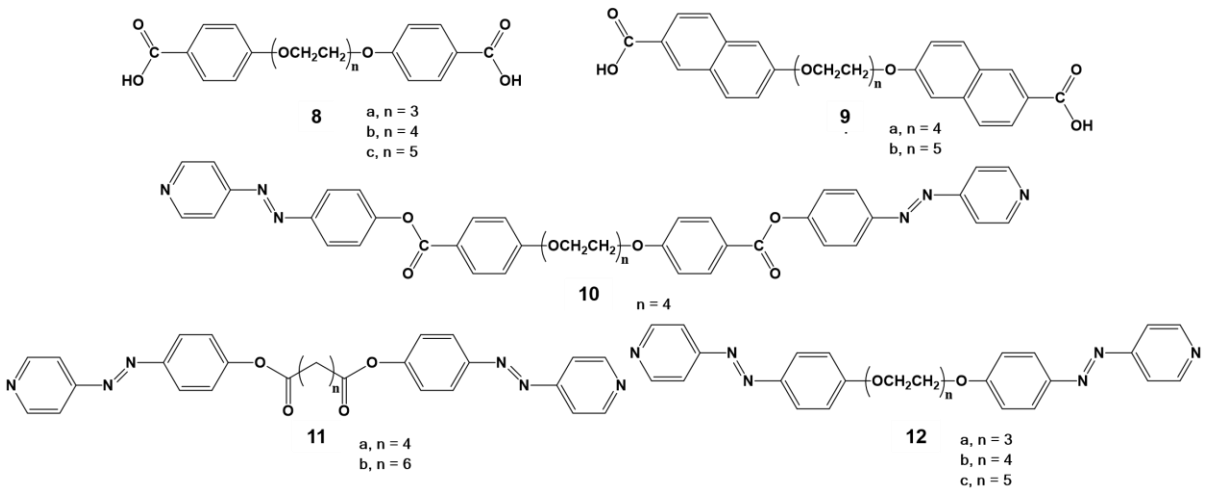

Figure 1-5 Ditopic diacids used as hydrogen bond donors (**8**-**9**) and azopyridine derivatives used as hydrogen bond acceptors (**10**-**12**)

A BSP with excellent stability and mechanical properties was prepared from **13** by Meijer *et al*. (Figure 1-6a).[50] FTIR indicated the self-association of **13,** through the characteristic absorptions of hydrogen bonded UPy end-groups, demonstrating that **13** formed a supramolecular polymer in bulk.[50] DSC revealed that the thermal behaviour of **13** was atypical for small molecules (Figure 1-6b). During the first heating cycle compound **13** melted at 112 °C (large endotherm); however, no recrystallization was observed during cooling or reheating. After melting, compound **13** was difficult to recrystallize despite annealing at 100 °C for 3 hours. Phenyl groups were added to the UPy group of **13** to disrupt hydrogen bond formation and subsequent supramolecular polymerization. The resulting compound displayed typical small-molecule behaviour and crystallized rapidly. This suggested that when first synthesized compound **13** was crystalline; however, upon melting, compound **13** associated to form a supramolecular polymer.[50] Furthermore, the steric effect of the supramolecular chains and their integrity (monomers do not dissociate) suppressed crystallization.[50] A glass transition was observed upon cooling and subsequent reheating at 25 °C (Figure 1-6b). Rheological investigation of compound **13** in the bulk revealed a rubbery plateau below 70 °C (Figure 1-6c).

Solid state nuclear magnetic resonance (NMR) spectra indicated that there were no microcrystalline domains present in the amorphous compound **13**. In the absence of physical cross-links, the presence of a rubbery plateau indicated chain entanglement.[50]

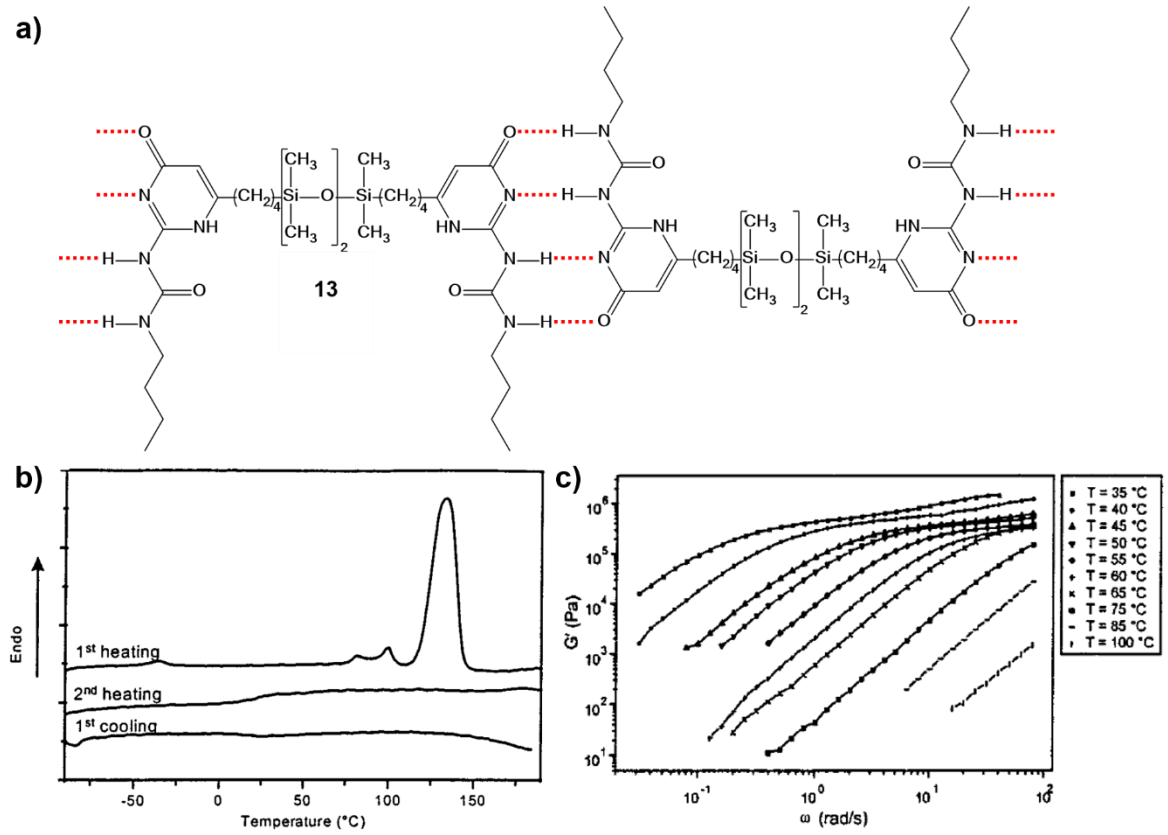

Figure 1-6 a) Supramolecular polymer formed by the self-association of compound **13** *via* UPy end-groups. b) DSC thermograms for compound **13**. c) Storage moduli of **13** at different temperatures. Images b) and c) reproduced with permission from reference 50. Copyright 1999 American Chemical Society.

This work demonstrated that small molecules can form BSP with appreciable mechanical properties. Furthermore, this work demonstrated that monomers must be heated to provide mobility so that supramolecular polymerization can occur. Lastly, this work highlighted the critical importance of using sufficiently strong intermolecular interactions, so that once the chains were formed, the monomers were sequestered and unable to crystallize. The steric effect of the chains also assisted in suppressing crystallization.

A detailed investigation of glasses formed by SP prepared from low molecular weight monomers was reported by Lacoudre *et al.* This work investigated the resulting glasses formed by mixtures of compound **14** with compounds **15** and **16** (Figure 1-7a).[77]

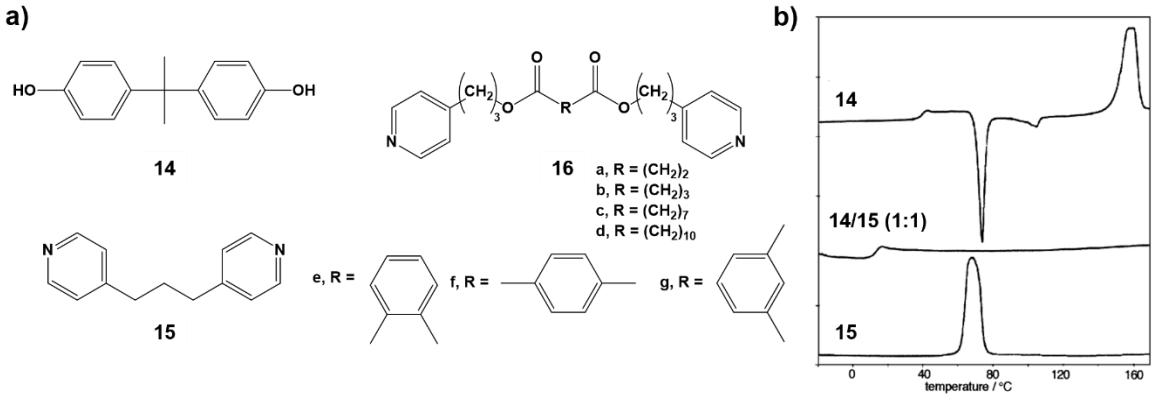

Figure 1-7 a) Structure of compounds **14-16 b**) DSC thermogram for compounds **14** and **15** as well as their mixture (1:1 ratio). Image b) reproduced with permission from reference 77.

Unlike pure compounds **14** and **15**, their 1:1 mixture resulted in a transparent stable glass with glass transition at 9 °C (Figure 1-7b). Notably, the 1:1 mixtures did not undergo crystallization even when using very slow temperature ramp rates (1 °C/min) indicating that the resulting SP were stable.[77] The formation of hydrogen bonds between compounds **14** and **15** was confirmed by FTIR and the stability of the glass was attributed to the strength of these hydrogen bonds. To investigate the influence of the spacer on the glass transition, compounds **16a-g** were prepared. Increasing the length of the alkyl spacer lowered the T_g, because of the increased mobility of the alkyl spacer.[77] Conversely, introducing a more rigid aromatic spacer resulted in a higher T_g. Lastly, mixtures prepared from the *para* isomer had a higher T_g than the *ortho* or *meta* isomers. The influence of the structure of the monomer on the T_g fit well with empirical relationships developed in the field of polymers.[77]

An excellent example of a linear main chain BSP prepared from carefully designed monomers **17** and **18** (Figure 1-8) was reported by Rowan *et al.*[78-79] This system harnessed the

well-known complementary hydrogen bonding between thymine and adenine to prepare an AA BB type supramolecular polymer Figure 1-9a.

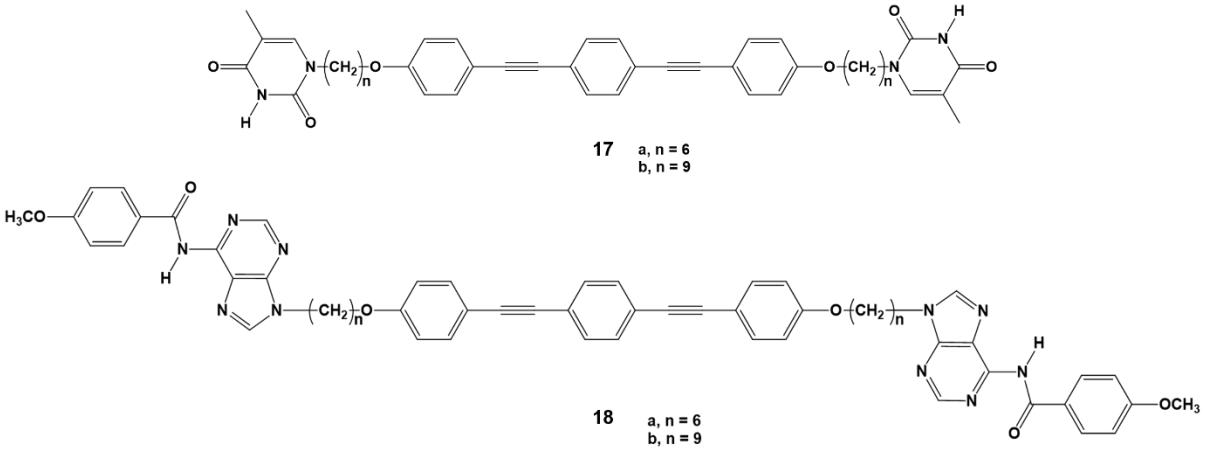

Figure 1-8 Chemical structure of compounds **17** and **18**.

The rigid spacer was chosen in order to impart liquid crystalline properties as well as fluorescence to the resulting supramolecular polymer.[78-79] To prevent self-dimerization, the adenine moiety on compound **18** was modified with N^6-anisoyl to increase the hydrogen bonding of the adenine moiety to the thymine moiety on compound **17**.[78-79] When compounds **17** and **18** were mixed in a 1:1 ratio, the mixtures did not crystallize upon cooling and displayed glass transition temperatures, indicative of SP chains (Figure 1-9b, c).[78-79]

Furthermore, a viscous birefringent phase was obtained as the mixtures were cooled after an initial heating cycle (Figure 1-10a, b). Upon further cooling, the viscous birefringent phase vitrified. This behaviour was attributed to the supramolecular polymer chains formed by the hydrogen bonding between **17** and **18**.[78-79] WAXD analysis of the vitrified birefringent phase identified low angle peaks which corresponded to the proposed length of the supramolecular polymer repeat unit in a smectic c arrangement. The chain structure was further supported by FTIR experiments as well as nuclear Overhauser effect (NOE) experiments in solution. The viscous birefringent phase was never observed during the initial heating cycle of

a 1:1 mixture (even if the mixture was obtained from a solution) and was only observed during subsequent heating and cooling cycles. This suggested that the birefringent phase only occurred after the thermal bulk supramolecular polymerization of the monomers.[78-79]

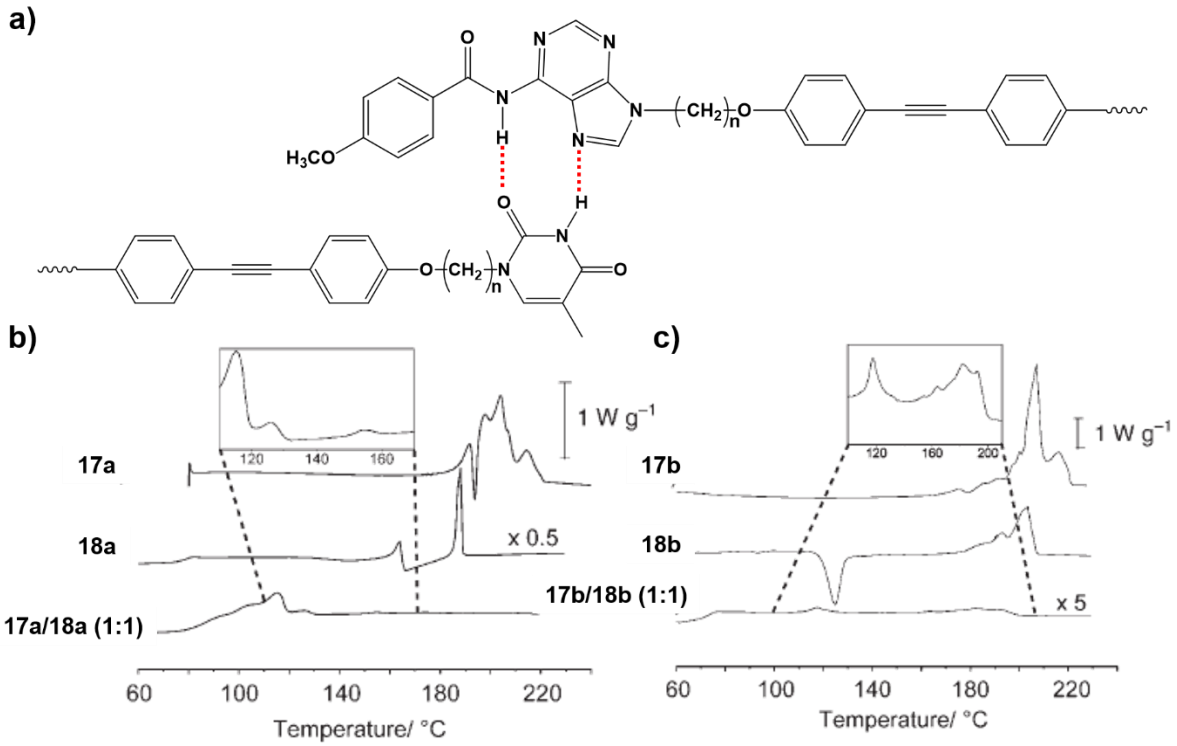

Figure 1-9 a) Hydrogen bonding between compounds **17** and **18**. b) DSC thermograms for compound **17a**, **18a** and their 1:1 mixture. c) DSC thermograms for compounds **17b**, **18b** and their 1:1 mixture. Images b) and c) reproduced with permission from reference 79.

Fluorescent fibres could be drawn from the melt (Figure 1-10c). The authors proposed that the assembly of compounds **17** and **18** into supramolecular chains increased the aspect ratio of the assembly compared to the monomers. This stabilized the assemblies, since the rigid high aspect ratio chains would have difficulty packing into a crystal lattice.[78-79]

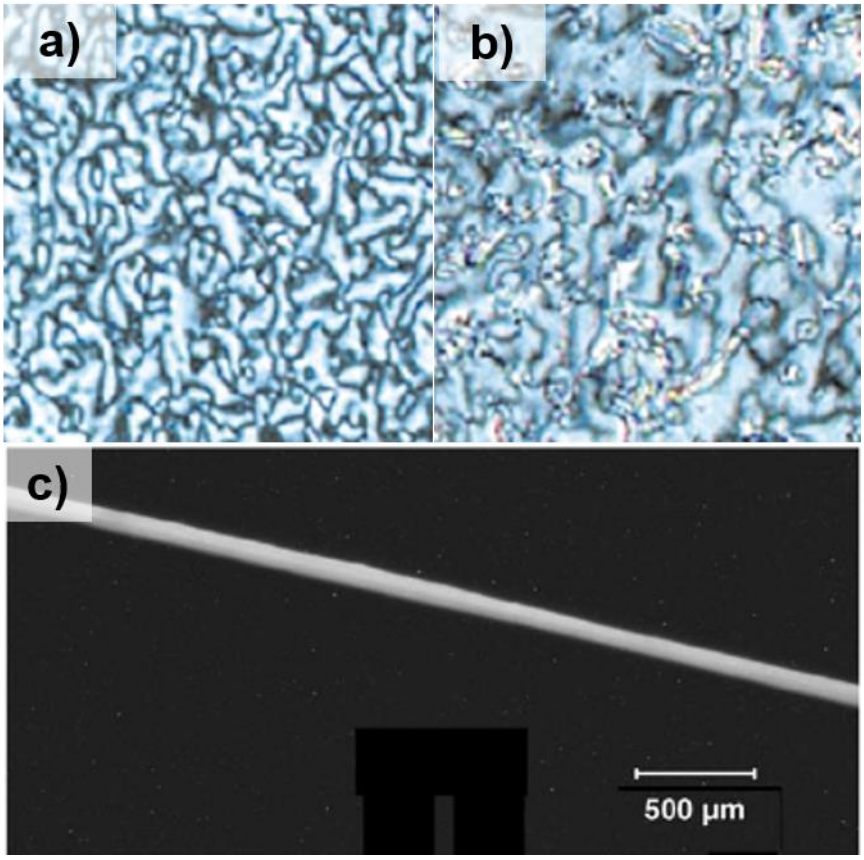

Figure 1-10 Polarized optical microscope images of the birefringent phase formed by mixtures of a) compounds **17a** and **18a** and b) **17b** and **18b**. Images reproduced with permission from reference 78. c) Image fibre drawn from a mixture of **17a** and **18b**. Image reproduced with permission from reference 79.

This work demonstrated how the careful design of monomers can produce stable linear main chain SP that can form fibres and a glassy state. Furthermore, additional properties can be incorporated into the spacer (i.e. fluorescence). Lastly, this paper highlights that the steric effect of the chain structure can also be a factor in suppressing crystallization.

All the examples discussed thus far incorporated spacers in between functional groups. These spacers imparted mobility to the monomers and assisted in suppressing crystallization. Linear BSPs from spacer-less monomers are quite rare. One such example, is compound **19a** reported by Araki *et al.*[80]

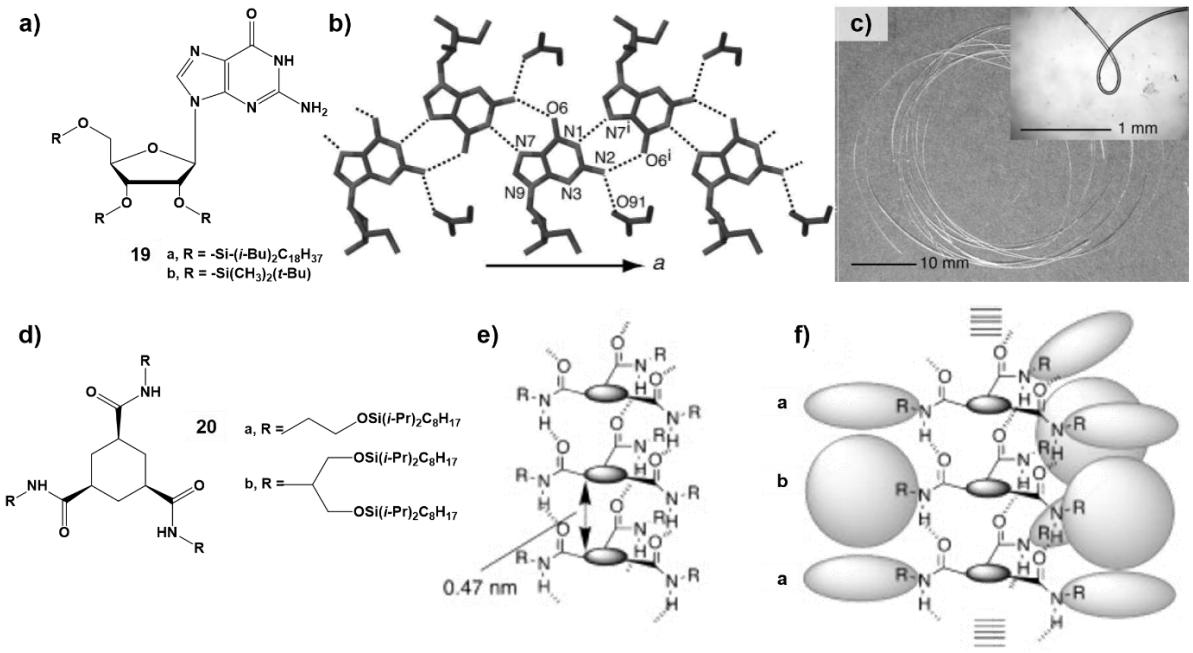

Figure 1-11 a) Chemical structure of compound **19**. b) Proposed chain structure formed by compound **19**. c) Fibre of **19a** formed by melt spinning. d) Chemical structure of compound **20**. e) Chain structure of compound **20** with an inter-monomer spacing of 0.47 nm. f) Chain structure of copolymer formed by **20a** and **b**. Images reproduced with permission from references 80 and 81.

Compound **19a** was able to form flexible fibres by melt spinning (Figure 1-11c). Crystal engineering was performed to determine the chain structure responsible for fibre formation. Unfortunately, single crystals suitable for X-ray diffraction could not be obtained from compound **19a**. Consequently, compound **19b** was prepared and successfully recrystallized. As shown in Figure 1-11b, compound **19a** formed tape-like chains in the *a* crystallographic direction induced by hydrogen bonding between molecules.[80] Compound **19a** and **19b** had the same IR spectral pattern for the amino stretching and deformation modes. Consequently, the authors attributed the fibre formation of compound **19a** to the same chain structure formed by compound **19b**.[80] X-ray diffraction of the resulting fibres revealed a peak corresponding to a repeat unit in the proposed chain structure. Tensile testing of the fibres

revealed they had a tensile strength of 1.91 ± 0.41 MPa at ambient temperature. DSC analysis suggested these fibres undergo crystallization and no glass transition was observed.[80]

Another interesting spacer-less system based on **20** is shown in Figure 1-11d.[81] Compound **20** was able to form a fibre *via* melt spinning.[82] Mixtures of compounds **20a** and **20b** were prepared by first dissolving the monomers in chloroform and then evaporating the solvent. The mixtures were heated to 150 °C and extruded.[81] The tensile strength of the resulting fibres was found to decrease with increasing mole fraction of compound **20b**. When the mole fraction of **20b** was increased past 50%, fibres could not be obtained. This was attributed to a lower degree of polymerization, since **20b** could not form hydrogen bonds with itself. X-ray diffraction of the fibres revealed peaks at $2\theta = 18.8°$ (d = 0.47 nm) along the long axis of the fibre which corresponded to the proposed chain structure shown in Figure 1-11e,f.[81] The IR spectra of mixtures of **20a** and **b** showed that both monomers were incorporated into the chain. While no glass transition was observed for the mixtures, fibres could be obtained which had a measurable tensile strength.[81] Both of the spacer-less systems described above used long flexible substituents to provide mobility to the monomers and delay crystallization. While these systems could form fibres, no other polymer-like behaviour was observed, such as viscoelasticity or a glass transition.

1.3.2 Network Main Chain Bulk Supramolecular Polymers

Network main chain BSP were developed concurrently with linear main chain BSP. The research was driven in part by the need to address the poor mechanical properties of linear main chain BSP and their tendency to crystallize. Griffin *et al.* expanded on previous work by increasing the number of hydrogen bonds between components to increase the polymer-like

behaviour. Consequently, compounds **20** and **21** (Figure 1-12a) were mixed with compound **3a** to create supramolecular polymer networks.[69]

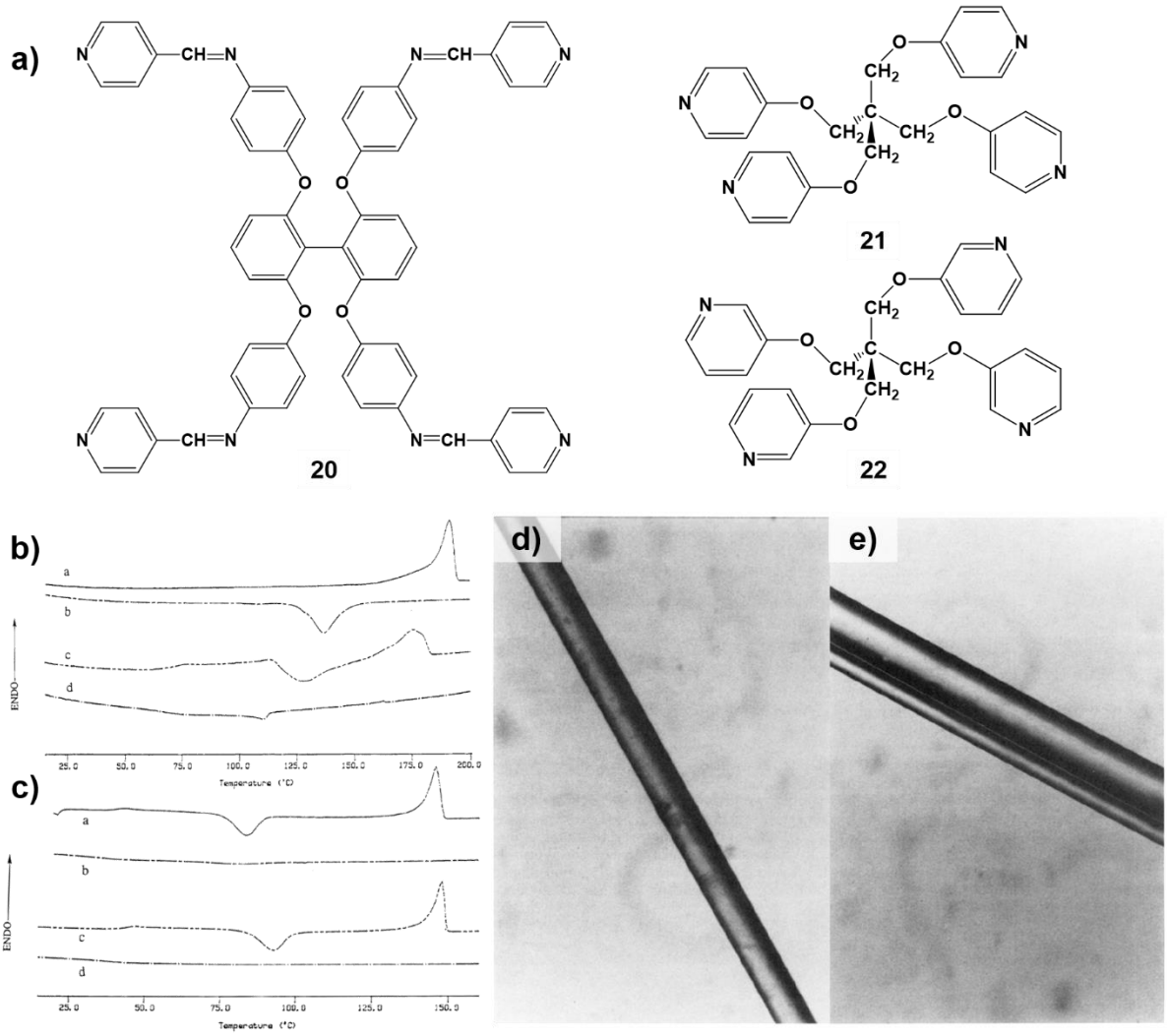

Figure 1-12 a) Chemical structure of monomers **20**-**22**. DSC thermograms for 1:1 mixtures of **20** and **3a** b) and 1:1 mixtures of **21** and **3a** c). Traces "a" and "b" represent normal heating and cooling cycles respectively. Traces "c" and "d" represent heating and cooling cycles after annealing at 200 °C. Photographs of fibres formed by 1:1 mixtures of **20** and **3a** d) and 1:1 mixtures of **21** and **3a** e). Images b-e reproduced with permission from reference 69. Copyright 1995 American Chemical Society.

These systems were prepared by melt mixing compounds **20** and **3a** or **21** and **3a**. As the temperature was decreased, FTIR confirmed complexation between the pyridyl and

carboxylic acid groups and a concomitant decrease in the adsorption of the carboxylic acid dimer was observed. This behaviour indicated that as temperature decreased, the dissociation of the hydrogen bonds was slowed and complexation between monomers increased.[69] Excitingly, fibres could be drawn from the melt as the temperature was lowered, which could not be done with mixtures prepared from **3** and **6**.[69]

Heating from room temperature, **20/3a** showed a broad melting endotherm suggesting that the sample became liquid-like over a broad temperature range (Figure 1-12b). While the samples would crystallize during cooling, crystallization could be suppressed by cooling rapidly. Interestingly, when the sample was cooled after heating at 200 °C, crystallization was suppressed. Upon reheating, a glass transition was observed and followed by cold crystallization (Figure 1-12b). Mixtures of **21** and **3a** did not recrystallize on cooling but underwent cold crystallization upon heating. While these mixtures did not display viscoelastic behaviour, fibres could be drawn from the melt and the mixtures could form glassy states. This demonstrated that the use of more hydrogen bonds and the formation of a network improved mechanical properties and helped to suppress crystallization.[69]

Further investigations revealed that the thermal behaviour of networks formed by mixing **21** or **22** with **3**, were affected by the number of heat-cool cycles and the length of time the monomers spent in the isotropic melt.[74] As the number of heat-cool cycles increased, the crystallization during cooling was gradually suppressed and cold crystallization increased during heating. When a mixture of **21** and **3a** was kept in the isotropic melt for longer periods of time (1 h, 3 h and 21 h), it behaved more like a system which had undergone multiple heat-cool cycles. Since ageing at room temperature had no effect on the thermal behaviour, a certain amount of energy must have been required for the reorganization of the network.[74] Once given

enough thermal energy the monomers rearranged into a more stable network structure that suppressed recrystallization. Therefore, the longer the time spent in the isotropic melt, the more time the monomers had to rearrange into the most stable structure.[74] Also, networks produced from diacids with shorter spacers and parapyridyls resulted in more crystallinity and required more time in the isotropic state to suppress crystallization.[74] This work highlighted the importance of spacer length and geometrical arrangement of the interactions on the suppression of crystallization. Also, this work demonstrated that supramolecular polymer networks require significant time in the isotropic melt to achieve a stable state.

Kihara *et al.* prepared a series of network main chain SP based on the combination of a non-mesogenic ditopic H-bond donor with a series of non-mesogenic tritopic H-bond acceptors (Figure 1-13).[83] These mixtures were prepared by mixing stoichiometric amounts of the H-bond donor and acceptors in pyridine. The solution was evaporated under reduced pressure and the resulting solid was dried in a vacuum for 24 hours. Upon drying, the mixtures displayed liquid crystalline behaviour indicating that the material maintained its supramolecular polymer nature. FTIR of the bulk samples confirmed the presence of intermolecular hydrogen bonds.[83] The thermal behaviour of the dried mixtures revealed that the mixtures underwent a glass transition during cooling and reheating, with the exception of a mixture of **23** and **28**.[83] All samples exhibited some crystallization during cooling and reheating, limiting their use as potential SP. The authors attributed the lack of a glass transition and crystallization with a mixture of **23** and **28,** to the symmetry of **28,** which facilitates crystallization.[83] Only one hydrogen bond was used to connect monomers, which likely contributed to the tendency of the mixture to undergo crystallization. It is important to note

that this work demonstrated that monomer asymmetry is an important factor to suppress crystallization.

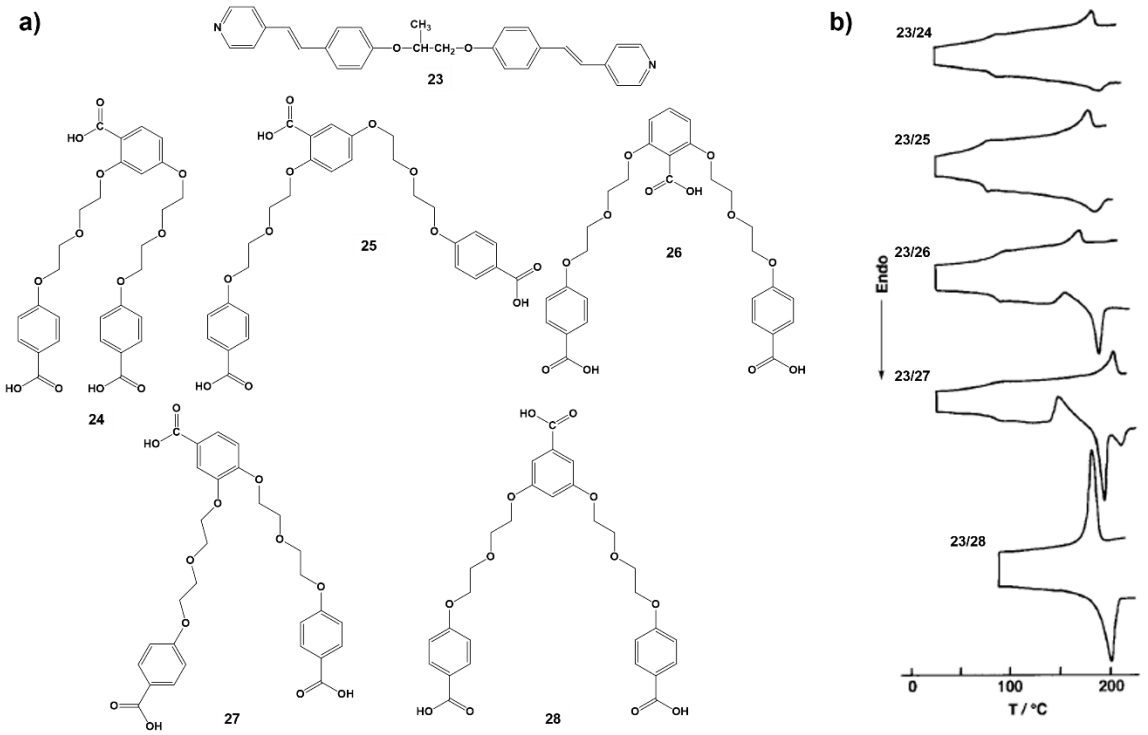

Figure 1-13 a) Chemical structure of compounds **23-28** b) DSC thermographs for 1:1 mixtures of monomer **23** with monomers **24-28**. Image b) reproduced with permission from reference 83.

After using crystal engineering to establish the hydrogen bonding motifs of aminotriazine,[84-86] Wuest *et al*. prepared a series of monomers shown in Figure 1-14a.[87] Each monomer had four aminotriazine functional groups each with two binding sites capable of forming two complementary hydrogen bonds (Figure 1-14b). After an initial cycle of melting and solidification, the monomers formed an amorphous material which was in the glassy state and underwent a glass transition. The use of longer alkyl chains resulted in lower T_g and melting temperatures. When the amorphous melts were characterized under steady shear stress, Newtonian behaviour was observed across all temperatures and stresses. It was found that increasing the length of the alkyl chain reduced the viscosity, possibly due to the disruption of

hydrogen bonding due to the steric effect of the alkyl chains.[87] These results demonstrated an improvement in the mechanical properties upon the addition of multiple hydrogen bonds.

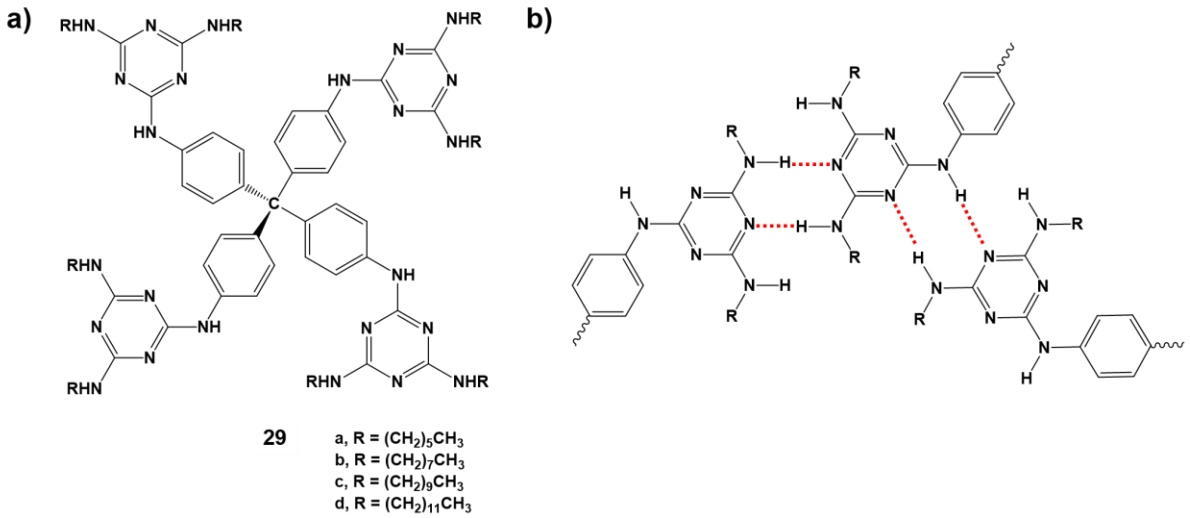

Figure 1-14. a) Chemical structure of monomer **29**. b) Intermolecular interactions between the aminotriazine functional groups.

An excellent example of functional network BSP was reported by Leibler *et al.*[49] This network BSP was composed of a mixture of complementary ditopic and tritopic monomers (Figure 1-15a), which resulted in a thermoreversible supramolecular polymer which displayed rubber behaviour and self-healing properties.[49] The tendency of small molecules to crystallize was overcome by using a mixture of small molecules with different associating end groups. Furthermore, the strong directional intermolecular interactions and the entropy of mixing helped to stabilize the chain structure and prevent phase separation of the monomers.[49] The resulting mixture of compounds was shown to be comprised of oligomers through a combination of NMR, size exclusion chromatography, and intrinsic viscosity measurements. FTIR spectroscopy confirmed the presence of multiple hydrogen bonds between N—H and C=O moieties.[49] DSC and X-ray scattering confirmed that the material was amorphous. This network BSP displayed a glass transition (T_g = 28 °C) and at 90 °C the material behaved like

a soft rubber. The material was able to return to its original dimensions after 100% strain deformation. To lower the T_g, the mixture was plasticized with dodecane (11% w/w). At room temperature, the plasticized material exhibited rubber behaviour as it could achieve high strains (Figure 1-15a). The material could almost completely recover the strain during creep recovery experiments (Figure 1-15b).

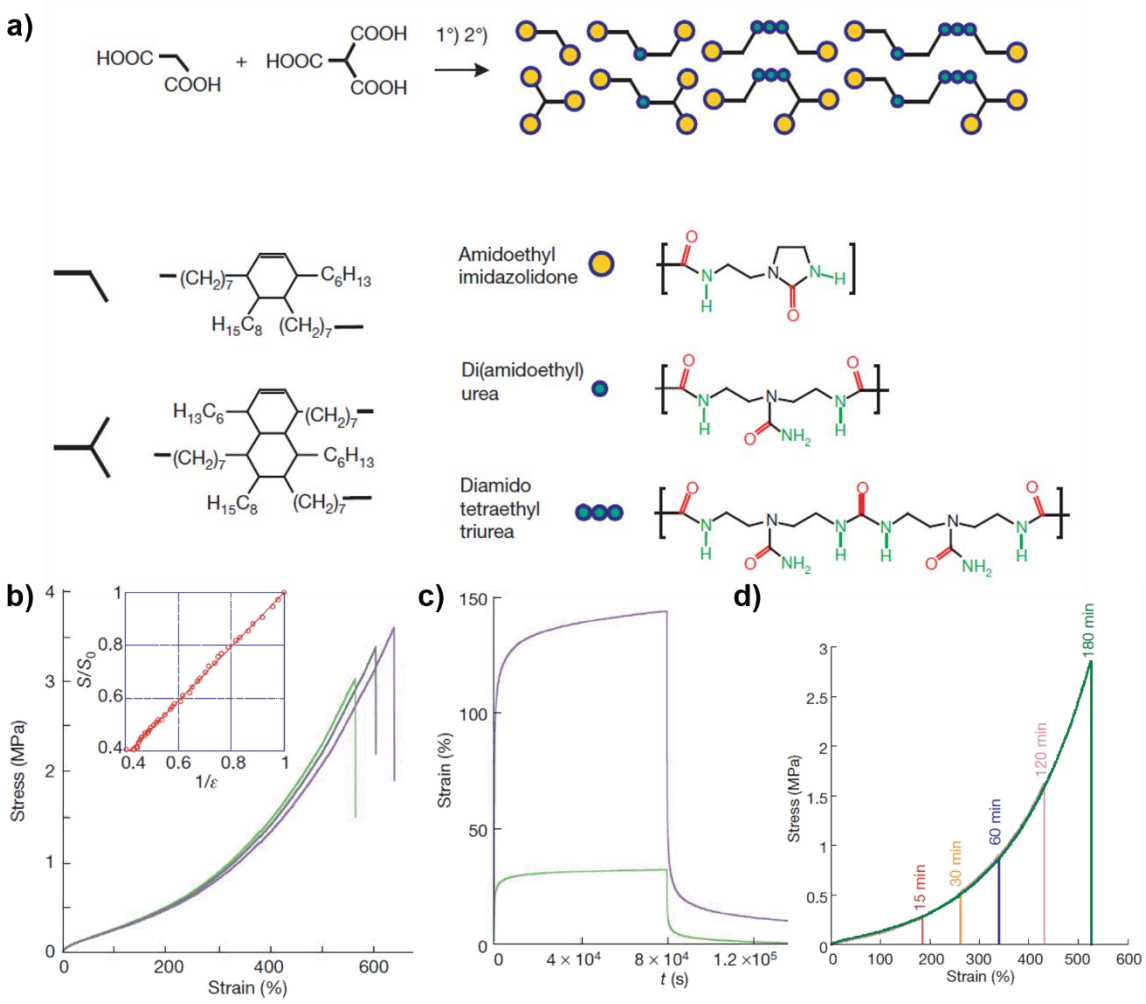

Figure 1-15 a) Network supramolecular polymer based on a mixture of tritopic and ditopic monomers. b) Stress strain curve for the plasticized network. c) Creep experiment for plasticized network with an applied stress of 5000 Pa (green) and 20000 Pa (purple). d) Stress strain curve after healing. Vertical lines represent strain at break after the designated healing time. Images reproduced with permission from reference 49.

The material was able to elongate to a maximum strain of 500% at break. Furthermore, the network BSP was able to return to its original dimension even after a strain of 300 %. The plasticized BSP was able to self-heal by holding the pieces together at 20 °C. As shown in Figure 1-15c, even after holding the pieces together for only fifteen minutes the sample could be deformed almost 200 %. After 180 minutes of contact time, the material healed to its original strength. The self-healing was attributed to the dissociated end-groups that could easily re-associate when the pieces were brought back into contact.[49] This was achieved thanks to the dynamics of the non-covalent interactions as well as the small size of the oligomers forming the network since they had better mobility than traditional polymers.[49]

A network main chain BSP with excellent functionality was reported by Weder *et al.*[61] This network BSP was based on a tritopic monomer which was functionalized with three UPy end-groups (Figure 1-16a). The monomers could be trapped in the amorphous network glass due to the high concentration of UPy end-groups and cross-linked nature of the network, which locked the monomers in the bound state.[61] These characteristics hindered molecular mobility thereby significantly reducing the tendency of the monomer to crystallize.[61] During the first heating cycle, this material displayed an endotherm attributed to the melting of crystalline regions (Figure 1-16b). After melting, powder X-ray diffraction (PXRD) showed only diffuse diffraction and subsequent heating and cooling cycles showed no recrystallization or cold crystallization. In addition, a glass transition was observed at approximately 100 °C.

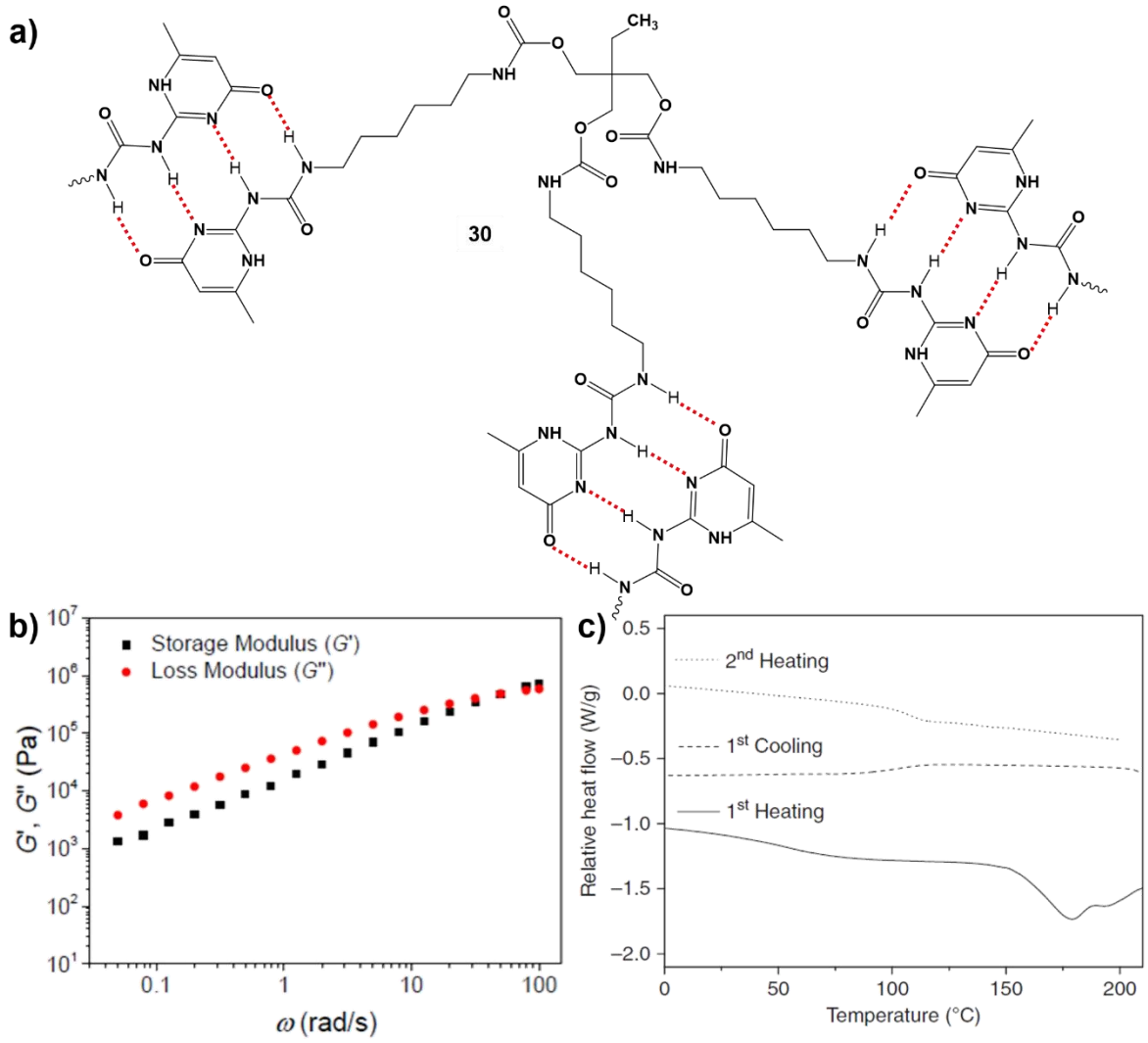

Figure 1-16 a) Complementary hydrogen bonding between UPy groups of compound **30**. b) Dynamic oscillatory experiments for compound **30** at 150 °C. c) DSC thermograms for compound **30**. Images b and c reproduced with permission from reference 61.

The material could be melt processed in a mould by heating to 200 °C and then cooling to room temperature. Compression moulding at 145 °C (5 tons, 5 s) resulted in self-supporting films which could be tested by dynamic mechanical analysis (DMA). DMA demonstrated that the material displayed a glassy state with a modulus of 3.6 GPa, up to 125 °C. Rheology experiments at 150 °C, showed that G' and G'' had a frequency dependence inferring polymer viscoelastic behaviour (Figure 1-16c). G' and G'' decreased upon heating suggesting that as

temperature increased the equilibrium was shifted to the unassociated state. As the sample was heated through the glass transition, the dynamic moduli (G' and G'') decreased. However, the network adhesion increased above T_g, which revealed that the UPy associations did not "switch off" above T_g.[61] Instead, the equilibrium between bound and unbound states shifted towards the unbound state.[61] The material displayed interesting stimuli-responsive behaviour. When exposed to UV light, the UPy groups generated heat locally, causing the monomers to shift to unbound states.[61] This caused de-bonding (in the event the material was used as a glue) and self-healing. The novelty of this material was that it was stiffer than any previously reported supramolecular polymer and was able to heal extremely fast. The triptopic UPy design proved extremely successful in preventing crystallization and imparting polymeric properties such as a glass transition, ability to form self-supporting films and frequency dependent G' and G''. The material displayed optical stimuli-responsiveness due to the generation of heat by UPy end groups when exposed to UV light.

In summary, BSP from small molecules are challenging to research, but have considerable potential as functional materials. BSP from small molecules typically require a cycle of heating to provide the monomers with the mobility to associate into the chain. Consequently, the key challenge associated with BSP from small molecules is preventing crystallization during cooling and subsequent reheating. Crystallization can be prevented by using strong cooperative intermolecular interactions to sequester the monomers into the chains. Another approach is to incorporate bulky substituents in the monomers. Furthermore, the overall symmetry of the monomer has been shown to have a significant role in preventing crystallization. The steric effect (i.e. bulkiness) and cross-linked nature of network main chain BSP significantly increases the stability of the resulting material. Consequently, network main

chain BSP often display superior mechanical behaviour as compared to linear main chain BSP. Successful monomer design requires special attention not only to the intermolecular interactions and mobility of the monomer, but geometry as well. Due to the complexities of monomer design, monomers have been typically developed from previously well-established intermolecular binding motifs (such as UPy, thymine and adenine). Consequently, innovation of new monomers based on novel binding motifs is almost non-existent, because of the lack of understanding of how intermolecular interactions in bulk work to create packing motifs. To overcome this barrier, techniques which provide direct insight into the solid-state packing motifs of molecules, such as crystal engineering, need to be employed in monomer design.

1.4 Crystal Engineering

Supramolecular chemistry involves the study of molecular assemblies and the intermolecular interactions which hold them together. The field of supramolecular chemistry has grown to involve the self-assembly or self-organization of molecules into larger arrays or structures through self-recognition.[88] Crystallization of organic compounds is a self-assembly process, which involves the self-organization of molecules through non-covalent interactions into large extended arrays.[89] The resulting molecular crystals are considered to be perfect "supermolecules" since they are the product of the self-recognition of many molecules organized by their intermolecular interactions.[90-91] Analysis of the single crystal structures can then provide valuable information about how the intermolecular interactions between molecules direct their self-assembly into the final solid-state structure.[92] This is accomplished by careful consideration of intermolecular distances and angles between adjacent molecules or by computational methods.[93] Thus crystal engineering is described as the study and understanding of intermolecular interactions for the purpose of bottom-up assembly of solid

state structures by the selection of the appropriate molecular building blocks.[94-95] Therefore, a chief goal of crystal engineering is to identify the intermolecular interaction(s) or "supramolecular synthon", which links the molecules in the single crystal structure together, so that suitable molecular building blocks can be selected.[92, 95]

Spectroscopic techniques are effective at identifying a variety of intermolecular interactions in solution and the solid state. As highlighted in the previous section, a variety of spectroscopic techniques such as FTIR, NMR and UV-Vis are routinely used to identify intermolecular interactions in solution and the solid state. However, spectroscopic techniques often struggle to detect "weak" interactions, such as C—H---O hydrogen bonding, especially in the solid state.[96] X-ray diffraction is one of the most reliable methods to obtain direct information about the intermolecular interactions in the solid state and is commonly used to confirm the intermolecular bonding motifs of molecules.[97] The chief difficulty of crystal engineering is obtaining suitable single crystals for X-ray diffraction.[97] Nevertheless, crystal engineering has elucidated how intermolecular interactions direct the organization of molecules in the solid state.[98]

1.4.1 Weak Hydrogen Bonding

Hydrogen bonding has been recognized as perhaps the most important and useful intermolecular interaction, since it plays a critical role in almost every biological process.[96] Thanks to the strength and directionality of the hydrogen bond, it is a useful synthon to direct supramolecular assemblies.[96] As shown in Figure 1-17a, the hydrogen bond consists of a donor referred to as X—H and an acceptor A—Y.[96] As defined by Steiner and Saenger, the hydrogen bond is "any cohesive interaction X—H---A where hydrogen carries a positive and A carries a negative (partial or full) charge and the charge on X is more negative than on H."[99] Due to

the long range nature of electrostatic interactions, it is possible for hydrogen bonding to be bifurcated or trifurcated as shown in Figure 1-17b.

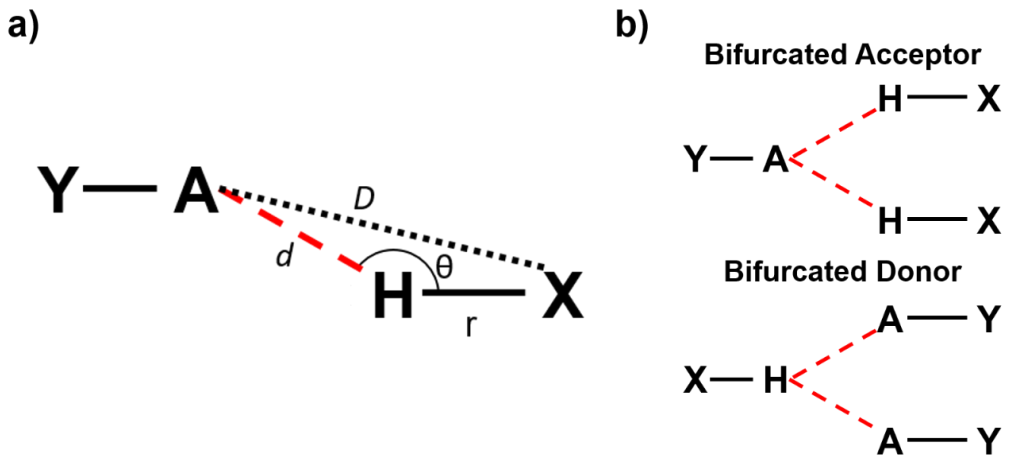

Figure 1-17 a) Structure of hydrogen bonding between a proton donor (X--H) and an acceptor (A--Y). The hydrogen bond is described in terms of the distance between hydrogen and acceptor *d* (bond distance), the donor hydrogen bond length *r*, θ the donor angle, and *D* the distance between acceptor and donor. b) Two structures of bifurcated hydrogen bonding.

The hydrogen bond can be described in terms of the distance between hydrogen and acceptor *d* (bond distance), the donor hydrogen bond length *r*, the donor angle θ, and the distance between acceptor and donor *D*.[96, 100] Thanks to crystal engineering, "weak" hydrogen bonding, such as C—H---O, began to gain widespread acceptance.[101-105] The use of distance cut offs is generally discouraged;[100-101] however, the length of C—H---O hydrogen bonds generally lies within $2.0 < d < 3.0$ Å or $3.0 < D < 4.0$ Å.[96, 100, 106-109] In C—H---O hydrogen bonds, the donor acidity strongly influences linearity. The more acidic the donor C—H is, the more the hydrogen bond angle tends to approach 180°.[107-109] However, weaker C—H---O hydrogen bonds are easily distorted and have bond angles within $110° < \theta < 180°$.[96, 104-105, 110] Like other hydrogen bonds, C—H---O hydrogen bonds are cooperative, meaning the energy

of an array of hydrogen bonds is greater than the sum of the individual bonds.[96] Recently it was demonstrated that the square-planar amphiphilic Pd(II) compound **31** (Figure 1-18a) is able to self-assemble into supramolecular polymer chains *via* C—H---O in solution, which could form hydrogels in water after ageing for two weeks (Figure 1-18b).[111-112]

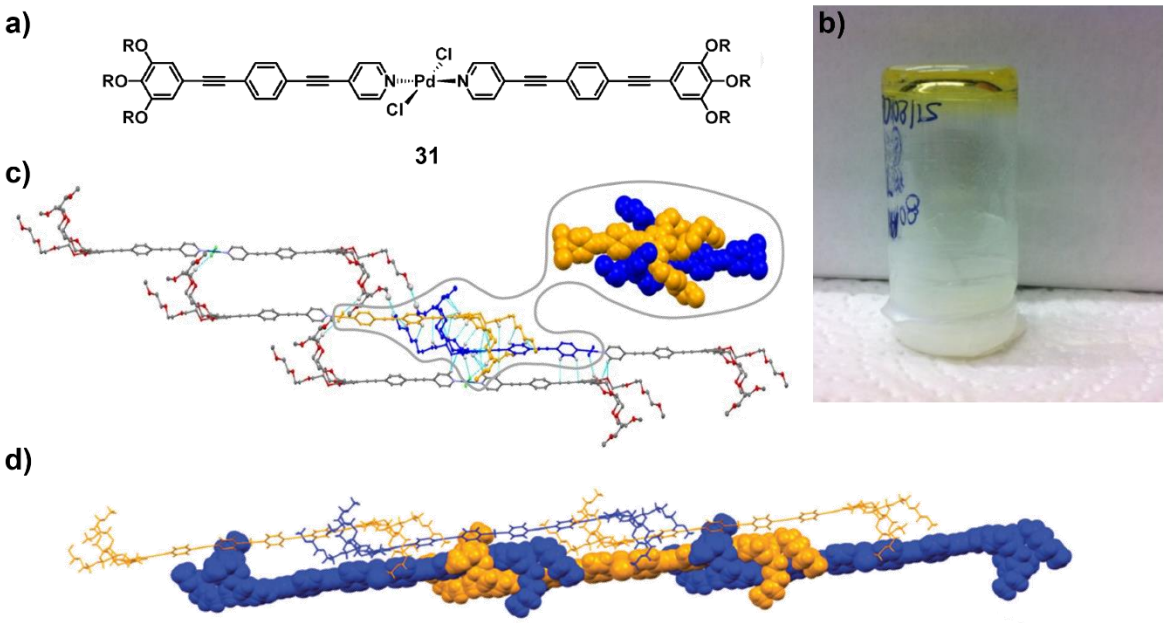

Figure 1-18 a) Square planar palladium compound **31**. b) Hydrogel formed after ageing for two weeks. c) Structure of compound **31** in the solid-state. Analysis of short contacts (drawn in light blue) reveals that the monomers form a "hand-shake" embrace driven by C—H---O interactions. d) Chain structure formed by compound **31** generated by repeating hand-shake embraces. Images reproduced with permission from reference 111.

Single crystal X-ray crystallography of **31** revealed that the packing of the palladium complex was driven by multiple C—H---O interactions (Figure 1-18c, d).[111-112] Consequently, compound **31** packs in a slipped fashion along the long axis of the molecule, resulting in a one dimensional chain structure formed by "hand-shake" embraces induced by C—H---O interactions and assisted by both aromatic interactions and C—H---Cl interactions (Figure 1-18c,d).[111-112] This progress highlights the ability of cooperative C—H---O hydrogen bonds

to form and stabilize chain structures in solutions. Despite this important step forward, the use of C—H---O hydrogen bonding to form a bulk supramolecular polymer remains unexplored.

1.4.2 Aromatic Interactions and Embraces

There are two general types of aromatic interactions that depend on the geometry of the interactions: offset face-to-face (OFF) interactions (Figure 1-19a) where the dihedral angle, α, between ring planes is 0° and edge-to-face (EF) interactions (Figure 1-19b) where α = 90°.[113-116] In addition, there are a variety of intermediate geometries, which arise from different ring tilts (0° < α < 90°) or offset between rings (Figure 1-19c).[113-116]

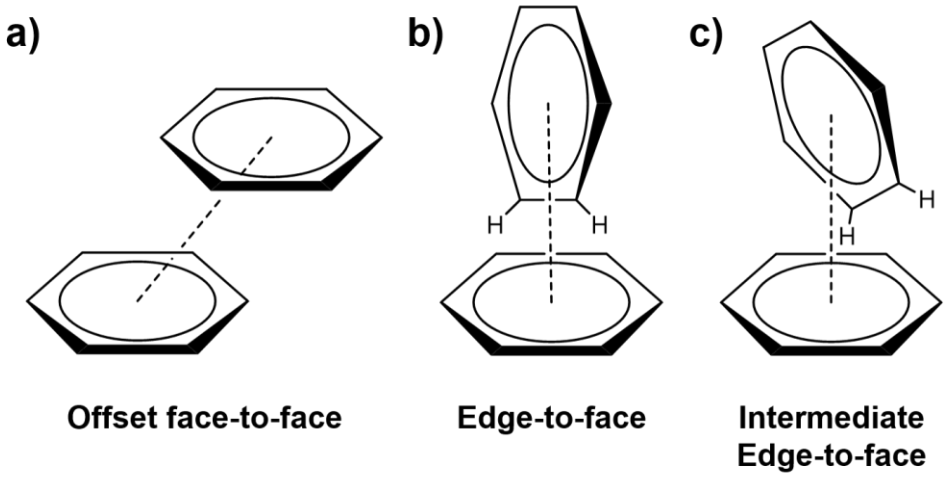

Figure 1-19 a) Geometry of offset face-to-face interaction (α = 0°) b) Geometry of edge-to-face interaction (α = 90°) c) Geometry of intermediate edge-to-face geometry where dihedral angle between rings is not perpendicular. (0° < α < 90°).

EF interactions can be considered a kind of weak hydrogen bond between the partially positive hydrogens of one aromatic ring and the electron rich π cloud of another ring.[114] The nature of the OFF interactions remains a matter of debate. One model proposed by Sanders and Hunter suggests that OFF interactions can be regarded as the attraction between an electron rich π cloud and the positively charged σ skeleton of another ring.[114, 116] Other work suggests that

London dispersion forces may play a more important role than the electrostatic nature of the interactions.[117] Nevertheless, these interactions can be identified in solid-state structures by calculating the distance between ring centroids and the dihedral angle between ring planes.[118]

Aromatic interactions play an important role in the organization of molecules in the solid state.[119] In particular, when molecules have multiple aryl groups, multiple OFF and EF interactions can work concertedly to organize two or more molecules into embracing motifs.[120-121] The term "embrace" refers to three primary attributes of these interactions: the involvement of two or more phenyl groups from each molecule involved in the interactions, the geometric cooperativity, and the strong mutual attraction.[121] Of particular interest are the embracing motifs created by molecules containing a propeller arrangement of three phenyl rings such as metal complexes of triphenylphosphine (PPh_3) or compounds containing the Ph_4P^+ cations.[120-121] In these systems, there are three common embracing motifs, which are described according to the type and number of aromatic interactions involved (see Figure 1-20).[120-121] The six-fold phenyl embrace (6PE) consists of three phenyl rings from each molecule interacting through six EF interactions (EF_6).[122-123] The parallel four-fold phenyl embrace P4PE involves two phenyl rings from each molecule interacting through one OFF interaction and two EF interactions OFF(EF_2).[124] In contrast, the orthogonal four-fold phenyl embrace O4PE involves two phenyl rings from each molecule interacting through 4 EF interactions (EF_4).[124]

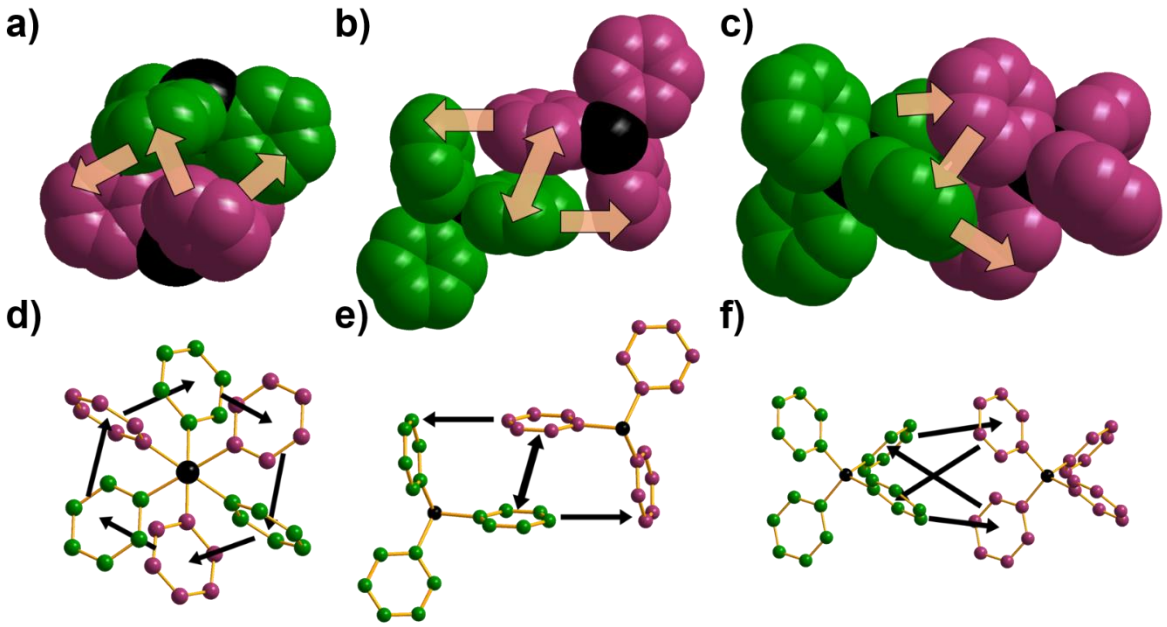

Figure 1-20 a) Spacefill representation of a six-fold phenyl embrace formed by six EF interactions between 2 $XPPh_3$ complexes. Three EF interactions are obscured. b) Spacefill representation of a parallel four-fold phenyl embrace formed by one OFF interaction and 2 EF interactions. c) Spacefill representation of an orthogonal four-fold phenyl embrace formed by 4 EF interactions. One EF interaction obscured. d) Top down view of a six-fold phenyl embrace e) Side view of a parallel four-fold phenyl embrace. f) Side view of a parallel four-fold phenyl embrace. Hydrogens have been omitted for clarity.

These embraces are quite strong; for example the 6PE embrace (EF_6) between two uncharged XPh_3 molecules (X = i.e. P) has an attractive energy of 13 kcal/mol.[125] In addition, O4PE and P4PE embraces can have attractive energies up to 8 kcal/mol.[120] The interaction energy of these embraces are comparable to some hydrogen bonds.[96] These systems are of interest to the field of SP because it has been shown that these bimolecular embracing motifs can interact with each other and generate linear chains of repeating embraces in crystalline solids.[120-121] In particular, a single compound can form chains which adopt a variety of morphologies. For example, Ph_4P^+ cations can form many chain morphologies, which include single columnar chains (Figure 1-21a,b) and ladder chains (Figure 1-21c,d).[120] In ladder chains,

the rails or edges of the ladder are comprised of O4PEs and the rungs are comprised of P4PE (Figure 1-21c, d) which are approximately orthogonal to the edges of the ladder.[120, 126] In some instances, the rails of the ladders can be formed by embraces consisting of 3 EF interactions, because the overall cooperative integration of embracing motifs is considered to be more important than a local embracing motif.[120] These embracing motifs are not unique to Ph_4P^+ and columnar chains have also been observed in various tris(bipryidyl)metal complexes.[127] While these motifs are able to form chains in crystalline materials, their application to SP in solution is hindered by the difficulty in characterizing aryl embraces in solution.[121] Furthermore, the use of embracing motifs to form BSP has not been realized.

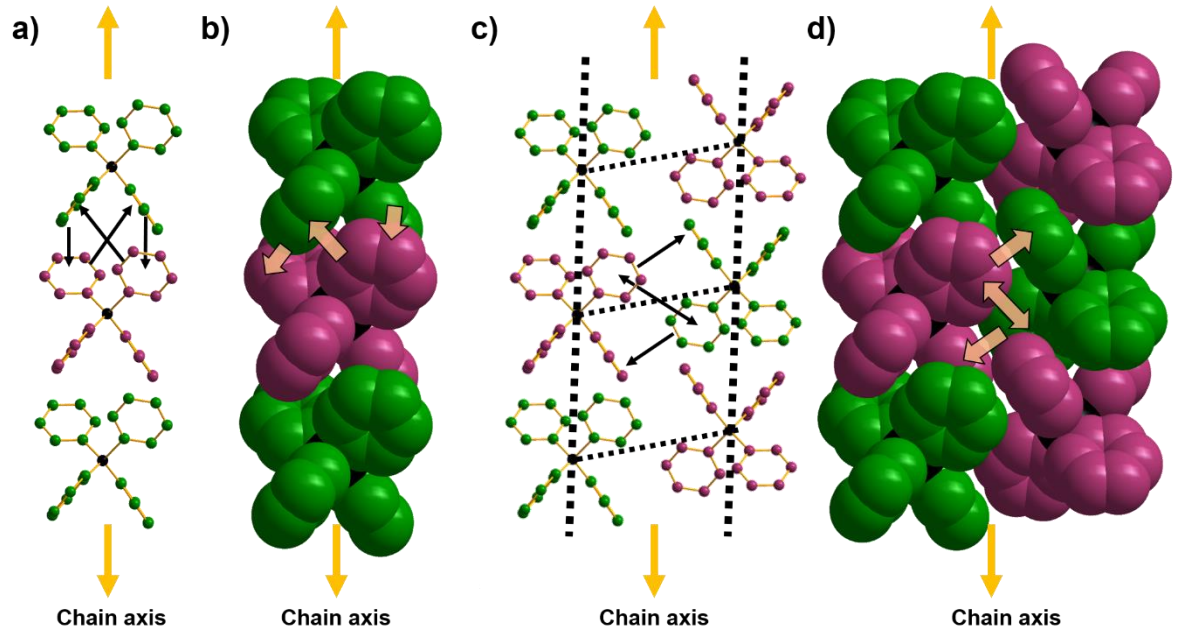

Figure 1-21 a) Columnar chain formed by repeating embraces O4PE. b) Spacefill representation of columnar chain structures by repeating embraces O4PE. c) Ladder chain formed by two antiparallel columnar chains (repeating O4PE embraces) connected at their edges by P4PE embraces. Rungs and rails of the ladder are outlined by a dotted black line between phosphorus atoms. d) Spacefill representation of the ladder chain structure. Yellow arrows represent chain long axis. Single headed arrows represent EF interactions and double headed arrows represent OFF interactions. Hydrogen atoms have been removed for clarity. Images were generated using the supramolecular structure (Cambridge Structural Database identifier: BITXUX) from reference 126.

1.5 Thesis Outline

The primary goal of this thesis was to investigate the bulk supramolecular polymerization of an organometallic monomer $CpFe(CO)PPh_3CO(CH_2)_5CH_3$ (FpC_6). Chapter 1 provides a literature review on both linear and network BSP prepared from small molecule monomers. In addition, Chapter 1 introduces several thesis related topics such as SP, crystal engineering and weak intermolecular interactions such as C—H---O hydrogen bonding and aromatic interactions. Chapter 2 discusses the synthesis and crystal engineering of FpC_6 and reports in

detail the intermolecular interactions and packing motifs of FpC_6 under different conditions. In Chapter 3, the bulk supramolecular polymerization of FpC_6 is investigated in detail. The identification of the chain structure in the amorphous material is discussed in detail. In addition, the thermal and mechanical behaviour are explored. Chapter 4 explores the effect of ageing and the influence of preparation conditions on the BSPs formed by FpC_6. Furthermore, Chapter 4 discusses a preliminary investigation into the bulk supramolecular polymerization of FpC_6 analogues (FpC_x, x = 5, 8 and 10). Finally, Chapter 5 provides a summary of the thesis and outlines suggested future work.

Chapter 2. Synthesis and Crystal Engineering

2.1 Overview

The first step in this thesis was to synthesize the organometallic small molecule $CpFe(CO)PPh_3CO(CH_2)_5CH_3$ (FpC_6). Once FpC_6 was successfully prepared, it was necessary to probe the capacity of FpC_6 to form chain structures in bulk. In order to do so, crystal engineering was performed by recrystallizing FpC_6 under different conditions. Five unique structural morphologies were obtained and thoroughly analyzed to understand intermolecular interactions and packing motifs of FpC_6.

In all solid-state structures, FpC_6 interacts through various synergistic combinations of embracing motifs (cooperative aromatic interactions) and C—H---O bonding. These interactions resulted in markedly different packing motifs between polymorphs that can be correlated to the influence of the recrystallization conditions (i.e. polarity of solvent, rate of solvent evaporation). In four out of five polymorphs, it was discovered that FpC_6 forms chain structures created by integrated repeating aromatic embrace motifs, demonstrating that FpC_6 has a propensity to form chain structures in the bulk. The structure of the chains was found to depend on the recrystallization conditions. Analysis reveals that the packing motifs and resulting chain structures were governed by the competition between the formation of aromatic embraces and the formation of C—H---O hydrogen bonding. When hydrogen bonding was disrupted, chains were obtained which did not contain any hydrogen bonds and were formed entirely of integrated aromatic embracing motifs. Furthermore, the FpC_6 molecules were organized to maximize aromatic interactions. Using non-polar recrystallization conditions, chains were obtained that contained both hydrogen bonding and integrated aromatic motifs. In addition, the packing of the FpC_6 molecules was influenced by considering both hydrogen

bonding and aromatic embraces whose balance was affected by the solvent evaporation rate. If the solvent evaporation rate was fast, the FpC_6 molecules tended to maximize aromatic interactions; however, if the evaporation rate was slow, the FpC_6 molecules packed to optimize the C—H---O hydrogen bonding. This work provided the fundamental knowledge required for the bulk supramolecular polymerization of FpC_6 discussed in later chapters.

2.2 Introduction

A unique feature of BSPs is that their dynamic backbone can reversibly lengthen or shorten.[1] To enhance this dynamic behaviour, it is desirable to construct the backbone using small molecules and weak intermolecular interactions. However, incorporating weak intermolecular interactions reduces chain stability, which can lead to crystallization.[69, 77, 83] The general strategy to improve chain stability is to use multiple strong non-covalent interactions,[2] but this is not always successful. While strong interactions may hold the chain together, they can also increase the tendency of small molecules to crystallize.[49] Successfully balancing the strength of intermolecular interactions against the tendency to crystallize is difficult. This is one of the key reasons why BSPs of small molecules, capable of forming glassy states and displaying viscoelasticity, are rare.[49-50, 61, 69, 77, 87, 128]

Despite the challenges, weak interactions have been incorporated into SPs and functional materials. Cooperative weak hydrogen bonding, such as C—H---O or C—H---π, along with aromatic interactions can generate SP in solution and preserve the chain structure in crystals.[35, 111-112] This discovery goes against the conventional intuition that weak hydrogen bonds, with low binding energy (< 4 kcal/mol) and limited bonding directionality,[96] are not useful for the synthesis of SPs. It is also surprising that even structural water can function as a co-monomer for a BSP with excellent adhesive properties.[129] However, in bulk, it is

challenging to elucidate the bonding motifs and chain structures. Consequently, crystal engineering is often carried out to establish the intermolecular interactions and packing motifs of monomers. Currently, there are no examples of BSPs formed *via* weak intermolecular interaction, due to the tendency of such systems to crystallize.[35, 111]

Previous research into BSPs from small molecules has focussed on the development of organic monomers and the use of metal-containing monomers remains unexplored. The incorporation of metal-containing monomers into solution SP has resulted in a wide variety of functional materials with useful properties such as self-healing, fluorescence, stimuli-responsive behaviour, and electro- and thermochromism. Therefore, it is worthwhile to investigate the incorporation of metal-containing monomers into BSP. Furthermore, the use of metal-containing monomers has great potential because of the unique metal coordination geometry, which can provide high functionality and different intermolecular interactions to a monomer resulting in novel complex chain structures.[130] Lastly, functional properties may be derived from the metal elements themselves (such as redox properties) and could impart additional functionality to the resulting materials. The organometallic monomer $CpFe(CO)PPh_3CO(CH_2)_5CH_3$ (FpC_6) was selected as a potential candidate for use as a monomer for BSP. Following successful synthesis, crystal engineering was required to elucidate the intermolecular interactions and packing motifs of FpC_6 to determine its propensity to form chains in bulk. The synthesis and crystal engineering of FpC_6 are discussed hereafter.

2.3 Materials

Potassium rod (99.5%, stored in mineral oil), sodium rod (99.9%), 1-bromohexane (98%), cyclopentadienyl iron (II) dicarbonyl dimer (99%), benzophenone (99%) and

potassium bromide (KBr) (≥ 99%) were purchased from Sigma-Aldrich. Triphenylphosphine (> 95%) was purchased from Tokyo Chemical Industries. Deuterated benzene (C_6D_6) (99.5 %) was obtained from Cambridge Isotope Laboratories Inc. All chemicals were used as received. Tetrahydrofuran (THF) was distilled over benzophenone and sodium under nitrogen to remove water.

2.4 Instrumentation

A Bruker-300 (300 MHz) spectrometer was used to record ^{1}H and ^{31}P NMR spectra at ambient temperature. ^{1}H NMR chemical shifts were reported relative to the residual C_6H_6 signal and ^{31}P NMR chemical shifts were referenced to an external standard sample of 85% H_3PO_4. FTIR spectra were acquired using a Bruker Tensor 27 spectrophotometer with a resolution of 1 cm^{-1}. Sample pellets were prepared by first mixing FpC_6 (2% by weight) with anhydrous KBr and compressing the mixture in a hydraulic sample press. X-ray data of single crystals was collected using Mo Kα radiation on a Bruker Kappa APEX II System with a CCD detector equipped with an OXFORD Cryosystems Cryostream 700 and an AD51 Dry air unit. Positive ion electrospray (ESI) experiments were performed with a ThermoFisher Scientific Q-Exactive hybrid quadrupole-orbitrap mass spectrometer.

2.5 Synthesis of Cyclopentadienyl Dicarbonyliron Potassium (FpK)

The synthesis of FpK was performed according to literature.[131] A 250 mL Schlenk flask was heated with a heat gun under vacuum to remove adsorbed water. Potassium benzophenone ketyl was prepared by stirring potassium (0.76 g, 19 mmol) and benzophenone (3.92 g, 22 mmol) in 50 mL of dry THF (see Scheme 1). The resulting dark blue solution was placed under a static nitrogen atmosphere and left to stir at room temperature for 12 h. Subsequently

cyclopentadienyl dicarbonyl iron dimer (4 g, 11 mmol) was added to the solution. The solution was stirred for 2 hours at room temperature under a nitrogen atmosphere. An orange/red precipitate formed and was allowed to settle. The supernatant was removed *via* cannula and the remaining THF was removed under vacuum. The resulting dark brown solid was washed with degassed toluene until the supernatant became clear. After removing the supernatant *via* cannula, the product was dried under vacuum yielding a bright orange powder (3.34 g, 87 %).

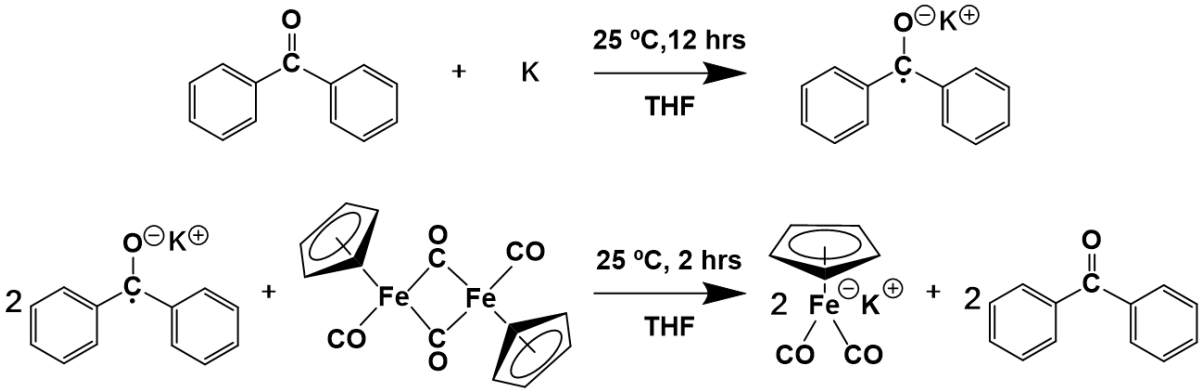

Scheme 1. Reaction scheme for the synthesis of FpK.

2.6 Synthesis of $CpFe(CO)PPh_3CO(CH_2)_5CH_3$ (FpC_6)

FpK (3.34 g, 15 mmol) was re-dissolved by adding dry THF (25 mL). 1-Bromohexane (2.33 mL, 17 mmol) was added dropwise to the FpK solution (see Scheme 2). The solution became olive green and a white precipitate was observed. The solution was left to stir for 1 hour at room temperature under a static nitrogen atmosphere. Subsequently, triphenylphosphine (PPh_3) (4.8 g, 18 mmol) was added to the solution and refluxed at 75 °C for 72 hours (see Scheme 2).

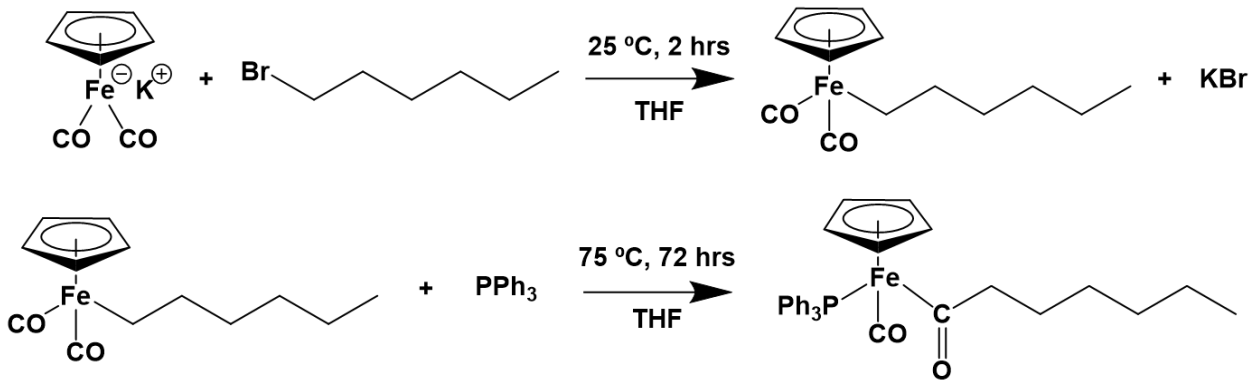

Scheme 2. Reaction scheme for the synthesis of FpC_6

THF was removed via rotary evaporation and a red-brown solid was obtained. The crude product was re-dissolved in a minimum of hexane yielding a turbid red/brown solution. This solution was then chromatographed on a silica gel column wet-packed using hexane. Once the crude product had been loaded onto the column using a syringe, the column was flushed with hexane and an orange band was observed during the flushing. This band was then eluted using a 1:1(v:v) mixture of hexane and dichloromethane. The band was collected and the solvent was removed using rotary evaporation. The red solid was placed under vacuum overnight (4.5g, 52%). The red solid was dissolved in deuterated benzene and characterized using ^{1}H and ^{31}P NMR with proton decoupling (see Figure 2-1). ^{1}H NMR (C_6D_6): 7.71 ppm (t, 6 H, meta $-C_6\mathbf{H}_5$), 6.95-7.09 ppm (b, 9H, ortho, para $-C_6\mathbf{H}_5$), 4.26 ppm (s, $C_5\mathbf{H}_5$), 3.00-3.15 ppm (m, 1H ,$-COC\mathbf{H}_2$), 2.84-2.97 ppm (m, 1H, $-COC\mathbf{H}_2$), 1.45-1.63 ppm (b, 1H, $-COCH_2C\mathbf{H}_2$), 1.30-1.43 ppm (b, 1H, $-COCH_2C\mathbf{H}_2$), 1.05-1.27 ppm (b, 6H, $-COCH_2CH_2(C\mathbf{H}_2)_3CH_3$, 0.86 ppm (t, 3H, $-COCH_2CH_2(CH_2)_3C\mathbf{H}_3$. ^{31}P NMR with proton decoupling (C_6D_6): 76.4 ppm. ESI-MS: 525.1653 m/z, which corresponds to $[M + H]^+$ with an elemental composition of $C_{31}H_{33}Fe\ O_2P$ ($\Delta m/z = 0.51$ mmu).

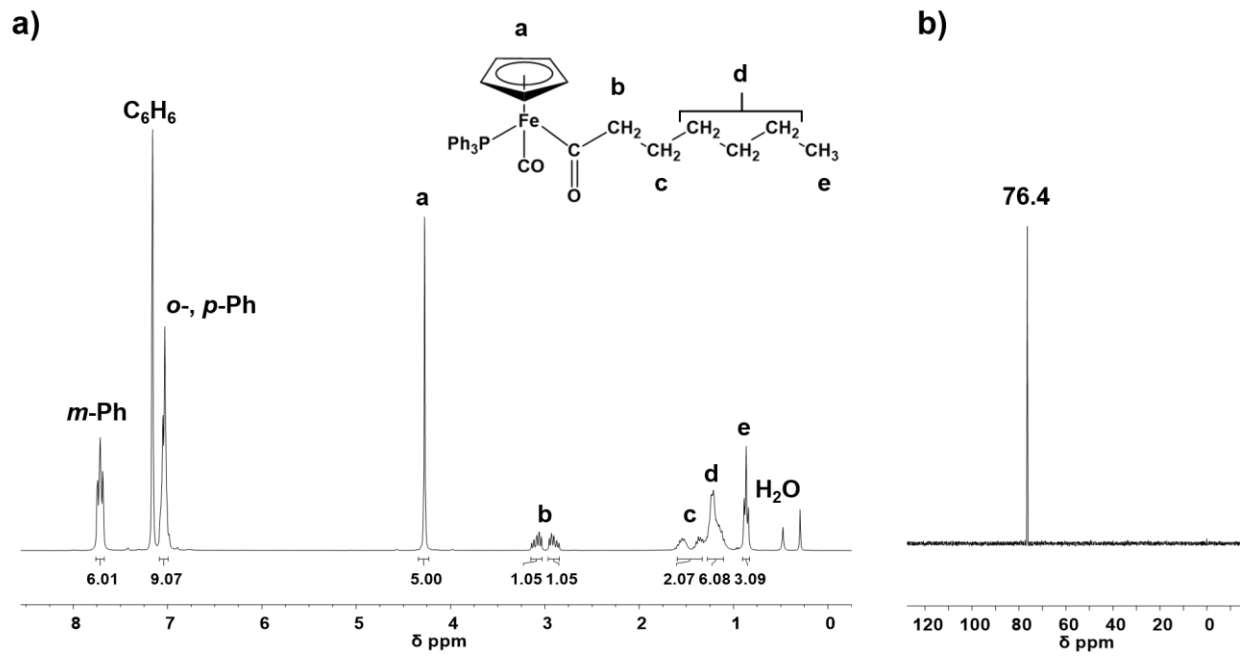

Figure 2-1 a) ^{1}H NMR and b) ^{31}P NMR spectra for FpC_6

2.7 Crystal Engineering of FpC_6

To investigate the intermolecular interactions of FpC_6 molecules, single crystals were prepared under various recrystallization conditions. The resulting structures were analyzed to probe the effect of external conditions on the balance between intermolecular interactions and the resulting changes in the packing motifs of FpC_6.

2.7.1 Recrystallization Conditions

Recrystallization conditions for supramolecular structure 1: A solution of FpC_6 in hexane (5 mg/mL) was prepared in a 20 mL scintillation vial and then transferred to a 12 x 75 mm culture tube. The culture tube was sealed using a plastic push cap lid and was then sealed with parafilm. The sample, after being sonicated for 90 minutes, was stored at room temperature and allowed to sit undisturbed in the dark. After a period of 31 days needle-like crystals were observed.

Recrystallization conditions for supramolecular structure 2: A solution of FpC6 in hexane (20 mg/mL) was prepared in a 20 mL scintillation vial and then transferred to a 12 x 75 mm culture tube. The culture tube was sealed using a plastic push cap lid and was then sealed with a Teflon film. This sample was placed in a fridge for 1 year. Alternatively, a solution of FpC_6 in pentane (10 mg/mL) was prepared in a 20 mL scintillation vial and transferred to a 10 mL push cap vial. The vial was sealed with a push cap lid and the sample was stored in the fridge. After 2 months crystals were observed.

Recrystallization conditions for supramolecular structure 3: A solution of FpC_6 in hexane (5 mg/mL) was prepared in a 20 mL scintillation vial and then transferred to a 12 x 75 mm culture tube. The culture tube was sealed using a plastic push cap lid. A needle was inserted into the push cap lid to increase the evaporation rate of the solvent. This sample was stored at room temperature. Crystals were observed within 2 weeks. The same supramolecular structure was obtained when a solution of FpC_6 in hexane (20 mg/mL) was prepared in a 20 mL scintillation vial and transferred to a NMR tube. The tube was seal with a push cap and stored at room temperature. Crystals were observed within 2 weeks.

Recrystallization conditions for supramolecular structure 4: A solution of FpC_6 in methanol (10 mg/mL) was prepared in a 20 mL scintillation vial. The vial was stored at room temperature and allowed to sit undisturbed in the dark. Plate-like crystals were observed in 4 days. This supramolecular structure was also obtained by recrystallization of a solution of FpC_6 (10 mg/mL) in a mixed solvent system (15 % water / 85 % ethanol) in a 10 mL push cap vial. The vial was sealed with a push cap and a needle was inserted into the cap. The crystals were obtained overnight.

Recrystallization conditions for supramolecular structure 5: A solution of FpC_6 (10 mg/mL) in mixed solvents (20% water / 80% ethanol) was prepared in a 20 mL scintillation vial and transferred to a 5 ml screw cap vial. This sample was stored in a drawer at room temperature. The crystals were observed after 1 month.

2.7.2 Supramolecular Structures of FpC_6

X-ray diffraction (XRD) of the resulting crystals revealed 5 unique supramolecular structures (see Table 2-1). While the crystal systems and space groups of the polymorphs are different, the structure of FpC_6 is similar in all polymorphs (see Figure 2-2). As shown in Figure 2-2, FpC_6 adopts a typical three-legged piano stool geometry. In addition, considerable disorder is observed in the alkyl chains due to the thermal displacement of the carbons in the chain.

Supramolecular structures **1** and **5** are missing a carbon from the alkyl chain giving the empirical formula $C_{30}H_{31}FeO_2P$. The missing CH_2 group is attributed to the poor quality of the single crystals and the flexibility of the alkyl chain. The crystals used to obtain crystal structures **1** and **5** were very thin (resulting in weak scattering) and had a significant amount of twinning. Furthermore, the thermal energy at room temperature generates considerable disorder in the alkyl chain which could not be resolved even by cooling to 200 K (see Figure 2-2). These two factors could obscure the electron density of the last carbon in the alkyl. The ESI mass spectrum of the FpC_6 used reveals a $[M + H]^+$ of 525.1653 consistent with the formula of $C_{31}H_{33}FeO_2P$. Consequently, supramolecular structures **1** and **5** were used to investigate the intermolecular interactions and packing motifs of FpC_6.

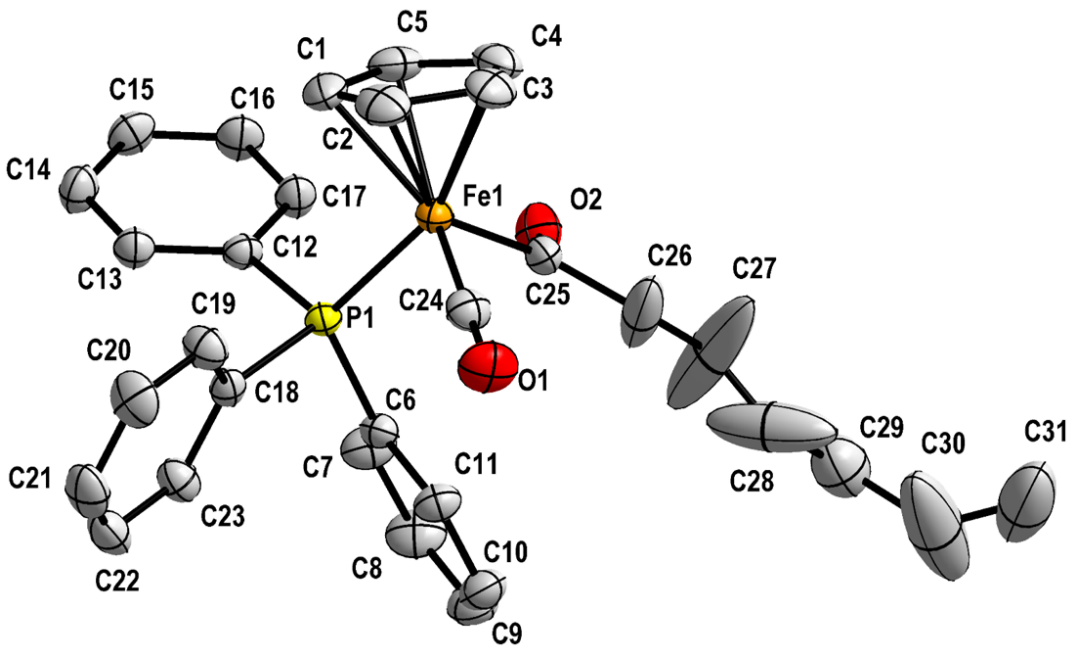

Figure 2-2 Supramolecular structure of FpC_6 (from supramolecular structure **4**) shown as thermal ellipsoids at a 50% probability level. Hydrogen atoms have been omitted for clarity.

Table 2-1 Summary of crystallographic data for supramolecular structures **1**-**5**

Supramolecular Structure	**1**	**2**	**3**	**4**	**5**
Empirical Formula	$C_{30}H_{31}FeO_2P$	$C_{31}H_{33}FeO_2P$	$C_{31}H_{33}FeO_2P$	$C_{31}H_{33}FeO_2P$	$C_{30}H_{31}FeO_2P$
Formula Weight (g/mol)	510.37	524.39	524.39	524.39	510.37
Temperature (K)	296(2)	296	200	200(2)	296
Wavelength (Å)	0.71073	0.71073	0.71073	0.71073	0.71073
Crystal System	Orthorhombic	Monoclinic	Monoclinic	Triclinic	Monoclinic
Space Group	***F**dd*2	***C***2/*c*	***P***2_1/*c*	$\mathbf{P\bar{1}}$	***P***2_1/*c*
a (Å)	41.3534(6)	46.1568(17)	11.5608(6)	9.2693(2)	9.3232(1)
b (Å)	64.6397(9)	8.1296(3)	22.2637(13)	9.4061(2)	33.6851(5)
c (Å)	8.13090(10)	31.9663(12)	22.6922(13)	15.4687(3)	16.8867(3)
α (°)	90	90	90	88.6025(8)	90
β (°)	90	109.024(2)	111.166(3)	87.6725(8)	91.5077(9)
γ (°)	90	90	90	80.3371(9)	90
Volume (Å^3)	21734.5(5)	11339.8(7)	5446.6(5)	1328.24(5)	5301.48(14)
Z	32	16	8	2	8
Calc. Density (g/cm^3)	1.248	1.229	1.279	1.311	1.279
Absorption Coefficient (mm^{-1})	0.637	0.613	0.638	0.654	0.653
F(000)	8576	4416	2208	552	2144
θ range for data collection	3.3 to 26.4°	3.0° to 26°	1.3° to 28°	1.3 to 26.4°	2.3° to 24.1°
Index Ranges *h*;*k*;*l*	−51,51;−80, 80; −10,10	−57,57;−10, 10; −39,39	−13,15;−29, 29; −26,29	−11,11; −11, 11; −19, 19	−10,10; −38, 38; −19,19
Reflections Collected	53776	11104	45195	39281	134597
Independent Reflections	10846	11104	13103	5430	8424
Completeness to θ = 25.242	0.994	0.998	0.998	0.999	0.944
Refinement method	Full-matrix least-squares on F^2	Full-matrix least-squares on F^2	Full-matrix least-squares on F^2	Full-matrix least-squares on F^2	Full-matrix least-squares on F^2
Data / restraints / parameters	10846 / 205 / 613	11104 / 225 / 601	13103 / 0 / 634	5430 / 104 / 316	8424 / 204 / 615
Goodness-of-fit on F^2	1.314	1.468	1.377	1.133	1.394
Final R indices [I>2σ(I)]	R_1 = 0.0466, wR_2 =0.0755	R_1 = 0.0683 wR_2 = 0.0961	R_1 = 0.0585 wR_2 = 0.1087	R_1 = 0.0558, wR_2 = 0.1123	R_1 = 0.0533 wR_2 = 0.1041
R indices (all data)	R_1 = 0.0813 wR_2 =0.0790	R_1 = 0.1436 wR_2 = 0.1034	R_1 = 0.1331 wR_2 = 0.1358	R_1 = 0.0588 wR_2 =0.1162	R_1 = 0.0811 wR_2 = 0.1119
Largest diff. peak and hole (e Å^{-3})	0.556, −0.211	0.468, −0.324	1.14, −0.615	1.637, −1.410	0.648, −0.551

2.7.3 Identification of Intermolecular Interactions and Packing Motifs of FpC_6

Potential interactions were identified by performing short contact analysis using both Platon[132] and Mercury[133-134] software packages. Subsequently, intermolecular interactions were identified based on the joint consideration of the bond distances and bond angles of potential interactions identified by short contact analysis. In the case of weak hydrogen bonding, short contacts were considered only if $d < 3.0$ Å and $120° \leq \theta \leq 180$.[96] Aromatic interactions were considered using similar criteria. In the case of offset face-to-face (OFF) π—π interactions, close ring interactions were only considered if $0° \leq \alpha \leq 5°$ and the centroid-to-centroid distance (C_d) ≤ 4.2 Å. Edge-to-face (EF) interactions between rings were considered if $55° \leq \alpha \leq 90°$ and $C_d \leq 5.5$ Å.[115, 135]

2.7.3.1 Supramolecular Structures 1 and 2

In supramolecular structures **1** and **2**, short contact analysis indicates that FpC_6 molecules interact through the same packing motifs and intermolecular interactions with only slightly different distances. In both structures, FpC_6 molecules are involved in a unique tetra-molecular embracing motif involving aromatic interactions from both Ph and Cp rings from four different FpC_6. This motif can be described as follows: (1) A bimolecular embrace between two FpC_6 molecules is formed *via* three EF interactions involving Cp and Ph rings as shown in Figure 2-3 a and b. The average distance between phosphorus atoms is 8.13 Å. (2) Two adjacent anti-parallel EF_3 bimolecular embraces are connected at their edges by an OFF interaction formed between Cp rings and two EF interactions between Cp and Ph rings ($OFF(EF_2)$) as shown in Figure 2-3 c and d.

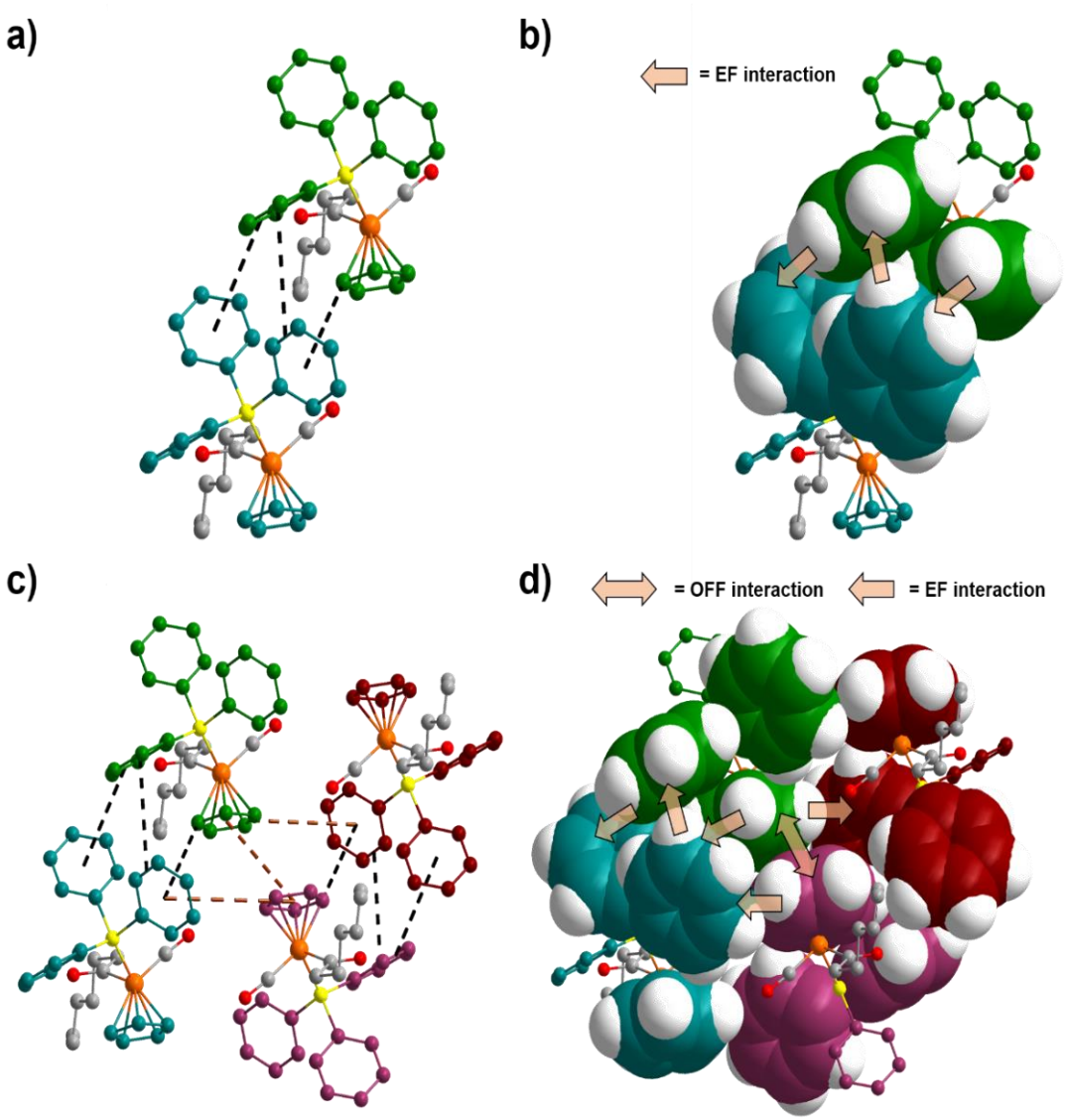

Figure 2-3 a) Bimolecular embrace formed by three EF interactions from aromatic groups from two different FpC_6 molecules (aromatic C atoms coloured green or blue). Hydrogen atoms have been omitted for clarity. b) Spacefill representation of FpC_6 bimolecular EF_3 embrace (aromatic C atoms coloured green or blue). Hydrogen atoms not involved in the aromatic embrace have been omitted for clarity. c) Final embracing motif OFF(EF_8) involving four different FpC_6 molecules (aromatic C atoms coloured green, blue, red and purple). The embrace involves two EF_3 embraces linked at their edges via an OFF interaction and two EF interactions. Hydrogen atoms have been omitted for clarity. d) Spacefill representation of OFF(EF_8) embrace between four different FpC6 molecules (aromatic C atoms coloured green, blue, red and purple). Three EF interactions are obscured. Hydrogen atoms not involved in aromatic embrace have been omitted for clarity.

Consequently, the embracing motif involving four FpC_6 molecules (shown in Figure 2-3a) is described as OFF(EF_8) and the interactions are summarized in Table 2-2. This embracing motif repeats by translation as shown in Figure 2-4a and b. Consequently, the repeating unit consists of four FpC_6 molecules in an OFF(EF_8) linked to another OFF(EF_8) *via* an OFF(EF_8) embrace as shown in Figure 2-4c and d.

Within the OFF(EF_8) embrace C—H---O hydrogen bonding is observed involving both the terminal carbonyl (*t*-CO) and the acyl carbonyl (*a*-CO) acting as acceptors for protons donated from Cp and Ph rings (Figure 2-5a). In total there are six C—H---O hydrogen bonds within the OFF(EF_8) embrace (Figure 2-5a). As shown in Figure 2-4 and Figure 2-5, "ladder" chains are formed by the repetition of both the embracing OFF(EF_8) motif and hydrogens bonds via translation of the repeat unit (Figure 2-16a).

Viewing supramolecular structure **1** in the (*b a*) plane, reveals that the unit cell consists of sixteen chain cross-sections (Figure 2-6a) and chains extend in the *c* crystallographic directions (Figure 2-5c). Conversely, viewing supramolecular structure **2** in the (*a c*) plane, reveals that the unit cell consists of eight chain cross-sections (Figure 2-6b) and the chains extend in the *b* crystallographic direction (Figure 2-5d). In both crystal structures **1** and **2**, the chains are aligned parallel to one another along their long axis. Adjacent chains are linked by two C—H---O hydrogen bonds per repeat unit and one EF interaction. It is noteworthy that the chains pack in the unit cell such that they are separated by regions or pockets of alkyl chains.

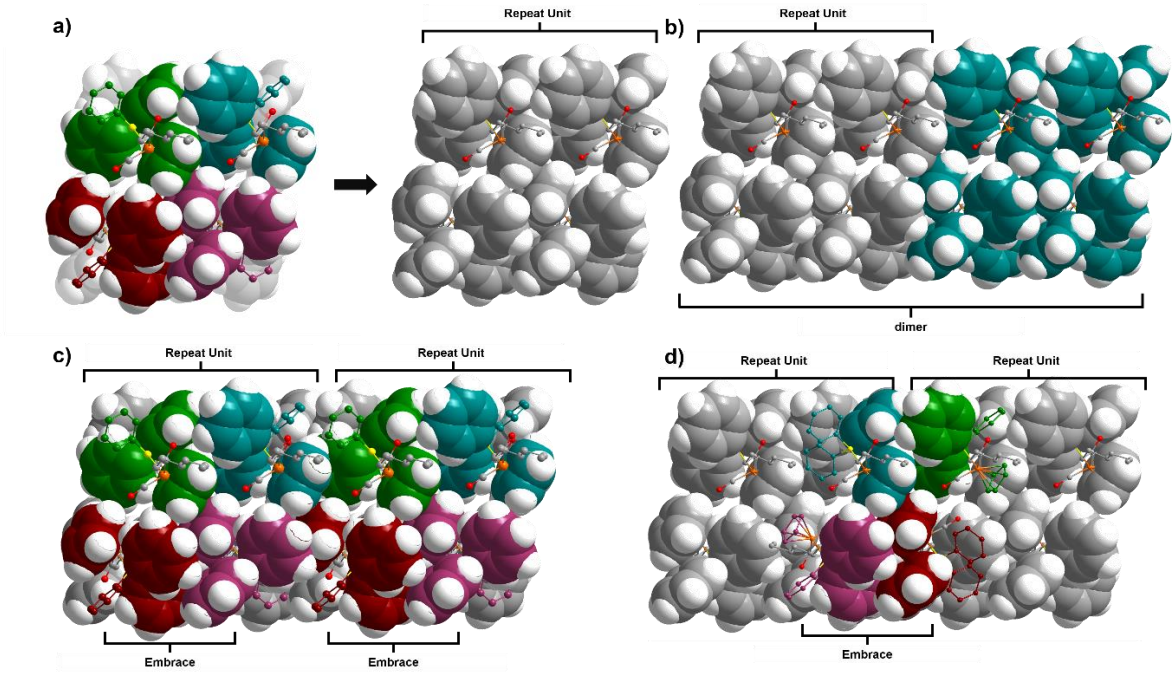

Figure 2-4 a) FpC_6 OFF(EF_8) embrace represented as a repeating unit of four FpC_6 molecules. b) Dimer formed by repeating unit. c) Representation of the OFF(EF_8) within each repeating unit in the dimer. d) Representation of the OFF(EF_8) embrace linking the repeating units.

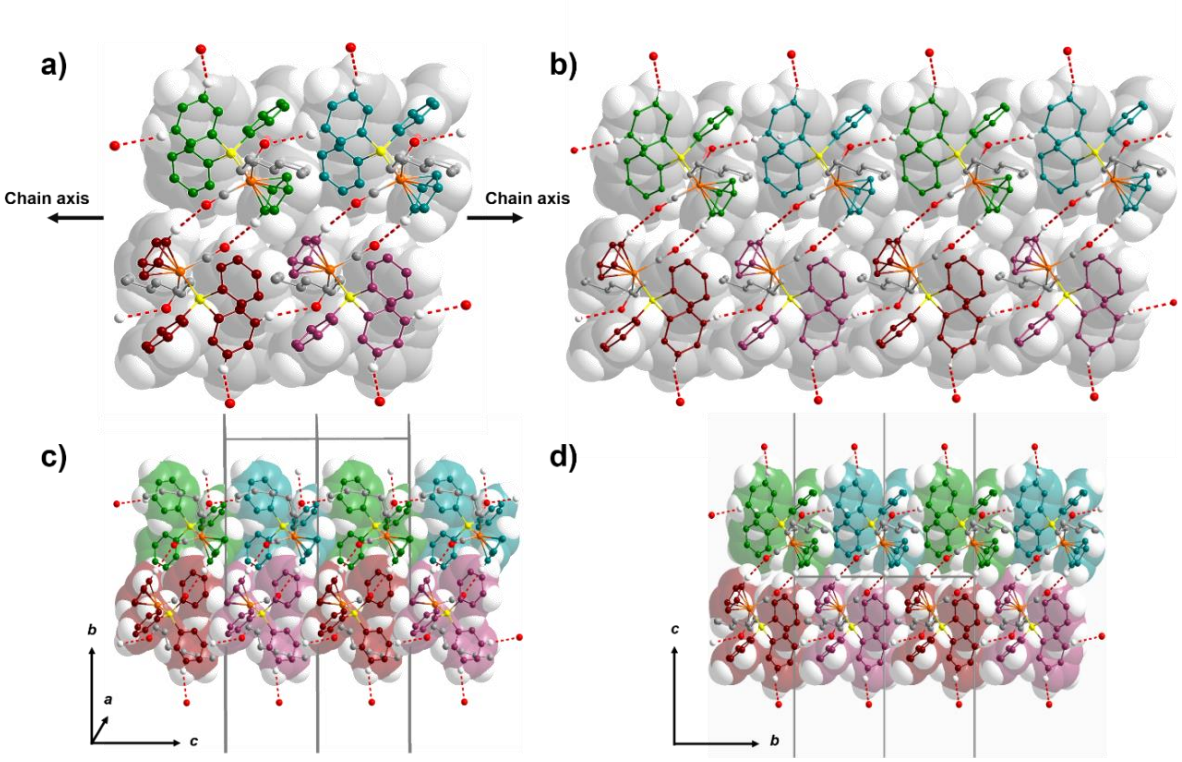

Figure 2-5 a) Hydrogen bonding with the repeating OFF(EF_8) embrace represented as red dashed lines. b) Extension of hydrogen bonding *via* translation of the repeat unit forming a duplex chain. c) Extension of the chain in the c direction in supramolecular structure **1** *via* translation of the OFF(EF_8) embrace. Unit cell edges shown by black lines. d) Extension of the chain in the b direction in supramolecular structure **2** *via* translation of the OFF(EF_8) embrace. Unit cell edges shown by black lines. Hydrogens not involved in hydrogen bonding have been omitted for clarity.

Ladder chains are typically observed for chains formed by phenyl embraces and are characterized according to the inter phosphorus distance between the rungs and rails of the ladder. In supramolecular structure **1**, the average P---P distance is 8.13 Å between rungs and 9.64 Å between rails. In supramolecular structure **2**, the average P---P distance is 8.13 Å between rungs and 9.54 Å between rails.

Table 2-2 Summary of aromatic interactions in supramolecular structures **1** and **2**.

Interaction	Average C_d (Å)		Average α (°)	
	1	**2**	**1**	**2**
OFF (Cp—Cp)	4	3.9	3	0
EF(Cp—Ph)	5.2	5.2	54	53
EF(Ph—Ph)	5.3	5.2	70	69

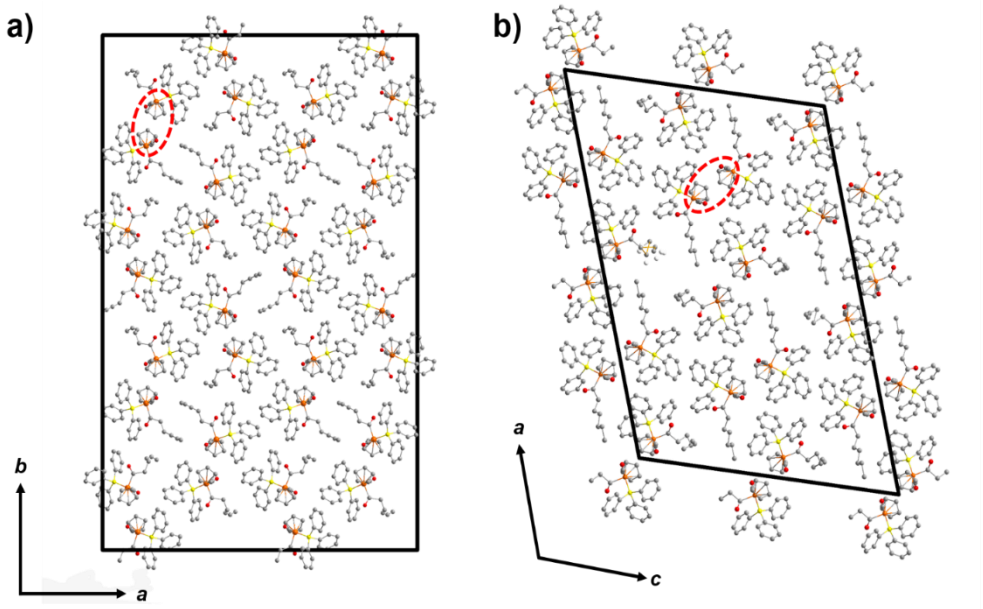

Figure 2-6 a) Projection of supramolecular structure **1** in the (*b a*) plane. Sixteen chain cross-sections can be observed. One chain cross-section circled in red. b) Projection of supramolecular structure **2** in the (*a c*) plane. Eight chain cross-sections can be observed. One chain cross-section circled in red. All hydrogens have been

2.7.3.2 Supramolecular Structure 3

Analysis of the short contacts in supramolecular structure **3** reveals that the FpC_6 molecules interact through a combination of hydrogen bonding and phenyl embrace motifs. In particular, the FpC_6 molecules are involved in a bimolecular embrace formed by three EF interactions (EF_3) (see Figure 2-7). The bimolecular embraces are connected at their edges to another bimolecular embrace *via* EF_3 interactions (Figure 2-8a). The bimolecular embraces form chains through a translational repetition of the molecules (Figure 2-8a) extending in the

a crystallographic direction (see Figure 2-9). The phosphorus atoms adopt a zig-zag arrangement (Figure 2-16b) and the average P---P distance is 7.7 Å. Within the chains, bifurcated C—H---O hydrogen bonding is observed occurring between *a*-CO and *t*-CO and protons donated from both Ph and Cp rings (Figure 2-8b and Table 2-6). Four hydrogens bonds are observed between the FpC_6 molecules involved in the chain (Figure 2-8a). The chains lie parallel to one another in the supramolecular structure and four chains are encompassed by the unit cell (see Figure 2-10a and b).

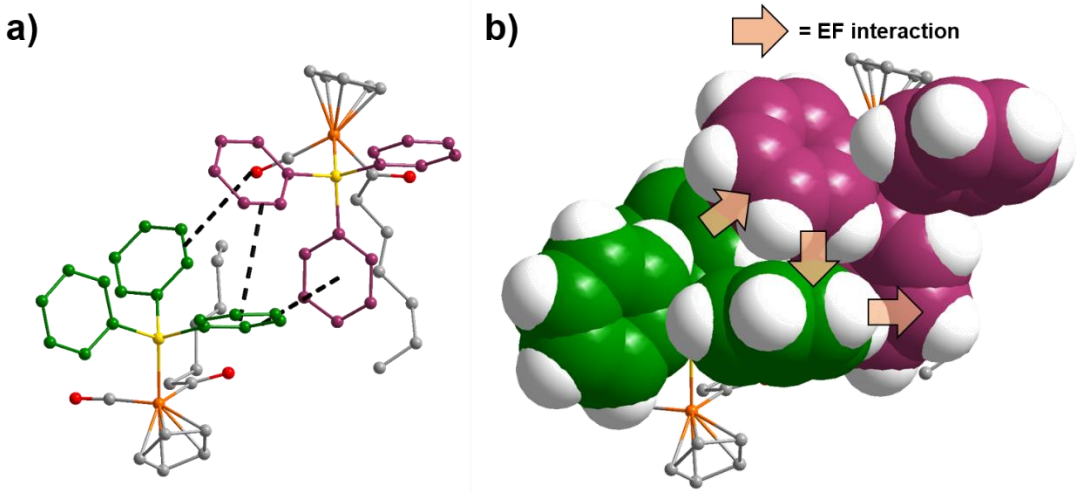

Figure 2-7 a) Phenyl embrace formed by three EF interactions between two PPh_3 groups from two different FpC_6 molecules (C atoms colour green, purple). Hydrogens removed for clarity. b) Spacefill representation of the phenyl embrace formed by three EF interactions between two PPh_3 groups from two different FpC_6 molecules (C atoms colour green, purple). Non-aromatic hydrogens removed for clarity.

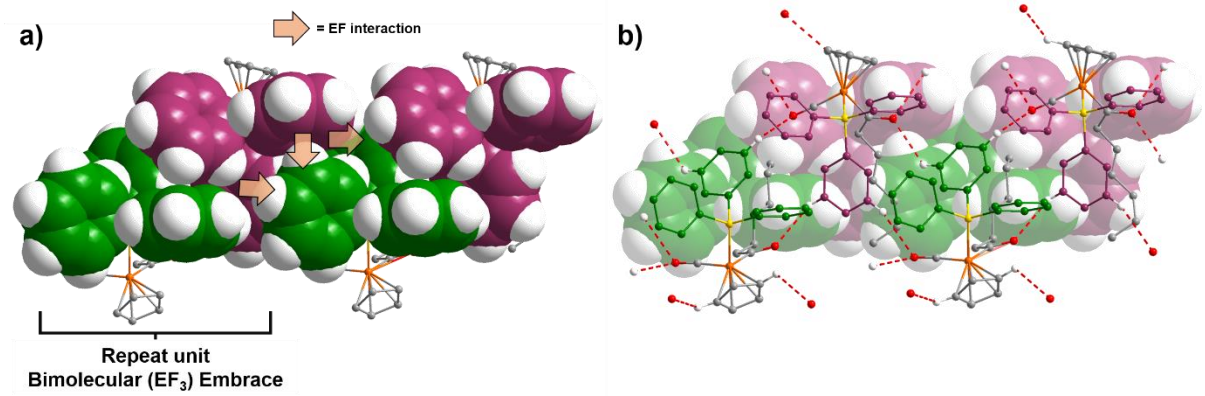

Figure 2-8 a) Extension of the bimolecular EF_3 embrace by translation. b) Hydrogen bonding within the chain formed by translating the EF_3 embrace. Hydrogen bonding is represented as dashed red lines.

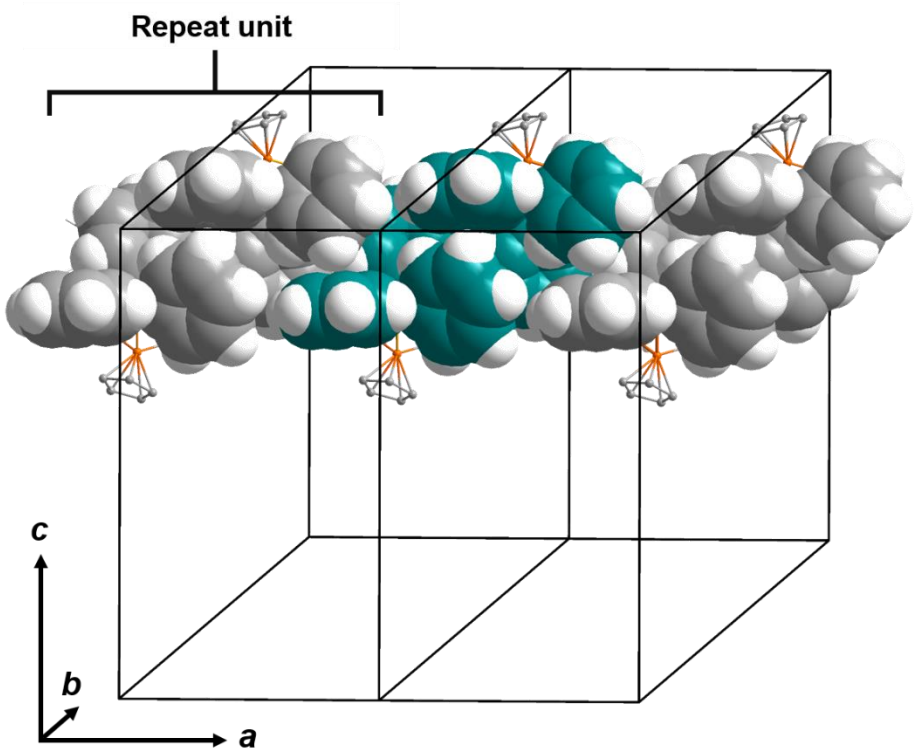

Figure 2-9 Extension of the chain in the *a* crystallographic direction

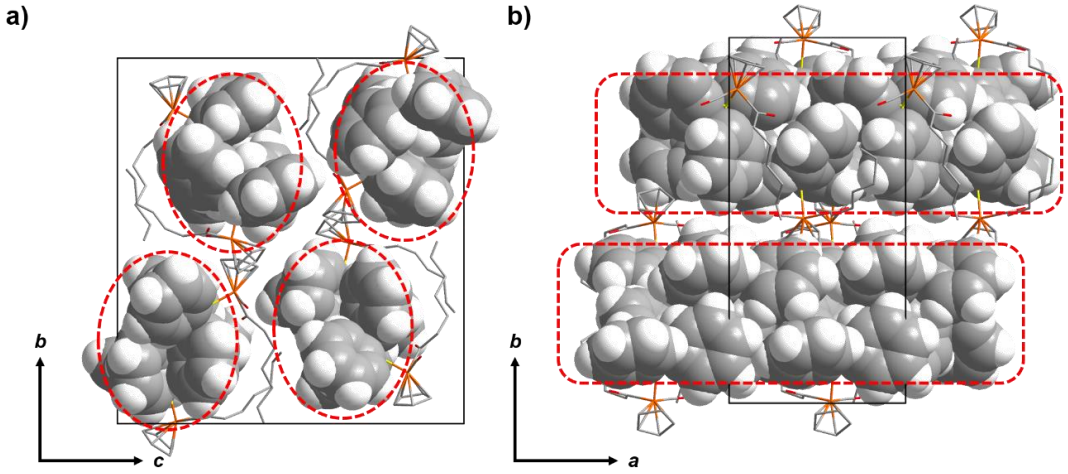

Figure 2-10 a) Projection of unit cell in the (*b c*) plane. Four chain cross-sections can be observed circled in red. b) Projection of unit cell in the (*b a*) plane. Two parallel chains can be observed outlined in orange. Non phenyl hydrogens have been omitted for clarity.

Table 2-3 Summary of aromatic interactions in supramolecular structure **3**.

Interaction	Average C_d (Å)	Average α (°)
EF_1 (Ph—Ph)	5.0	67

2.7.3.3 Supramolecular Structure 4

Analysis of supramolecular structure **4** reveals FpC_6 molecules interacting primarily through aromatic interactions. The unit cell consists of two FpC_6 molecules involved in a bimolecular embrace (see Figure 2-11) created through four EF interactions between both Ph and Cp (see

Table 2-4). The distance between phosphorus atoms in the bimolecular embrace is 7.14 Å. Extending the supramolecular structure in the *a* direction reveals that the bimolecular embrace is connected at its edges to another bimolecular embrace through one OFF interaction between Cp rings and two EF interactions between Cp and Ph rings (

Table 2-4 and Figure 2-12a). These interactions link the bimolecular embraces together and this pattern repeats in the *a* direction creating a chain of repeating embraces (Figure 2-12). Consequently, each FpC_6 molecule is involved in six EF interactions and one OFF interaction. The resulting chain structure forms a "firecracker ladder" and is formed by repeating bimolecular embraces connected by OFF(EF_2) (Figure 2-16c). The chains are then packed parallel to one another in the supramolecular structure. Despite being crystallized from a methanol solution (methanol is known to disrupt hydrogen bonding), a complementary C—H---O hydrogen bond involving *a*—CO group acceptor and hydrogen donated from a phenyl ring is observed in the *c* crystallographic direction (see Table 2-6). These hydrogen bonds extend between the chains and are located in a pocket consisting of alkyl and aryl substituents, suggesting that these hydrogen bonds arise due to the parallel packing of the chains.

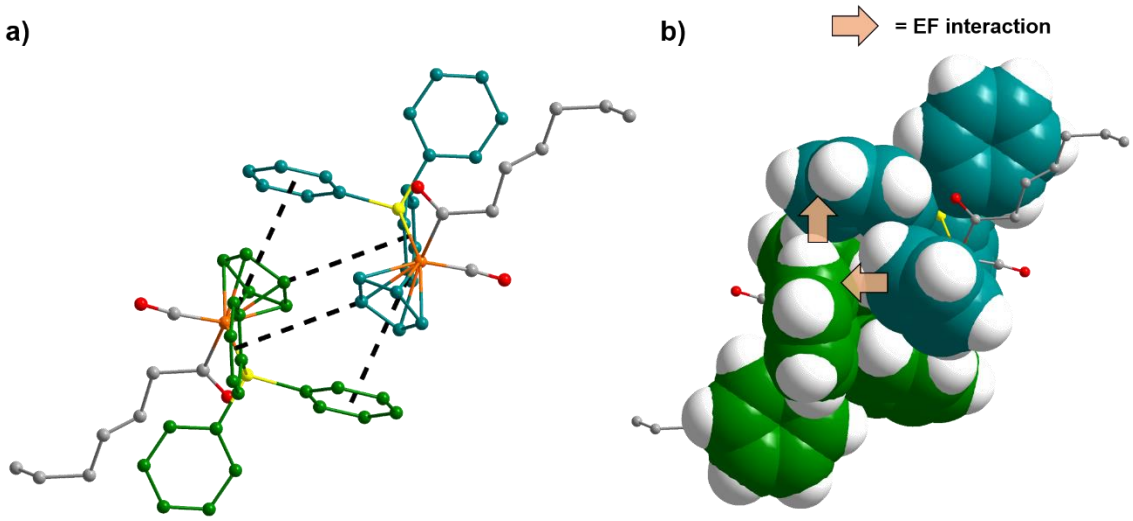

Figure 2-11 a) Bimolecular embrace formed by four EF interactions from aromatic groups from two different FpC_6 molecules (aromatic C atoms coloured green or blue). b) Spacefill representation of FpC_6EF_4 bimolecular embrace. Two EF interactions are obscured (aromatic C atoms coloured green or blue). Non-aromatic hydrogens have been removed for clarity.

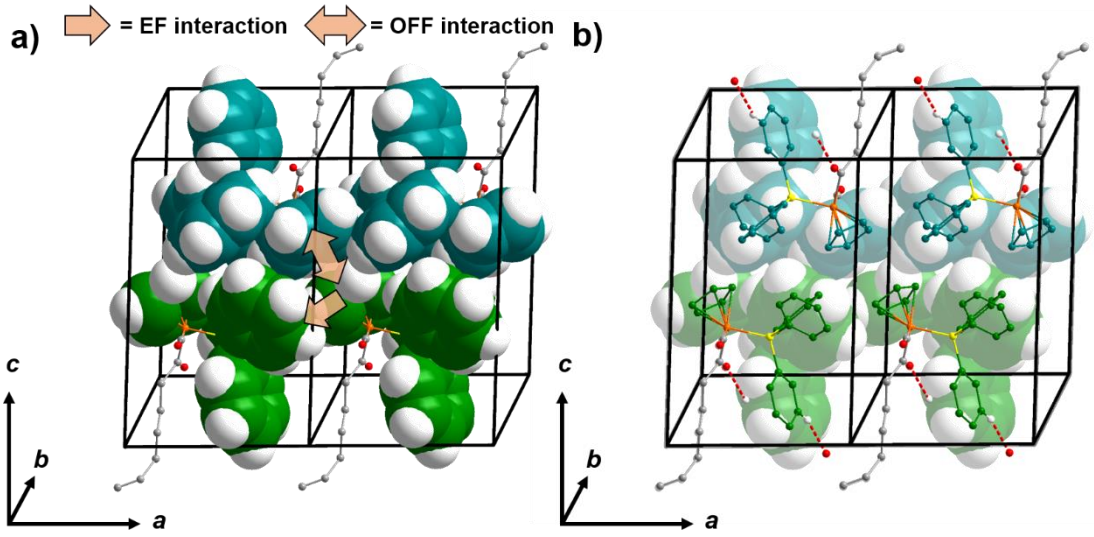

Figure 2-12 a) Extension of the FpC_6 EF_4 embraces through translation in the *a* crystallographic direction. Each embrace is connected to another *via* an OFF(EF_2) embrace (one EF interaction is obscured). Non-aromatic hydrogens have been removed for clarity. b) Hydrogen bonding within supramolecular structure **4**. No hydrogen bonds are observed within the embrace chain; however, hydrogen bonding extending between chains is observed. Hydrogens not involved in hydrogen bonding have been omitted for clarity.

Table 2-4 Summary of aromatic interactions in supramolecular structure **4**.

Interaction	Average C_d (Å)	Average α (°)
OFF(Cp—Cp)	4.2	0.0
EF(Ph—Ph)	5.2	81
EF(Cp—Ph)	5.2	59

2.7.3.4 Supramolecular Structure 5

In supramolecular structure **5**, analysis of the short contacts reveals that FpC_6 molecules are involved in a series of embraces dominated by aromatic interactions. In the unit cell, pairs of FpC_6 molecules are involved in a typical parallel four-fold phenyl embrace (P4PE) denoted as P4PE-1 as shown in Figure 2-15. The aryl groups are involved in one OFF interaction and two EF interactions. In P4PE-1, complementary hydrogen bonding between *t*-CO and a proton donated from the phenyl ring involved in the OFF interaction is observed (see Figure 2-13a).

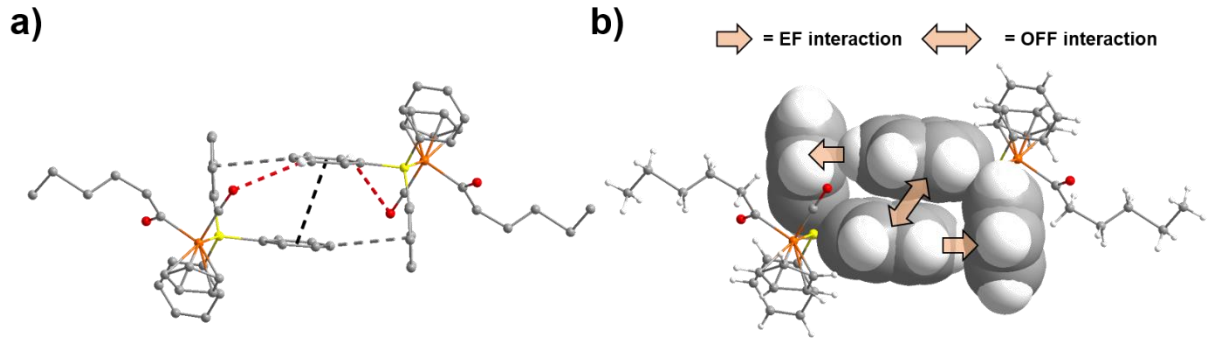

Figure 2-13 a) Parallel four-fold phenyl embrace (P4PE) P4PE-1 formed by FpC_6. Black dotted lines represent OFF interactions and grey dotted lines represent EF interactions. Red dotted lines represent hydrogen bonding. Hydrogens not involved in hydrogen bonding have been omitted for clarity. b) Spacefill representation of P4PE formed by FpC_6.

Further analysis indicates that these P4PE-1s are linked at their edges to another slightly different P4PE denoted as P4PE-2 by an EF interaction between Cp and Ph rings and

complementary hydrogen bonding involving *t*-CO groups and a proton donated from the phenyl ring involved in the EF interaction (see Figure 2-14a and b). In P4PE-2, the interaction distances are slightly different from P4PE-1 and no hydrogen bonding is observed between *t*-CO and a proton donated from the phenyl ring involved in the OFF interaction (see Table 2-5).

Table 2-5 Summary of aromatic interaction in P4PE-1 and P4PE-2

Interaction	Average C_d (Å)		Average α (°)	
	P4PE-1	P4PE-2	P4PE-1	P4PE-2
OFF(Ph—Ph)	3.9	4.4	0.0	0.0
EF(Ph—Ph)	5.4	5.1	84	90
EF(Cp—Ph)	5.0	5.0	83	83

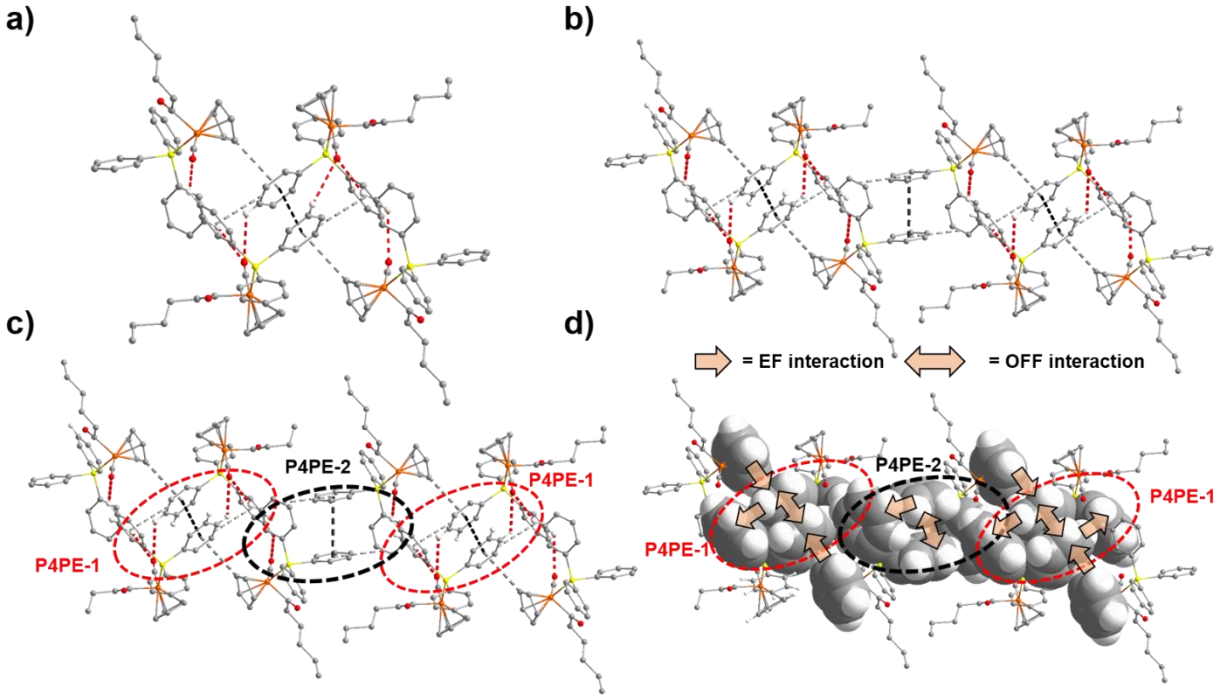

Figure 2-14 a) Intermolecular interactions between P4PE-1 and P4PE-2. b) Extended sequence of intermolecular interactions between FpC_6. c) Zig-zag chain obtained through the alternating association between phenyl embraces P4PE-1 and P4PE-2. d) Space fill representation of zig-zag chain. Two EF interactions are obscured. Grey dashed lines represent EF interactions. Black dashed lines represent OFF interactions. Red dashed lines represent hydrogen bonding. Hydrogens not involved in hydrogen bonding have been omitted for clarity.

The P4PE-1 and P4PE-2 embraces repeat in an alternating pattern and an extended zig-zag sequence "P4PE-1 ---- P4PE-2 ----P4PE-1" is obtained (Figure 2-14b, c and d). The supramolecular structure consists of these alternating sequences extending in the (1 0 1) plane, as seen in Figure 2-15a, and the sequences can be seen to lie parallel to one another when the supramolecular structure is viewed along the *a* crystallographic direction (see Figure 2-15b). Between each extended sequence there are EF interactions between each P4PE-1 and P4PE-2.

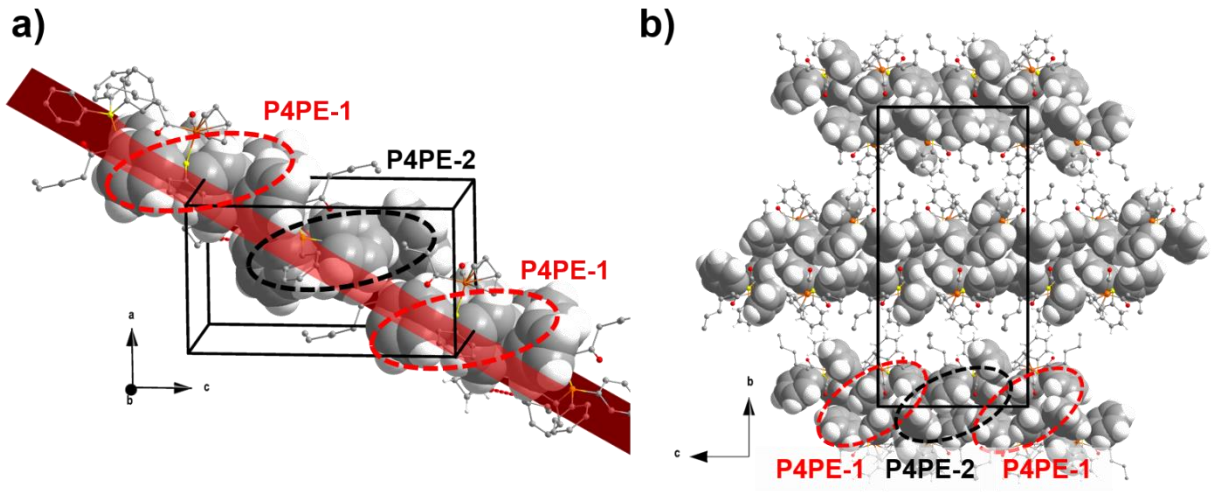

Figure 2-15 a) Image of P4PE-1---P4PE-2 sequence in the (1 0 1) plane. b) Projection of supramolecular structure **5** in the (*b c*) plane. The alternative sequences align parallel to one another. Hydrogens not involved in intermolecular interactions have been omitted for clarity

2.7.4 Analysis of Intermolecular Interactions and Packing Motifs of FpC_6

Analysis of the supramolecular structures reveals that the packing motifs of FpC_6 involve C—H---O hydrogen and phenyl embraces. Since these crystalline solid-state structures were obtained *via* different external conditions it is possible to compare the different packing motifs with respect to their external conditions. Doing so provides information about the balance between competing interactions (embracing motifs vs. hydrogen bonding) to direct self-assembly and how external conditions influence this.

Supramolecular structures **1-3** were obtained through the recrystallization of FpC_6 from non-polar hexane solutions; whereas, supramolecular structure **4** and **5** were obtained through the recrystallization of FpC_6 from a methanol solution and an ethanol/water solution (20/80 v/v), respectively. When polar protic solvents were used during recrystallization, the amount of intermolecular C—H---O hydrogen bonding in the resulting supramolecular structures was reduced (see Table 2-6).

FpC_6 formed chains in all supramolecular structures except supramolecular structure **5**. In supramolecular structure **5**, no integrated chain structures were formed and instead alternating sequences of P4PEs were observed (Figure 2-14 c, d and Figure 2-15a). This suggests that when water is introduced into the system, FpC_6 molecules do not form chains and form P4PEs instead. This change in packing motif may be caused by the hydrophobic effect and disruption of inter FpC_6 hydrogen bonding (Table 2-6).

Table 2-6 Summary of hydrogen bonding in supramolecular structures **1-5**.

Supramolecular Structure	t-CO---H—C (Cp)		a-CO---H—C (Ph)		t-CO---H—C (Ph)		Number of hydrogen bonds per mol.
	d (Å)	θ (°)	*d* (Å)	θ (°)	*d* (Å)	θ (°)	
1	2.7	166	2.6	154	N/A	N/A	5
2	2.8	162	2.6	151	N/A	N/A	5
3	2.7	122	2.7	137	N/A	N/A	7
4	N/A	N/A	2.4	163	N/A	N/A	2
5	N/A	N/A	N/A	N/A	2.6	157	2

Different recrystallization conditions resulted in significantly different chain structures (see Figure 2-16). Consequently, in supramolecular structures **1** and **2**, the chains were formed through a combination of integrated phenyl embraces and hydrogen bonding (Figures Figure 2-4 and Figure 2-5) and a ladder chain structure was obtained (Figure 2-16a). The rails of the ladder are formed by repeating EF_3 embraces and the rungs of the ladder are formed by repeating OFF(EF_2) embraces (Figure 2-17). While the chain in supramolecular structure **3** is

also formed through a combination of integrated phenyl embraces and hydrogen bonding (Figure 2-8), a zig-zag chain is obtained instead of a ladder chain (Figure 2-16b). The zig-zag chain is formed by adjacent bimolecular EF_3 embraces interacting at their edges through an EF_3 embrace (Figure 2-17).

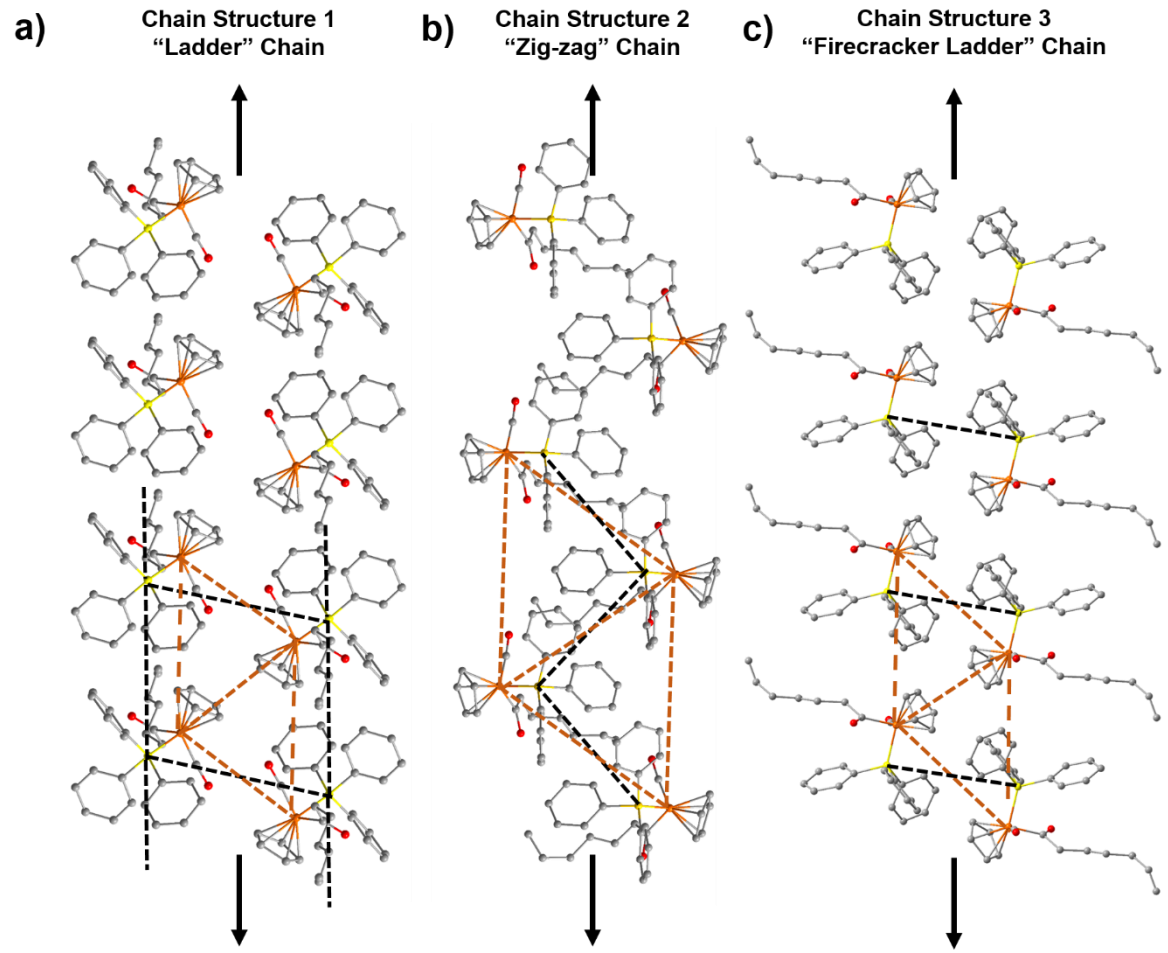

Figure 2-15 a) Ladder chain structure observed in supramolecular structures **1** and **2**. b) Zig-zag chain structure observed in supramolecular structure **3**. c) "Firecracker" chain structure observed in supramolecular structure **4**. Orange dashed lines indicate inter iron distances. Black dashed lines indicate relevant phosphorus distances outlining the chain's morphology. Arrows indicate the long axis of the chain. Hydrogen atoms have been omitted for clarity.

In supramolecular structure **4**, there are no hydrogen bonds within the chain structure, because of the disruption of hydrogen bonding by methanol. Consequently, the chain structure

is formed entirely through repeating phenyl embraces (Figure 2-11 and Figure 2-12) and a firecracker ladder chain is obtained (Figure 2-16c and Figure 2-17). The rungs of the firecracker ladder are formed by bimolecular EF_4 embraces which are linked to another EF_4 at their edge *via* an OFF(EF_2) embrace (Figure 2-17). In all the chain forming supramolecular structures, the chains are packed such that they are separated by regions or pockets of alkyl chains (see Figure 2-6, Figure 2-10a, and Figure 2-12a).

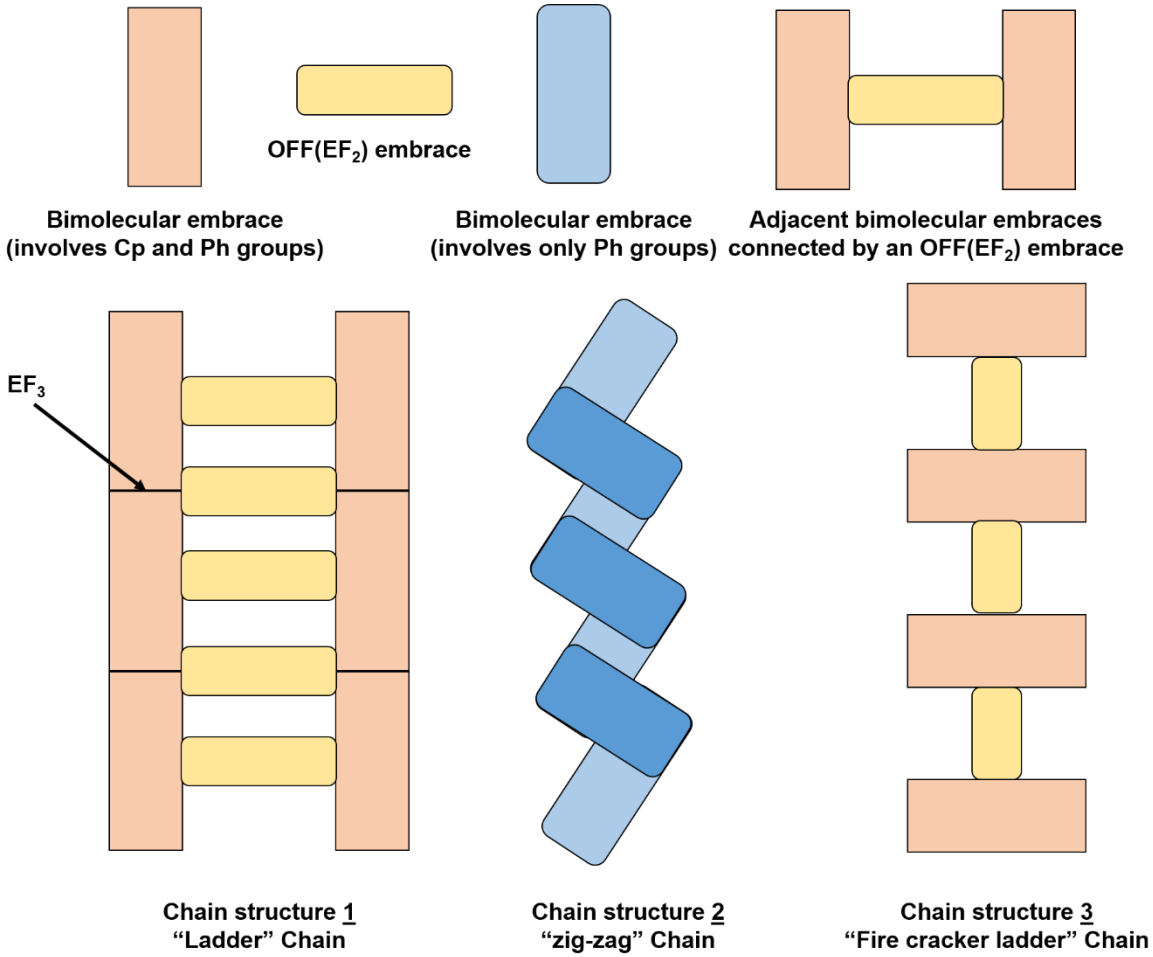

Figure 2-16 Cartoon representation of the three chain structures formed by FpC_6. Chain structure **1** is observed in supramolecular structures **1** and **2**. Chain structure **2** is observed in supramolecular structure **3**. Lastly, chain structure **3** is observed in supramolecular structure **4**.

While at first glance the embracing motif in supramolecular structure **4** may appear similar to that observed in supramolecular structures **1** and **2**, there are a number of significant differences. Firstly, the FpC_6 molecules involved in the bimolecular embrace in supramolecular structure **4** interact through four EF interactions (Figure 2-11) rather than three EF as seen in supramolecular structures **1** and **2** (Figure 2-3). As a result, the P---P distance in supramolecular structure **4** is 7.14 Å, whereas in supramolecular structure **1** and **2** it is 8.13 Å. The closer P---P distance indicates a stronger embrace, which suggests that the FpC_6 molecules are packing to maximize the EF interactions in supramolecular structure 4. This packing behaviour is reasonable since hydrogen bonding between FpC_6 molecules was disrupted and FpC_6 molecules could then interact primarily through aromatic interactions. In supramolecular structures **1** and **2**, the bimolecular embrace is formed by only three EF interactions rather than four as observed in supramolecular structure **4**. The reason for this is that the FpC_6 molecules involved in the embrace are rotated so that their *t*-CO ligands point in the same direction. This occurs so that the *t*-CO ligands can form the hydrogen bonding involved in the bimolecular embrace in supramolecular structures **1** and **2** (Figure 2-3a). On the other hand, in supramolecular structure **4**, the *t*-CO ligands point in opposite directions maximizing the aromatic interactions (Figure 2-11a). It can be concluded that when hydrogen bonding is disrupted, the FpC_6 molecules pack to maximize the aromatic interactions. This subtle change in packing behaviour results in a drastic change in chain structure as shown in Figures Figure 2-16 and Figure 2-17. This change in packing behaviour demonstrates the crucial role of C—H---O bonding directing the packing of the FpC_6 molecules.

While supramolecular structures **1-3** were all obtained from non-polar conditions, the chain structure (**1**) observed in supramolecular structures **1** and **2** is significantly different

compared with the chain structure (**2**) observed in supramolecular structure **3**. While each chain structure incorporates hydrogen bonding, there are twice the number of hydrogen bonds involved in chain structure **1** than in chain structure **2**. Another difference between the supramolecular structures is the inter phosphorus distance. In supramolecular structures **1** and **2**, the P---P distance in the bimolecular embrace is 8.13 Å and it is 7.75 Å in supramolecular structure **3**. The closer phosphorus distance indicates that the embrace in supramolecular structure **3** is stronger than in supramolecular structures **1** and **2**. This suggests that FpC_6 molecules in supramolecular structure **3** are packing in order to maximize the aromatic interactions of the phenyl rings. These differences can be rationalized by considering the faster evaporation used to obtain supramolecular structure **3**, which resulted in a faster crystallization rate. Supramolecular structure **3** may arise due to a much faster nucleation-growth process. As a result, the supramolecular structure may arise from a more kinetically favourable process. It is reasonable that the chain structure observed in supramolecular structure **3** is kinetically more favourable since it involves less FpC_6 molecules to form one repeat unit of the chain and there are less steric considerations since only one embracing motif is involved. Based on these observations it can be concluded that in non-polar environments FpC_6 forms integrated chains through cooperative hydrogen bonding and repeating embracing motifs. With slow crystallization rates, FpC_6 packs to form ladder chains based on repeating embracing motifs and maximizes hydrogen bonding. With fast crystallization rates, FpC_6 packs to create zig-zag chains which maximize the aromatic interactions between phenyl rings. These results demonstrate that while FpC_6 packing is governed by the need to optimize both hydrogen bonding and aromatic interactions, kinetic factors play an important role in the chain structures.

2.8 Conclusions

In summary, the organometallic small molecule FpC_6 was successfully synthesized. By varying the recrystallization conditions five unique structural morphologies were obtained. Analysis of the intermolecular interactions and packing motifs revealed that FpC_6 molecules interact with one another through a variety of C—H---O hydrogen bonding and aromatic embracing motifs. In supramolecular structures **1** and **2**, the FpC_6 molecules pack to form integrated ladder chains formed through cooperative hydrogen bonding and a repeating embrace motif OFF(EF_8). In supramolecular structure **3**, the FpC_6 molecules pack to form a zig-zag chain consisting of repeating EF_3 embracing motifs and hydrogen bonding. In addition, supramolecular structure **4** consisted of a firecracker ladder chain formed through a repeating motif of EF_4 embraces linked at their edges through an OFF(EF_2) embrace. Lastly, supramolecular structure **5** consisted of FpC_6 molecules packed into alternate sequences of P4PE. The packing motif of FpC_6 is found to be controlled by a balance between hydrogen bonding and aromatic interactions. FpC_6 has a tendency to form chains created by embracing motifs and hydrogen bonding; however when water is present, FpC_6 does not form chains and an alternating sequence of P4PEs is obtained instead. When recrystallized in a polar environment, the resulting chains are formed through repeating embracing motifs as FpC_6 molecules pack to maximize aromatic interactions. Similarly, in non-polar environments with fast crystallization rates, FpC_6 molecules form chains which optimize the aromatic interactions rather than hydrogen bonding. Lastly, in non-polar environments with slow crystallization rates, FpC_6 molecules pack to form ladder chains which optimize both the aromatic interactions and hydrogen bonding. FpC_6 has a propensity to form chains in the crystalline material and these chains are separated by regions of packed alkyl chains. It may then be possible to disrupt

the three-dimensional supramolecular structure by the addition of thermal energy and obtain supramolecular polymer chains in the bulk amorphous material.

Chapter 3. Supramolecular Polymerization of FpC_6

3.1 Overview

After determining that FpC_6 was capable of forming one dimensional chains in a crystalline material, the second step in this project was to determine if these chains were present in the amorphous material after melting. After melting, FpC_6 displayed characteristic polymer behaviour, such as the ability to draw fibres from the melt and form standing films, suggesting the presence of chains in the amorphous material. To identify the chain structure, powder X-ray diffraction (PXRD) was used to characterize the amorphous material. PXRD revealed a double peak pattern, characteristic of ladder polymers. The position of the first peak matched the inter-iron spacing corresponding to the repeat unit of chain structure **1**, and the position of the second peak matched that expected of aromatic interactions. Regardless of the initial crystalline solid-state structure, PXRD after melting indicated that chain structure **1** was always obtained. PXRD at high temperatures indicated that chain structures were present well above the crystalline melting temperature, highlighting the stability of the supramolecular polymer formed by cooperative C—H---O hydrogen bonds and aromatic embraces. DSC revealed that the FpC_6 supramolecular polymer chains underwent a glass transition and were stable enough to suppress crystallization on the time scale of the DSC experiments. The dielectric constant and refractive index were determined in order to establish the potential of FpC_6 for use in optical and electronic application. Dynamic oscillatory experiments revealed that freshly melted FpC_6 behaved like a viscous liquid, whereas aged FpC_6, displayed viscoelastic behaviour, indicative of chain entanglement. This suggested that the FpC_6 chains might elongate during the ageing process. Furthermore, time sweeps revealed that G' increased over time during measurements, suggesting that FpC_6 chains were sensitive to measurement history.

3.2 Introduction

BSP formed by small molecules have considerable potential for functional materials, with properties such as self-healing and stimuli-responsiveness. These systems typically require a cycle of heating to provide the monomers the mobility to associate into the chain. Consequently, the key challenge associated with using small molecules to prepare BSP is preventing crystallization during cooling and subsequent reheating. The ability of the supramolecular chains to suppress crystallization is an important factor in the stability of BSP. Additionally, at the temperatures BSP form, the degree of polymerization can be very low. This makes achieving polymer-like mechanical properties very challenging. Consequently, BSP assembled from small molecules which can form a glassy state and display viscoelastic behaviour are rare.[49-50, 61, 69, 77, 87, 128] Furthermore, previous literature shows that it is challenging to investigate BSP formed by small molecules because of their sensitivity to thermal history, crystallization, complex mechanical behaviour and the lack of understanding of intermolecular interactions in bulk.[5, 49, 68, 70, 87, 129] Historically, well characterized strong hydrogen bonding motifs have been used to minimize these challenges. While weak interactions, such as C—H---O and C—H---π hydrogen bonds, have been used to prepare SP in solution, no examples currently exist in bulk. Despite the associated challenges of using weak intermolecular interactions, research of new monomers is necessary to advance the field and explore BSP formed by weak intermolecular interactions.

Crystal engineering demonstrates that FpC_6 is capable of forming a variety of chain structures in solid-state structures *via* C—H---O hydrogen bonds and aromatic embraces. Consequently, FpC_6 presents a unique opportunity to explore the potential formation of the first bulk supramolecular polymer *via* C—H---O hydrogen bonds and aromatic interactions.

By disrupting the three-dimensional ordering of the crystalline material, it may be possible to generate SP. To explore this possibility, crystalline FpC_6 was melted in order to provide the mobility necessary for the monomers to assemble. The resulting amorphous material displayed characteristic polymer-like behaviour, suggesting that supramolecular polymerization had occurred. Subsequently, the amorphous material was characterized in order to determine the chain structure responsible for the polymer-like behaviour. Additionally, the thermal behaviour of bulk FpC_6 was investigated to understand the conditions required for the formation of the chains and determine their stability. Finally, the effect of ageing and temperature on its mechanical behaviour was studied to investigate the dynamic behaviour of the backbone assembled from C—H---O hydrogen bonds and aromatic embraces.

3.3 Instrumentation

X-ray data of powder samples were collected using two instruments. Firstly, X-ray data were collected using Mo Kα radiation on a Bruker Kappa APEX II System with a CCD detector equipped with an OXFORD Cryosystems Cryostream 700 and an AD51 Dry air unit. Alternatively, X-ray data were acquired using an Inel XRG 3000 Powder X-ray Diffractometer with a position sensitive detector using Cu Kα radiation. Fourier transform infrared (FTIR) spectra were obtained using a Bruker Tensor 27 spectrophotometer with a resolution of (1 cm^{-1}). Samples were prepared by mixing FpC_6 and anhydrous KBr using a mortar and pestle. The mixture was then pressed in a pellet using a hydraulic press. Attenuated total reflectance (ATR)/FTIR Spectra were obtained using a germanium crystal Pike MIRacle^{TM} ATR attachment by Pike Technologies. Solution FTIR/ATR was carried out by placing a drop of solution directly onto the crystal. Thermal gravimetric analysis (TGA) was performed using a TGA Q50 by TA instruments. TGA experiments were carried out using a heating rate of 10

°C/min with a nitrogen flow rate of 40 mL/min. Differential Scanning Calorimetry (DSC) was performed using a Q20 DSC equipped with a RCS 90 cooling system from TA Instruments. All experiments were carried out using T_{zero} aluminum pans. Unless otherwise specified, all DSC measurements were performed using a heating rate of 10 °C/min with a nitrogen flow rate of 50 mL/min. Rheology experiments were carried out using either a Bohlin Rheometer CS (controlled stress) using 20 mm parallel plates or a Rheometrics RDS II (controlled strain) using 25 mm parallel plates. Ellipsometry data were obtained using an ALPHA-SE ellipsometer manufactured by J.A. Woollam Co. The permittivity of FpC_6 was extracted from capacitance measurements made using an Agilent 4284A LCR with Agilent 16451B Test Fixture. Film thickness measurements were obtained using a DEKTAK 8 stylus profilometer.

3.4 Experimental

Preparation of amorphous FpC_6 for PXRD experiments using the Bruker Kappa APEX II: Crystalline FpC_6 was placed in a round bottom flask and heated in an oil bath to 110 °C for 5 minutes. The molten FpC_6 was drawn into the tip of a Pasteur pipette, removed from heat and allowed to cool to room temperature. The pipette tip containing vitrified FpC_6 was cut and sealed using a torch. Subsequently, the sample was mounted into the goniometer head on the Bruker Kappa APEX II System. The temperature was then adjusted using an OXFORD Cryosystems Cryostream 700 series.

Preparation of amorphous FpC_6 for powder X-ray diffraction experiments using the Inel XRG 3000: Amorphous samples were prepared by filling an aluminum sample holder with crystalline FpC_6. The sample holder was heated on a hot plate at 65 °C for 10 minutes, until the FpC_6 became liquid-like and translucent. Subsequently, the sample holder was placed into the instrument and X-ray data were collected for 60 to 90 minutes.

Sample preparation for rheological experiments: Aged FpC_6 samples were shaped into discs by compressing them between Teflon sheets. The FpC_6 discs were loaded onto the bottom plate of the rheometer. The sample was heated to 40 °C while the top plate was lowered to ensure sample contact with the top plate. The top plate was lowered until a 1 mm gap was obtained. Excess FpC_6 that flowed outwards was trimmed using a scoopula. Freshly melted samples of FpC_6 could be directly loaded onto the bottom plate of the rheometer without having to shape the samples into discs. The top plate was then lowered until a gap of 1 mm was obtained. No heating was necessary as the sample flowed easily. Excess FpC_6 that flowed outward was trimmed using a scoopula. Samples were allowed to equilibrate for 5 minutes before taking measurements after loading and after each temperature change. Measurements were carried out at least twice to ensure reproducibility.

Ellipsometry measurements: A thin film of FpC_6 was prepared on a silicon wafer by spin coating a 10 mg/mL toluene solution of FpC_6 at 5000 rpm for 1 minute. Ellipsometry measurements of the film were made from 380 to 900 nm at incidence angles of 65°, 70° and 75°.

Capacitance measurement: A 1 mm film was prepared by compressing an FpC_6 pellet between two Teflon sheets. The film and the Teflon sheets were placed in an Agilent 16451B Test Fixture and the capacitance was measured using an Agilent 4284A LCR using the Rigid Metal electrode method (contacting electrode method). The measurements were compensated for the capacitance of the Teflon sheets by measuring the capacitance of the Teflon sheets separately and adjusting the measurements accordingly.

3.5 Bulk Behaviour of FpC_6

After melting, FpC_6 does not immediately crystallize and instead forms a soft sticky red solid (see Figure 3-1). Over time (hours to days depending on storage conditions), this red material darkens and becomes much stiffer and resin-like (see Figure 3-1).

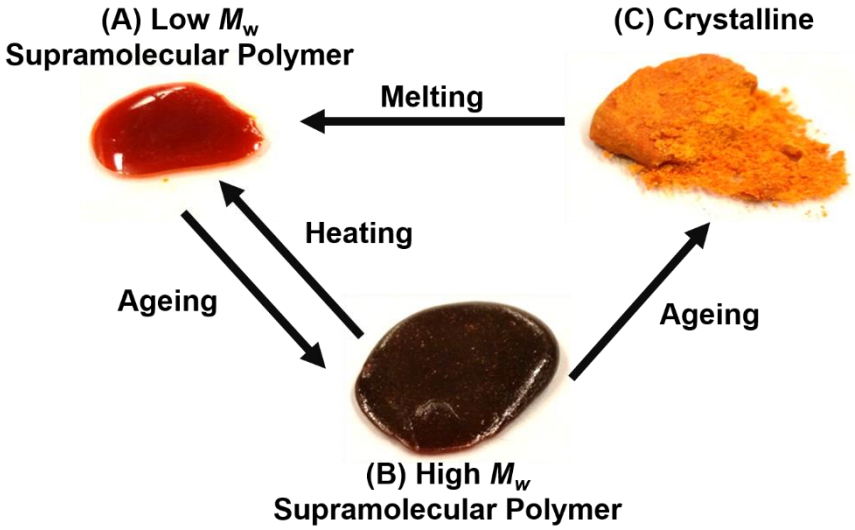

Figure 3-1 Freshly melted (A), aged (B) and crystalline (C) FpC_6

As illustrated in Figure 3-2a, fibres could be drawn from both the soft red solid and the resin-like material at temperature between ca. 20-50 °C.[136] Additionally free-standing films can be formed *via* compression moulding (Figure 3-2b). Freshly prepared FpC_6 (after solvent removal) forms a large free-standing bubble when placed in a vacuum oven (Figure 3-2c).[136] The resin-like material can be extruded from a syringe forming long strands (Figure 3-2d) and moulded into a variety of shapes at room temperature (Figure 3-2e-g). This behaviour is characteristic of polymers and is indicative that FpC_6 forms supramolecular chains. While the resin-like material can be moulded to form shapes, the freshly melted FpC_6 red solid is unable to hold its shape, which suggests that it may be formed by shorter chains.

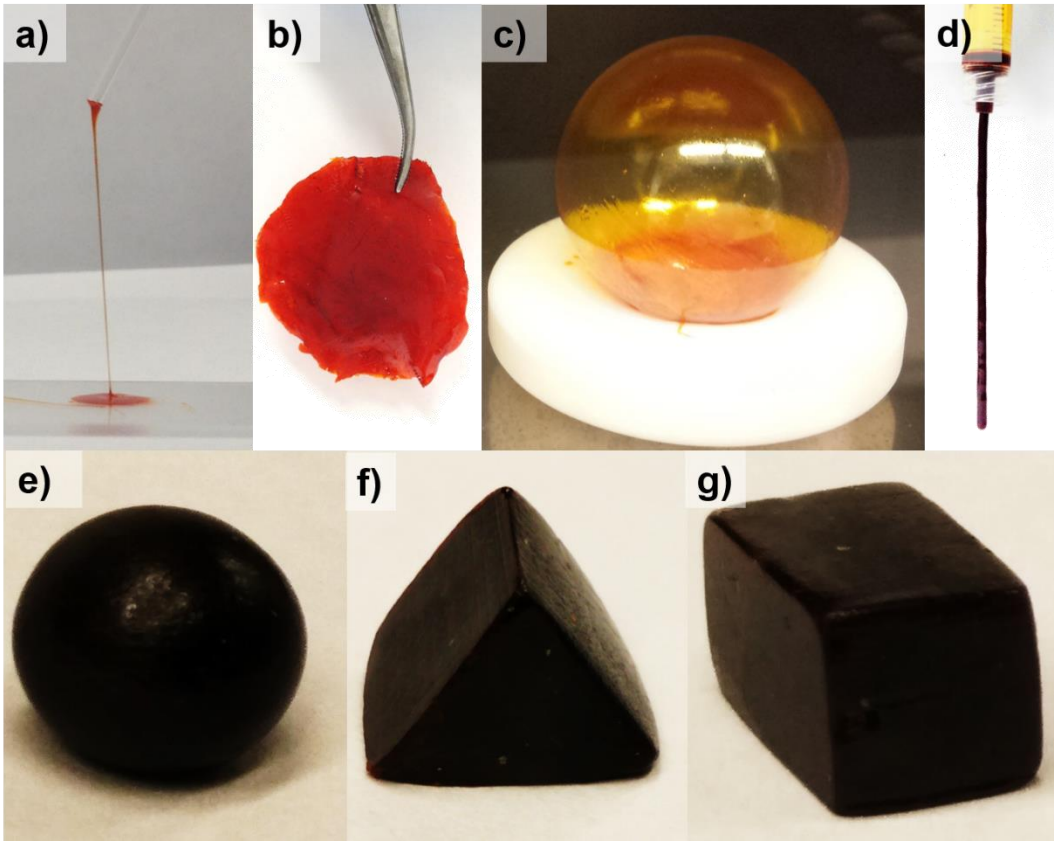

Figure 3-2 a) Fibre drawn from freshly melted FpC_6. b) Free-standing film formed by compression molding of freshly melted FpC_6. c) Free standing bubble formed by freshly melted FpC_6. d) Strand formed by extruding aged FpC_6 through a syringe. Aged FpC_6 can be moulded into a variety of shapes including a sphere e), triangular prism f) and a rectangular prism g).

If stored at room temperature, the resin-like FpC_6 crystallizes over approximately two weeks (see Figure 3-1). By comparing the experimental and simulated PXRD diffractograms as shown in Figure S3-1b, the final crystalline structure was determined to be supramolecular structure **3**. When the resin-like material was stored at 4 °C, the crystallization of the samples was further slowed and took approximately 30 days to complete (Figure 3-3).[136] Interestingly, crystallization in the fridge sometimes resulted in the formation of supramolecular structure **1** (Figure S3-1a). When stored at −50 °C, the resin-like material did not crystallize even after four months (Figure S3-4). This slow crystallization behaviour is characteristic of

supramolecular chains; however, it also reveals that the chains are metastable and crystallize over time.

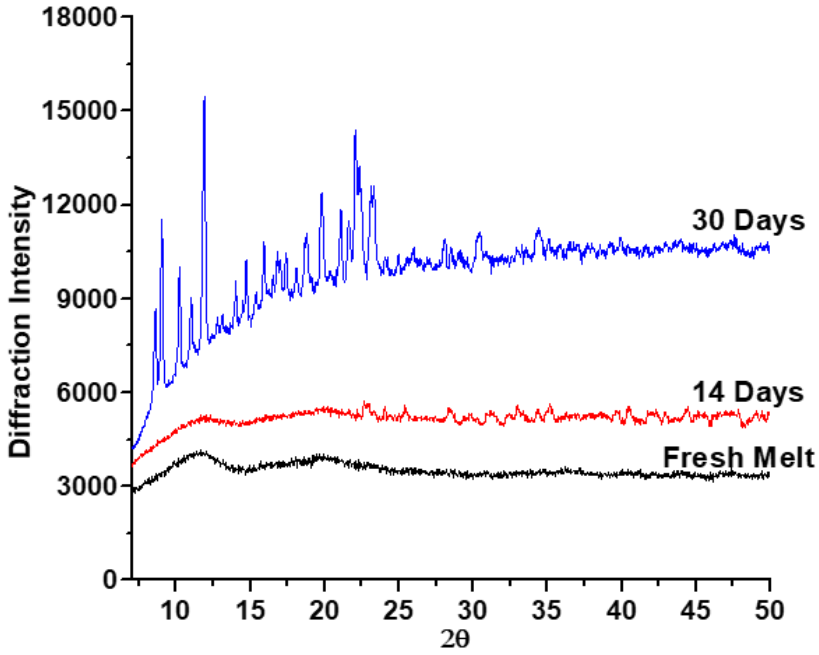

Figure 3-3 Time-dependent PXRD diffractograms for FpC_6. The sample was prepared by heating a portion of crystalline FpC_6 (supramolecular structure **1**) at 65 °C for 10 minutes. The sample was stored in the fridge at 4 °C. After 30 days the samples had completely crystallized back into supramolecular structure **1**.

3.6 Identification of Chain Structure in Amorphous Material

Crystal engineering reveals that FpC_6 can adopt three different chain structures in crystalline material (Figure 2-16). PXRD of amorphous FpC_6 was performed to determine the chain structure responsible for the polymeric behaviour of FpC_6. The resulting diffractograms always displayed a double peak pattern characteristic of ladder polymers (Figure 3-4a).[137-140] Silicon based ladder polymers, such as polysilsesquioxanes, display a characteristic double peak pattern, wherein the first peak is attributed to the spacing between the rails of the ladder and the second peak is attributed to the chain thickness or spacing between chains.[137-140]

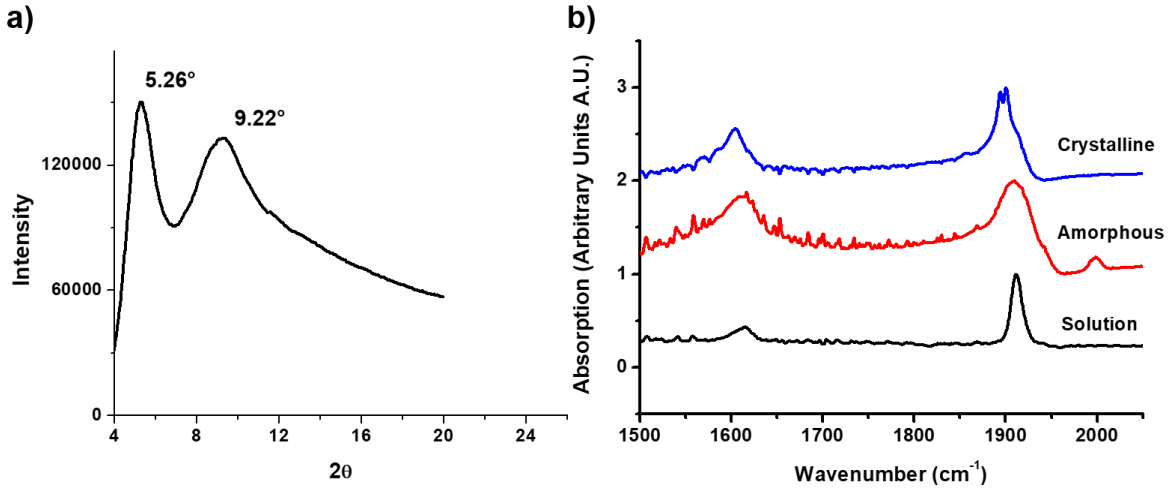

Figure 3-4 a) PXRD of freshly melted FpC_6. A characteristic double peak pattern is observed. The first peak ($2\theta = 5.26°$) corresponds to a distance of 7.5 Å. The second broad peak ($2\theta = 9.22°$) corresponds to a distance of 4.4 Å. b) Normalized FTIR/ATR of crystalline, amorphous and a 50 mg/mL solution of FpC_6. The peak near 1900 cm^{-1} corresponds to the *t*-CO stretching frequency. The broad peak centered near 1600 cm^{-1} corresponds to the *a*-CO stretching frequency.

In the case of FpC_6, the first peak at $2\theta = 5.26°$ corresponds to a distance of 7.5 Å and the second broad peak at $2\theta = 9.22°$ represents a distance of 4.4 Å (see Figure 3-4). Compared to oxygen or carbon, iron and phosphorus both have a large number of electrons which scatter more X-rays. Therefore, the average inter-iron and phosphorus distances can act as indicators of the chain structure. The weighted average inter iron and phosphorus distances of the chain structures repeat unit were calculated (Figure 3-5) and are summarized in Table 3-1.

Table 3-1 Summary of inter iron and phosphorus distance in chain structures **1**-**3**

Chain Structure	Average inter Fe distance (Å)	Average inter P distance (Å)
1	7.4 Å	8.3 Å
2	10.4 Å	7.8 Å
3	8.2 Å	8.2 Å

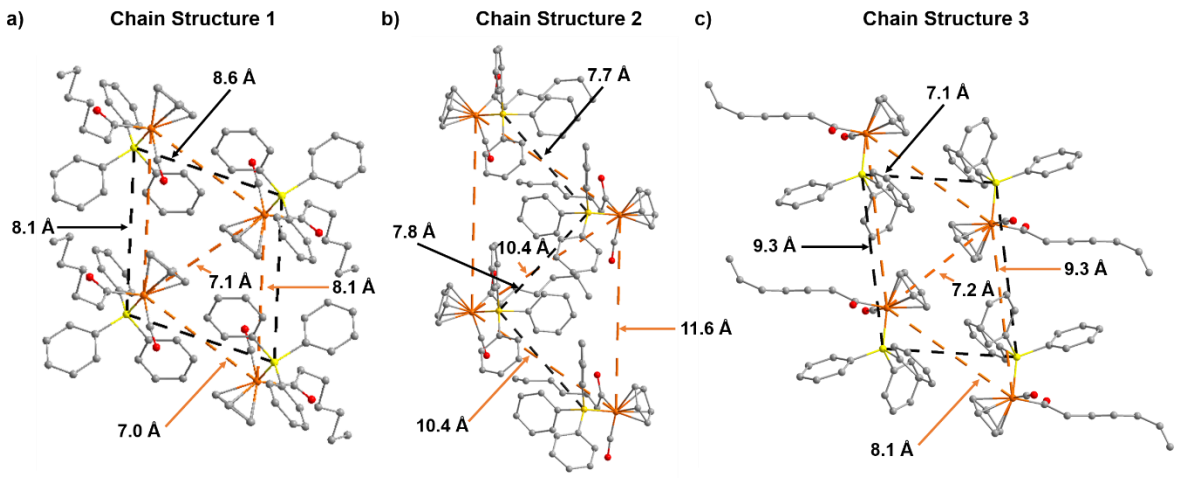

Figure 3-5 a) Inter iron and phosphorus distance in repeat unit of chain structure **1**. b) Inter iron and phosphorus distance in repeat unit of chain structure **2**. c) Inter iron and phosphorus distance in repeat unit of chain structure **3**. Repeat units of chain structures **1**-**3** were obtained directly from the supramolecular structures.

As shown in Table 3-1, the average inter iron distance of chain structure **1** matches very closely the first peak observed in the diffractogram. The average iron distance in chain structure **1** are representative of both the distance between the rails and rungs of the ladder. Furthermore, chain structure **1** is the only chain structure which adopts a ladder structure, similar to polysilsesquioxanes, which are known to generate double peak patterns. Chain structure **2** does not form a ladder structure and the average inter iron and phosphorus distances do not match the peaks in the diffractogram. While chain structure **3** adopts a pseudo ladder structure, the average inter iron and phosphorus distances do not match the PXRD peak positions.

FTIR/ATR spectra for amorphous and crystalline FpC_6 (supramolecular structure **1**) were compared to that of an FpC_6 benzene solution (50 mg/mL) to characterize the hydrogen bonding in bulk FpC_6 (Figure 3-4b). The FTIR/ATR of the FpC_6 benzene solution shows that the absorption frequencies of the *a*-CO and *t*-CO were 1618 cm^{-1} and 1912 cm^{-1}, respectively. These stretching frequencies are considered to be associated with FpC_6 molecules with no

significant hydrogen bonding. For amorphous FpC_6, the *a*-CO and *t*-CO stretching frequencies shift to 1610 cm^{-1} and 1910 cm^{-1}, respectively. The shift in the stretching frequencies to lower wavenumbers is indicative of hydrogen bonding in the amorphous material.[96] Furthermore, the involvement of both *a*-CO and *t*-CO groups in hydrogen bonding is expected for chain structure **1**. The stretching frequencies of the *a*-CO and *t*-CO groups shifted to even lower wavenumbers in the crystalline material further demonstrating the presence of hydrogen bonding.[96] Based on the FTIR/ATR and PXRD experiments it can be concluded that FpC_6 adopts chain structure **1** in the bulk amorphous material.[136]

The formation of chain structure **1** is reasonable, since it is observed in crystals recrystallized from non-polar environments. It is interesting that chain structure **1** (obtained from supramolecular structure **1**) is formed rather than chain structure **2** (obtained from supramolecular structure **3**), since both are observed in crystals recrystallized from non-polar environments. This suggests that chain structure **1** is more stable than chain structure **2**, which is reasonable since the chain is formed by more C—H---O hydrogen bonding and aromatic interactions. As previously discussed, when stored at room temperature, the amorphous FpC_6 SP with chain structure **1** (from supramolecular structures **1** and **2**) slowly crystallizes into supramolecular structure **3**. This indicates that the chains are metastable. Furthermore, while chain structure **1** may be more stable than chain structure **2** in the amorphous material, the final crystalline solid-state structure appears to be determined by other factors.

3.7 Thermal behaviour and Bulk Supramolecular Polymerization of FpC_6

The prevention or suppression of crystallization is a key measure of the integrity of BSP from small molecules. Furthermore, the strength of the association between monomers can be indirectly investigated by determining the temperatures at which the chains dissociate

into monomers. The higher the temperature at which dissociation occurs, the stronger the association between monomers and the higher the thermal stability. To understand the formation, stability and integrity of the chains, the thermal behaviour of bulk FpC_6 was first investigated using thermal gravimetric analysis (TGA). TGA indicates the onset of decomposition (corresponding to a 1 % weight loss) occurs at 136 °C (see Figure S3-2).

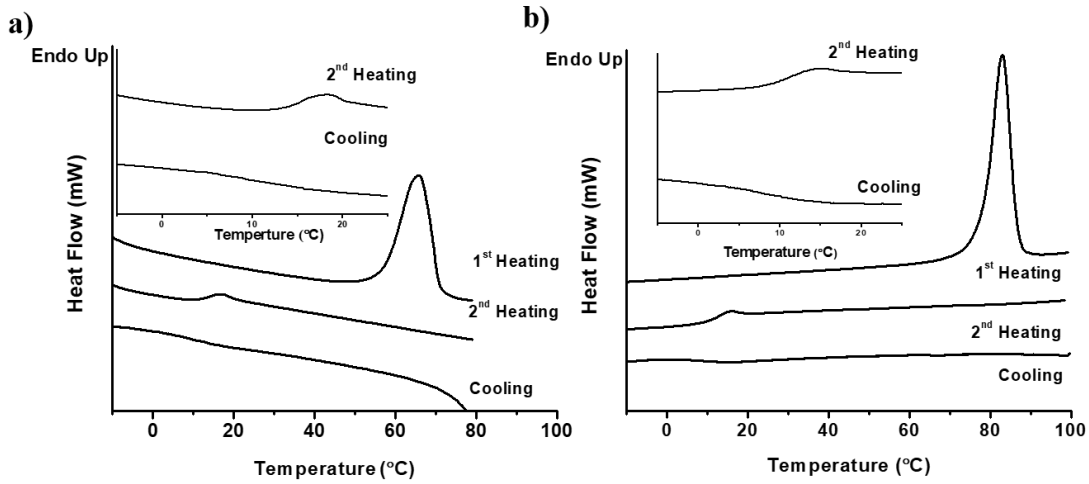

Figure 3-6 a) DSC trace (ramp rate 5 °C/min) of FpC_6 with supramolecular structure **1**. Inset: Glass transition region using ramp rate of 10 °C/min. b) DSC trace (ramp rate 5 °C/min) of FpC_6 with supramolecular structure **3**. Inset: Glass transition region using ramp rate of 10 °C/min.

Subsequent DSC experiments (Figure 3-6), indicate that during the first heating cycle, crystalline FpC_6 melts at 65 °C (supramolecular structure **1**) or 85 °C (supramolecular structure 3). During the cooling and reheating cycles, no recrystallization or cold crystallization occurs. Subsequently, the molten samples undergo a glass transition at ca. 8 °C during the cooling cycle and at ca. 13 °C during the second heating cycle (Figure 3-6). PXRD of the molten samples shows the presence of the duplex chains corresponding to chain structure **1**, indicating that FpC_6 BSP formed *via* chain structure **1** can be created by heating regardless of the initial crystalline solid-state structure of the material.

Crystallization is suppressed during the DSC experiments which allows FpC_6 to undergo a glass transition. In fact, no crystallization is ever observed on the DSC after melting, even when a temperature ramp rate of 1 °C/min is used or after annealing at 50 °C for 2 hours during the cooling cycle (see Figure S3-3). In addition, PXRD of an annealed sample (at 50 °C for 3 hours) showed no crystalline peaks (see Figure S3-4b). These results indicate that FpC_6 does not recrystallize on the time scale of the DSC experiments. The suppression of the crystallization in BSP is attributed to the presence of chains and the sequestration of the monomers inside them.[49-50, 141] All previously reported BSP rely on "strong hydrogen bonding" to integrate the monomers into the chains and prevent crystallization. The thermal behaviour of FpC_6 BSP demonstrates that cooperative weak hydrogen bonding and aromatic embraces are able to sequester monomers in the chains, which significantly hinders crystallization. This remarkable behaviour is attributed to the cooperative effect generated by the arrangement of the non-covalent and the steric effect of the ladder chains.

3.8 Stability of FpC_6 Supramolecular Polymers

To investigate the thermal stability, FpC_6 BSP were characterized by PXRD at high temperatures. A round bottom flask containing FpC_6 was heated to 110 °C for 10 minutes under nitrogen. Then FpC_6 was drawn into the tip of a Pasteur pipette and allowed to cool to room temperature. The pipette tip containing the sample was cut and then mounted into the diffractometer. Subsequently, the sample was heated to 100 °C and allowed to equilibrate for a minimum of 5 minutes. The diffraction pattern was collected at 100 °C and is displayed in Figure 3-7a**.** The resulting diffractogram shows the characteristic double peak pattern, indicating that the FpC_6 chains are present at 100 °C. To investigate if the chain structure is present above 100 °C, a sample of FpC_6 was heated in a round bottom flask to 130 °C using

an oil bath under nitrogen. The sample was allowed to equilibrate for 10 minutes and was subsequently drawn into the tip of a Pasteur pipette and quenched in liquid nitrogen. The diffraction pattern was then collected at room temperature and is shown in Figure 3-7b. The double peak pattern, characteristic for chain structure **1** was observed, suggesting the chains are present even at 130 °C. These results highlight the remarkable thermal stability of the FpC_6 supramolecular chains, which demonstrate the strength of the integrated aromatic embraces and cooperative C—H---O hydrogen bonding.

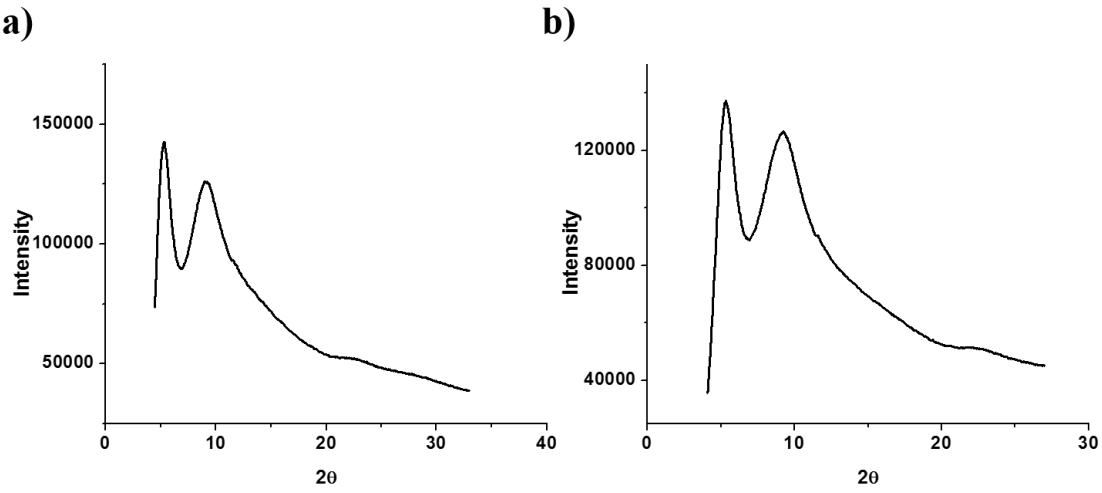

Figure 3-7 a) PXRD of FpC_6 collected at 100 °C. b) PXRD of a quenched sample of FpC_6. The PXRD pattern was collected at room temperature.

The crystallization of polymorphic compounds remains an active field of research.[95] However, some comments can be made regarding the crystallization behaviour of FpC_6 with respect to the thermal behaviour and its supramolecular polymer nature. Ultimately, the BSP formed by FpC_6 crystallizes in bulk into two different supramolecular structures (**1** and **3**). Interestingly, the T_m of supramolecular structure **1** is lower than supramolecular structure **3**. This indicates that supramolecular structure **3** is more thermodynamically stable and one would expect chain structure **2** to form after melting. However, melting crystalline material with

either supramolecular structure **1** or **3**, always results in supramolecular chains with chain structure **1**. Furthermore, chain structure **1** is even observed at 130 °C, approximately 50 °C above the melting temperature of supramolecular structure **3**. Regardless of the stability of the supramolecular structures, chain structure **1** is the most stable chain structure in the amorphous material.

In the case of supramolecular structure **1**, the structure consists of supramolecular FpC_6 chains packed parallel to one another in the crystal lattice. Thus supramolecular structure **1** can be considered to form by the crystallization of the supramolecular chains of FpC_6. Consequently, melting supramolecular structure **1**, involves providing the thermal energy necessary to disrupt the inter-chain interactions and disrupt the packing of the chains. On the other hand, the melting of supramolecular structure **3**, results in the formation of chain structure **1**. This would require the disruption of all the intermolecular interactions in the crystal, to allow the reorganization of FpC_6 molecules into chain structure **1**. As indicated by the higher melting temperature of crystalline material with supramolecular structure **3**, this process requires significantly more energy. In summary, melting supramolecular structure **3** involves disrupting all the intermolecular interactions and providing the mobility necessary for FpC_6 to assemble into chain structure **1** (i.e. the bulk supramolecular polymerization). The melting of supramolecular structure **1** involves the disruption of interactions between FpC_6 supramolecular polymer chains and providing the chains mobility.

Supramolecular structure **1** can be obtained by crystallization at low temperatures (4 °C), indicating that the chains can be preserved in the supramolecular structure (Figure 3-3). When stored at room temperature, FpC_6 BSP crystallizes into supramolecular structure **3**. This suggests that the nucleation rate of supramolecular structure **3** (crystallization of monomer)

may be faster than supramolecular structure **1** (crystallization of polymer) at room temperature (Figure 3-8) and that there is an energy barrier to the nucleation process required to obtain supramolecular structure **3**.

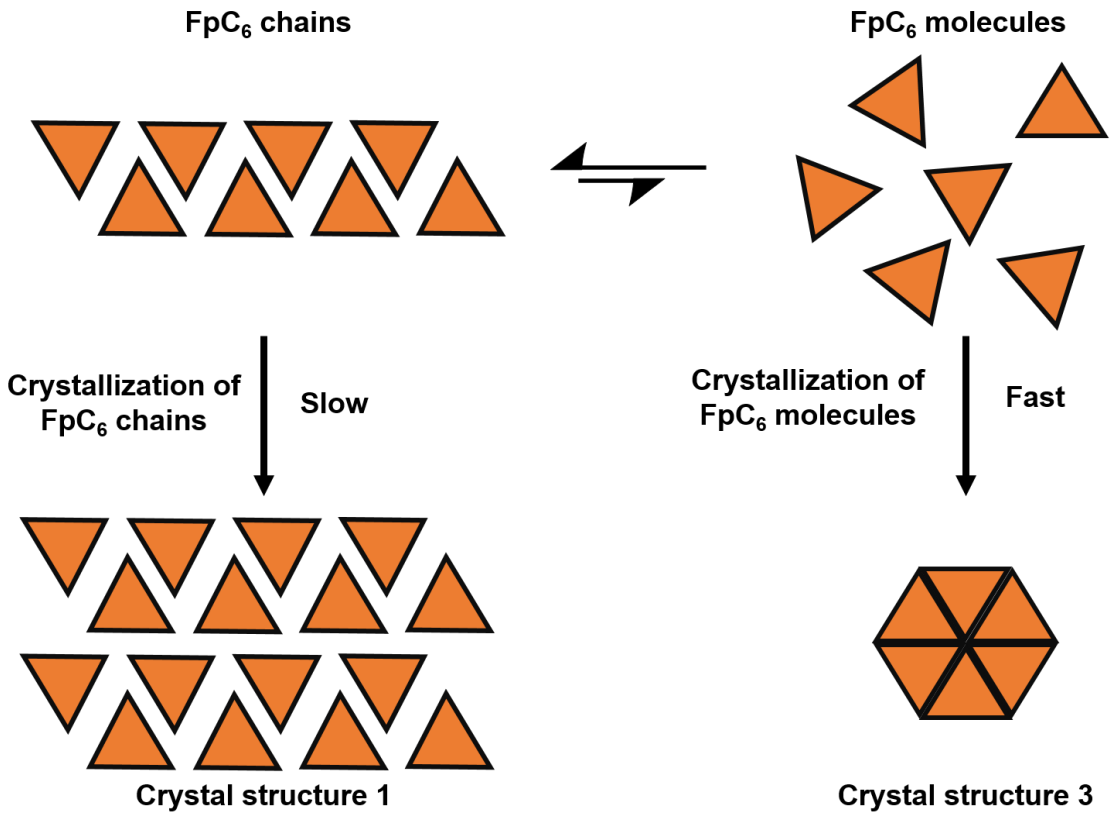

Figure 3-8 Cartoon depiction of crystallization pathway of FpC_6. The supramolecular chains are at equilibrium with unassociated monomers. The nucleation rate of supramolecular structure **3** may be faster than supramolecular structure **1**. As a result, unassociated monomers may crystallize into supramolecular structure **3**. Depletion of unassociated monomers from the system would drive further disassembly of the chains.

At room temperature, the BSP exist at equilibrium with some unassociated monomer (Figure 3-8). The nucleation of supramolecular structure **3** may be rapid. Once nucleation occurs, unassociated monomers will begin to crystallize. Since crystallization is not reversible, the crystallization process would deplete unassociated monomers from the system, driving the disassembly of chain structure **1** in order to re-establish equilibrium.

3.9 Refractive Index and Dielectric Constant of FpC_6

To determine the suitability of FpC_6 BSP for optical or electronic applications, such as an anti-reflective coating or a dielectric layer, the refractive index and dielectric constant were characterized. A thin film (30 nm thick from profilometer measurements) of FpC_6 was characterized by ellipsometry to determine the refractive index (RI). The resulting data were modelled by a single non-absorbing Cauchy layer on a silicon substrate using the CompleteEASE software. The model parameters were as follows: A = 1.748, B = 0.00067916, C = 0.0, k = 0, band edge = 400 nm. The model fit the data well and had a mean squared error of 4.775 (see Figure S3-5a). The film thickness according to the model was 28.44 ± 0.02 nm and was in agreement with the thickness obtained *via* profilometer measurements. The refractive index of FpC_6 according to the model was 1.75 at 632.8 nm. The high refractive index of FpC_6 was comparable to that of polyferrocenylsilanes and had potential applications for optical and electronic devices.[142]

The relative permittivity of FpC_6 was extracted from capacitance measurements of a 1 mm film. The resulting dielectric constant of FpC6 as a function of frequency is displayed in Figure S3-5b. The relative permittivity of FpC6 was 3.4 at 1 MHz, close to that of SiO_2 (3.9). Therefore, FpC_6 is potentially useful as a dielectric material for printed electronics where low-temperature processability is required.

3.10 Mechanical Behaviour of FpC6

3.10.1 Rheological Behaviour of Freshly Melted FpC_6

Freshly melted samples of FpC_6 (Figure 3-1) were loaded onto either a stress-controlled or a strain-controlled rheometer. Using a CS Bohlin stress-controlled rheometer, the linear

viscoelastic regime was determined at 26 °C (see Figure 3-9). Only stresses which produce measurable deformation are displayed. It is observed that at a fixed frequency, both G' and G'' are independent of stress. In addition, G' and G'' increase as higher frequencies are used, which suggests non-Newtonian behaviour. Subsequent dynamic oscillatory measurements were carried out using a stress of 4700 Pa.

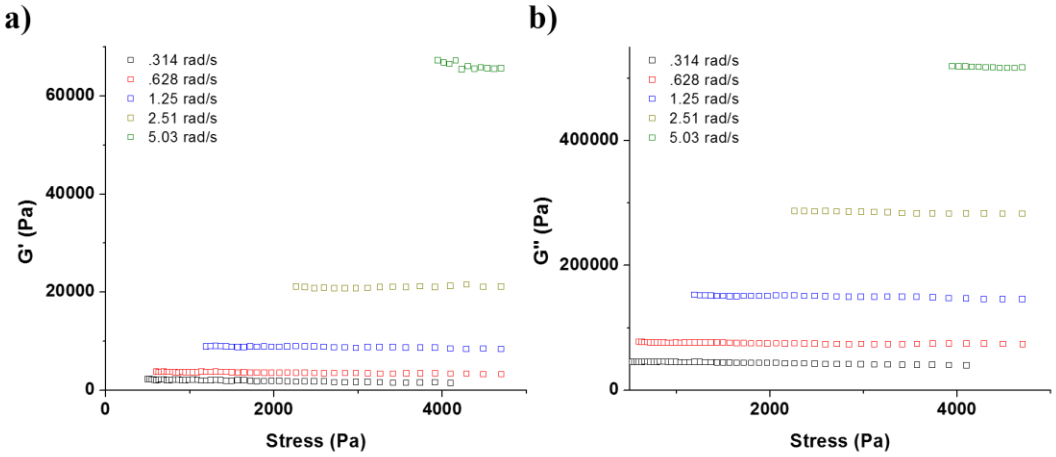

Figure 3-9 Results of stress sweep at 26 °C. a) Storage modulus (G') vs. stress at various frequencies. b) Loss modulus (G'') vs. stress at various frequencies. Only values above the minimum strain of the CS Bohlin rheometer are included in the results.

Using a RDS II strain controlled rheometer, strain sweeps were performed on freshly melted FpC_6 at 26 °C to determine the LVR at frequencies of 1, 3 and 5 rad/s. Representative results are shown in Figure 3-10. At a frequency of 1 rad/s, G' and G'' were independent of strain from 4 to 20 % strain and the stress strain curve was linear. This indicates that the measured strains lie in the LVR. At higher frequencies, G' was not measurable because the phase angle (δ) was greater than 90° (this instrument artifact will be discussed in Section 3.10.6). However, G'' was independent of strain and the stress strain curve was linear. This suggests that the strain values measured still lie in the LVR. In order to protect the transducer from damage at higher frequencies, the strain was limited to 4%.

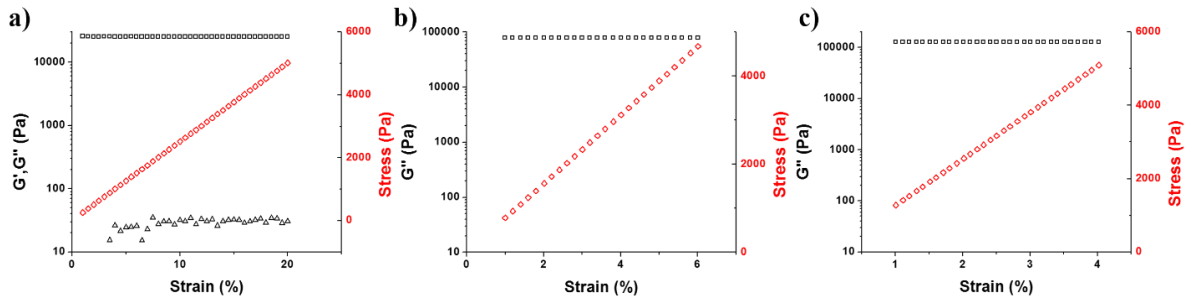

Figure 3-10 Results of strain sweep at 26 °C on the RDS II rheometer. Storage modulus (G'), loss modulus (G'') and stress vs. strain a) at 1 rad/s, b) at 3 rad/s and c) at 5 rad/s.

The results of the dynamic oscillatory experiments on freshly melted FpC_6 are shown in Figure 3-11a, b. On both instruments, the loss modulus (G'') is greater than the storage modulus (G') over the entire frequency range investigated (Figure 3-11a, b). These results indicate that FpC6 behaves like a viscous fluid. While PXRD shows the presence of chains in freshly melted samples (Figure 3-4a), the lack of viscoelastic behaviour indicates that these chains are too short to entangle. On the stress-controlled rheometer, a large tan δ peak appears at 0.44 rad/s and is accompanied by a change in the slope of G' (Figure 3-11a). As shown in Figure 3-11a, G' begins to increase more steeply with frequency after 0.44 rad/s, which indicates that FpC6 begins to behave more elastically with increasing frequency. When the strain-controlled rheometer was used, the measured phase angle (δ) exceeded 90° at the tan δ peak (Figure 3-11b). This reproducible instrument artifact occurred only when FpC_6 was analyzed on the RDS II. Viscous liquids did not generate this response. This artifact will be discussed in a following section. When an absolute value of G' is used, the mechanical behaviour of freshly melted FpC_6 on both rheometers is similar (Figure 3-11a and Figure S3-6a).

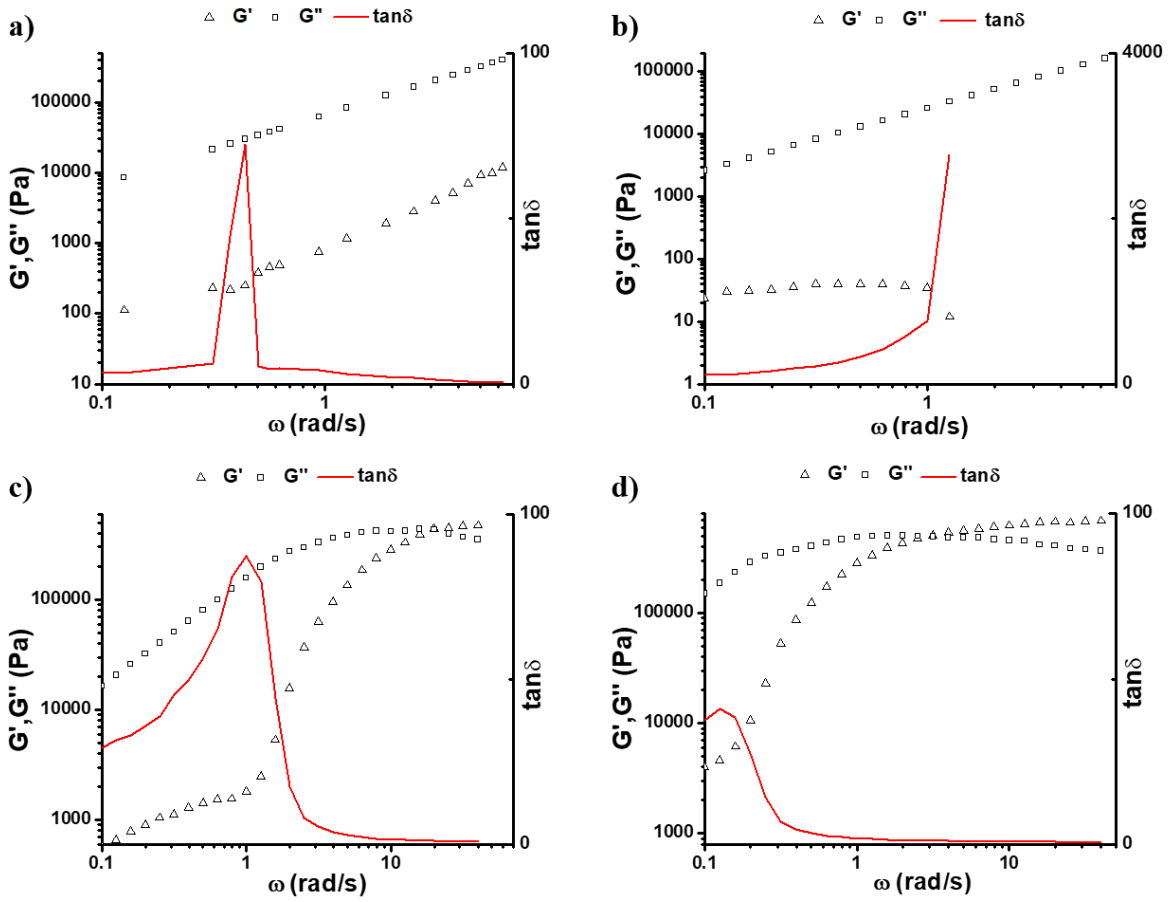

Figure 3-11 Results of dynamic oscillatory experiments. Mechanical behaviour of a) freshly melted FpC_6 characterized using a stress-controlled rheometer at 26 °C (applied stress = 4700 Pa), b) freshly melted FpC_6 characterized using a strain-controlled rheometer at 26 °C (applied strain = 4 %). Note: after 1.26 rad/s, the mesured phase angle exceeds 90°. As a result, the rheometer reports negative G' and tan δ values, which are not displayed, c) aged FpC_6 characterized using a strain-controlled rheometer at 32 °C (applied strain = 1 %), d) aged FpC_6 characterized using a strain-controlled rheometer at 26 °C (applied strain = 1 %).

3.10.2 Mechanical Behaviour of Aged FpC_6

Aged FpC_6 (Figure 3-1) was stiffer than freshly melted FpC_6, suggesting that the mechanical properties have improved. The stress-controlled instrument could not be used to characterize aged FpC_6, because the stiffness of the sample was beyond the measurement capability of the instrument. The mechanical behaviour of an aged sample was characterized at different

temperatures by cooling from 40 °C to 26 °C on the strain-controlled rheometer. At temperatures above 32 °C, the samples exhibited the aforementioned instrument artifact (Figure S3-6b), consistent with freshly melted FpC_6 (Figure 3-11b). In contrast, when experiments were performed at 32 °C and below, the mechanical behaviour was coherent over the entire frequency range (Figure 3-11c, d).

At both temperatures (32 and 26 °C), aged FpC_6 displayed viscous behaviour (G'' > G') at low frequencies, and behaved elastically (G' > G'') at higher frequencies. This viscoelastic behaviour is characteristic of chain entanglement. The cross-over point (G' = G'') of aged FpC_6 at 26 °C (Figure 3-11d) appeared at a lower frequency (2.6 rad/s) than that at 32 °C (20 rad/s) (Figure 3-11). The sample at 26 °C exhibited a well-defined "rubbery" plateau (Figure 3-11d). For covalent polymers, the average molecular weight between entanglements (M_e) can be determined from the plateau modulus (G_e) using the following equation:[143]

$$\boldsymbol{M_e = \frac{\rho RT}{G_e}}$$

Assuming this equation is valid for FpC_6 and that the rubbery plateau is caused by chain entanglements, the M_e can be approximated using the density from supramolecular structure **1** (1.31 g/cm^3) and the plateau modulus from the dynamic oscillatory experiment at 26 °C (0.64 MPa).

$$\boldsymbol{M_e \approx \frac{1.31\ \frac{g}{cm^3} * 8.314\ \frac{cm^3 MPa}{Kmol}\ * 299.15\ K}{0.64\ MPa} \approx 5091 \frac{g}{mol}}$$

An M_e of 5091 g/mol corresponds to a degree of polymerization of 9.71. This suggests that there are approximately 10 FpC_6 molecules between entanglements. Comparing the dynamic oscillatory experiment of the aged and unaged samples at 26 °C reveals that the aged sample

yields larger G' values and displays a viscoelastic response (Figure 3-11d vs Figure 3-11b). This suggests that the ageing process lengthens the chains so that they become long enough to entangle. While PXRD and DSC show no evidence of crystallization in the aged samples, the presence of micro-crystallites cannot be ruled out.

3.10.3 Origin of Tan δ Peak

A tan δ peak, which represents a mechanical relaxation, is observed during all dynamic oscillatory experiments on both rheometers. The behaviour of the dynamic moduli before and after the tan δ peak may provide insight into the mechanical relaxation responsible for the tan δ peak. In the case of freshly melted FpC_6 (Figure 3-11a, b), G' is frequency-independent (typical of Newtonian liquids) before the appearance of the tan δ peak, and is very small compared to G'' (G' < 1.5% of G''). After the tan δ peak, G' becomes frequency-dependent and its magnitude relative to G'' increases with frequency, suggesting the presence of structure in the sample, which can be attributed to the chains that were detected by PXRD. In aged samples (Figure 3-11c), G' increases slightly with frequency before the tan δ peak, which is similar to the behaviour of viscous liquids with short chains present. After the tan δ peak, G' increased at a much faster rate and eventually became greater than G''. This viscoelastic behaviour is characteristic of chains long enough to entangle. In summary, before the tan δ peak, the sample behaves as if there were no chains or only short chains were present in the sample. After the tan δ peak the sample behaves as if chains were present.

This suggests that chain scission may be the mechanical relaxation represented by the tan δ peak. If the measurement timescale (inversely related to the frequency, ω) is longer than the average lifetime of the polymer chains (τ_b), then chain scission can be observed. Once the timescale of the measurement is shorter than the τ_b, no chain scission would occur during the

measurement. Therefore, at low frequencies (before the tan δ peak), FpC_6 BSP may undergo chain scission during the measurements. In freshly melted samples, the chain length may be quite short. When chain scission occurs, the sample may behave as if no chains were present (Figure 3-11a, b), resulting in the frequency independent G'. In an aged sample, the chains may be longer, so that when chain scission occurs, the samples behave as if oligomers were present. At frequencies above the tan δ peak, FpC_6 chains will relax *via* chain-like relaxations depending on their length, i.e. short chains will relax *via* viscous flow (Figure 3-11a) and longer chains will relax *via* reptation (Figure 3-11c).

3.10.4 Complex Viscosity of Aged FpC_6

The complex viscosity (η*) as a function of frequency at different temperatures was obtained from the dynamic oscillatory experiments. As shown in Figure 3-12, η* increases as the temperature is lowered. Furthermore, at temperatures above 32 °C, the complex viscosity of FpC_6 is independent of frequency. At 32°C and below, η* of FpC_6 was frequency-dependent and displayed shear thinning behaviour. Interestingly, the onset of shear thinning occurred only at frequencies after the tan δ peak occurred. Therefore, polymer-like behaviour is only observed once τ_b becomes long enough (by lowering the temperature), to enable the measurement of polymer relaxation. This is illustrated by the onset frequency where the viscosity of FpC_6 starts to depend on frequency, once the chains no longer undergo chain scission during the deformation.

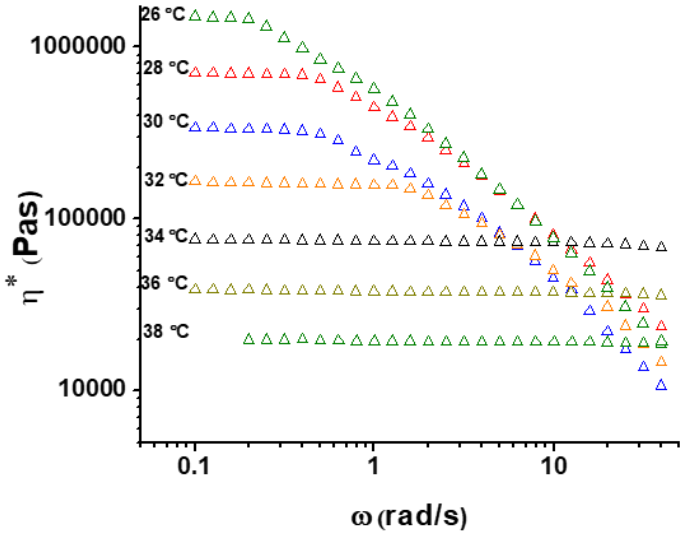

Figure 3-12 Complex viscosity of FpC_6 vs. angular frequency at different temperatures.

3.10.5 Effect of Temperature and Ageing on Tan δ Peak:

As shown in Table S3-1, as the temperature is lowered the position of the tan δ peak shifts to lower frequencies. An illustrative example of this behaviour can be seen in Figure 3-11c and d. At 32 °C, the tan δ peak is observed at 1 rad/s; however, at 26 °C, the frequency at which the tan δ peak occurs shifts from 1 rad/s to 0.13 rad/s. This behaviour suggests that as the temperature is lowered, the τ_b of the supramolecular polymer chains increases. This occurs because as the temperature is decreased, the intermolecular interactions become stronger increasing the τ_b.[2] Interestingly, the position of the tan δ peak at 26 °C for aged FpC_6 is 0.13 rad/s and for un-aged FpC_6 is 1.6 rad/s. This result indicates that τ_b increases during the ageing process. This may occur since the mechanical behaviour indicates that the chains lengthen during the ageing process. Longer chains may have a higher τ_b, because their anisotropy may enhance the association of the monomers.[65]

3.10.6 FpC_6-Induced Instrument Artifacts

When FpC_6 was characterized using the RDS II strain controlled rheometer, the phase angle δ often exceeded 90° during dynamic mechanical experiments. This reproducible artifact only occurred when FpC_6 was analyzed on the RDS II instrument. Viscous liquid samples (δ ≈ 90°) and viscoelastic standards did not generate this response. Nevertheless, an improperly corrected phase angle could cause this artifact. Measured phase angles must be corrected by a correction factor representing the phase shifts caused by the rheometer's electronic servo system. The phase angle correction factor was calibrated using a steel standard. Testing with a viscous standard (δ ≈ 90°) indicated that the RDS II was operating correctly and within tolerance, ruling out the possibility of an improperly corrected phase angle. This type of artifact can occur on stress-controlled instruments due to improper corrections for instrument compliance. However, it is unlikely that this artifact was caused by instrument inertia effects, since the RDS II is a strain controlled rheometer and uses a force rebalance transducer, which has negligible compliance. Therefore, it appears that the nature of FpC_6 causes this instrument artifact. When this artifact occurs (δ > 90°), it always appears at or above the frequency corresponding to the maximum of the tan δ peak, regardless of frequency sweep direction. The tan δ peak is observed on the stress-controlled rheometer, indicating that it is real and not a product of the RDS II instrument artifact. If the tan δ peak represents chain scission it could be possible that chain scission affects the ability of the RDS II to accurately measure the phase difference between the measured torque signal and the strain signal. The dynamic nature of FpC_6 may generate a noisy torque signal, which could make accurately determining the phase difference challenging. Currently, it is not possible to predict when the artifact will occur, making reproducibility of measurements challenging.

3.10.7 Time Sweep of FpC_6

Time sweeps were carried out in order to investigate the build-up or breakdown of the network structure of FpC_6 during measurements. A time sweep was carried out at 40 °C and revealed that both G' and G'' increase slowly over time (Figure 3-13a). Furthermore, δ decreases over time, indicating that FpC_6 becomes slightly more elastic.

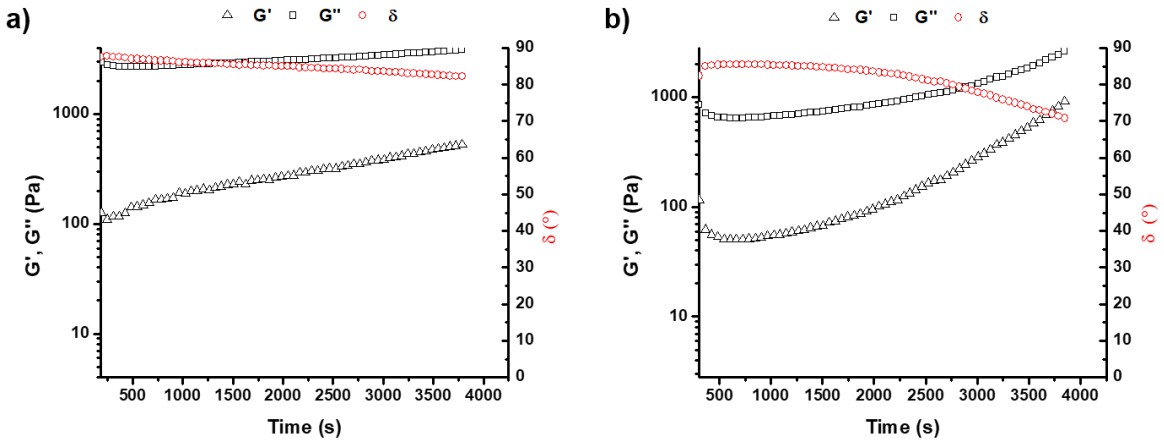

Figure 3-13 a) Time sweep at 40 °C using a strain of 3%. Measurements were made over 60 s intervals using a frequency of 1 rad/s. An initial delay of 180 s was used to allow the sample to equilibrate to 40 °C. b) Time sweep at 50 °C using a strain of 30 % during the second hour. Measurements were made over 60 s intervals using a frequency of 1 rad/s. An initial delay of 300 s was used in the second hour to allow the sample to re-equilibrate to 50 °C from room temperature.

A two-hour time sweep was carried out in one hour segments at 50 °C. During the first hour, the sample behaved similarly to the one hour time sweep at 40 °C (Figure S3-8). However, during the second hour, G' and G'' both increased significantly (Figure 3-13b). Additionally, there is a pronounced decrease in δ demonstrating that the sample is becoming significantly more elastic. These results demonstrate that the mechanical behaviour of FpC_6 changes over time, which suggests that the mechanical behaviour is sensitive not only to ageing and temperature but to measurement history as well. DSC and PXRD experiments at 50 °C,

indicate that no crystallization occurs. This suggests that the chains may elongate or the network builds-up during measurements. Consequently, the reproducibility of measurements becomes challenging, because making measurements appears to change the behaviour of the sample.

3.10.8 Summary of Mechanical Behaviour

The mechanical behaviour of FpC_6 was found to be very rich and complex. Freshly melted FpC_6 displays viscous behaviour, indicating that the chains are not long enough to entangle. Aged FpC_6 displays viscoelastic behaviour, characteristic of chain entanglements, suggesting that ageing increases the length of the chains. While PXRD and DSC show no evidence of crystallization in aged samples, the presence of micro-crystallites cannot be ruled out. A tan δ peak is observed during all dynamic oscillatory experiments and is tentatively attributed to chain scission. Before the tan δ peak, FpC_6 behaves as if no chains or only very short assemblies are present. After the tan δ peak, FpC_6 behaves as if chains are present. The dynamic nature of FpC_6 appears to induce an instrument artifact on the RDS II rheometer. Time sweeps reveal that the FpC_6 network changes during measurement. It is possible that chains elongate or are aligning during measurements. Consequently, the reproducibility of the mechanical behaviour of aged FpC_6 between different samples is extremely challenging and is exacerbated by instrument artifacts.

3.11 Conclusions

After melting, FpC_6 does not immediately recrystallize and instead forms a bulk supramolecular polymer. PXRD of FpC_6 BSP reveals a distinctive double peak diffraction pattern which corresponds to chain structure **1**, previously identified by crystal engineering. As a result FpC_6 is the first reported BSP formed by C—H---O hydrogen bonding and aromatic embraces. FpC_6 BSP exhibits typical polymer behaviour, such as the ability to form fibres, to form free-standing films and to be moulded into different shapes above its T_g. Furthermore, high temperature PXRD and quenching experiments demonstrate that the chains are present even at 130 °C. These results highlight the remarkable stability of chain structure **1**, which is attributed to the cooperativity associated with the C—H---O hydrogen bonding and the integrated aromatic embrace motif. DSC reveals that after melting, during the initial heating cycle, no recrystallization or cold crystallization is observed within the time scale of the DSC experiments. Furthermore, the FpC_6 SP undergoes a glass transition during cooling at ca. 8 °C and at 13 °C during reheating. This result illustrates that aromatic embraces and C—H---O hydrogen bonds are strong enough to sequester the monomer into the chain structure. The chains are metastable and crystallize over time into supramolecular structures **1** or **3**. The stability of the chain may be affected by the competing nucleation of supramolecular structure **3**, which could drive the disassembly of the chains. The refractive index of the supramolecular polymer chains was determined to be 1.75 at 632.8 nm. In addition, the dielectric constant of FpC_6 was determined to be 3.4 at 1 MHz. The mechanical behaviour of FpC_6 was found to be rich and complex. Freshly prepared FpC_6 behaves like a viscous liquid, indicating that the chains are too short to entangle. In contrast, aged FpC_6 displays viscoelastic behaviour which suggests the chains are long enough to entangle. The average molecular weight between

entanglements is approximated to be 5,091 g/mol, which is approximately 10 FpC_6 molecules. During dynamic oscillatory experiments, a large tan δ peak is observed. The tan δ peak is tentatively attributed to chain scission resulting from the dynamic nature of the supramolecular chains. As temperature is decreased, the tan δ peak shifts to lower frequencies, which is consistent with the expected increase in τ_b as the temperature decreases. Additionally, the tan δ peak of an aged FpC_6 sample occurs at a lower frequency than that of freshly melted FpC_6, indicating that τ_b increases with ageing. Time sweeps reveal that the FpC_6 networks change during measurements, becoming more elastic over subsequent measurements. The sensitivity to ageing, temperature and measurement history make the reproducibility of the mechanical behaviour of aged FpC_6 extremely challenging. To achieve reproducible results between samples, the thermal bulk supramolecular polymerization of FpC_6 must be understood in detail to establish a protocol for the preparation of the FpC_6 supramolecular polymer. Once the starting point can be established for all samples, the ageing process and its influence on mechanical properties can be studied in depth. Once the ageing process can be controlled, a more detailed investigation into the mechanical behaviour may be possible.

Chapter 4. Influence of Thermal History on the Supramolecular Polymerization of FpC_6 and Preliminary Investigation of FpC_x Analogues

4.1 Overview

The purpose of this chapter is two-fold. Firstly, as discussed in Chapter 3, the mechanical behaviour of FpC_6 is very rich and complex. Factors such as ageing, temperature and measurement history influence the mechanical properties of FpC_6, making reproducibility challenging. This chapter seeks to understand what occurs to the FpC_6 polymer chains immediately after melting in order to establish a reproducible initial state. Only by establishing a reproducible initial state will it become possible to study the ageing process. Secondly, FpC_6 supramolecular polymer chains are metastable and crystallize over time. This chapter provides a preliminary investigation of FpC_6 analogues, FpC_x (x = 5, 8, 10), to determine if these analogues are capable of forming SP. Furthermore, this chapter endeavours to understand the influence of the alkyl chain length on the thermal behaviour.

FpC_x analogues were synthesized and their thermal behaviour was found to be similar to that of FpC_6. After the initial heating cycle all FpC_x (x = 5, 8, 10) analogues undergo a glass transition during cooling and reheating. No recrystallization was observed on the timescale of the DSC experiments. Interestingly, FpC_{10} never crystallizes even after storing at room temperature for over 1 year. PXRD experiments showed that melts of all the FpC_x analogues displayed a characteristic double peak pattern, suggesting that they all form BSP with chain structure **1**. Additionally, it was found that increasing the length of the alkyl chain reduced the T_g.

Investigation of the thermal behaviour of FpC_6 and FpC_8, revealed that when the material was heated to higher temperatures, the T_g decreased. The T_g also decreased with increasing annealing time at temperatures above T_m. PXRD experiments of aged FpC_6 show that the samples become more disordered as temperature increases. These results suggest that the supramolecular chains shorten at higher temperatures and that the system is not under equilibrium control. Hysteresis and annealing experiments showed that little to no repolymerization occurs at the temperatures investigated. The dissociation of FpC_8 appears to be faster than FpC_6, possibly due to the increased mobility of the monomers.

4.2 Introduction

Researching BSP from small molecules is known to be challenging, because of their sensitivity to thermal history, tendency to crystallize, complex mechanical behaviour and the lack of understanding of intermolecular interactions in bulk.[5, 49, 68, 70, 87, 129] Chapter 2 illustrated how crystal engineering can provide a detailed understanding of intermolecular interaction in bulk, thereby overcoming this challenge. In chapter 3, the complexity and challenges associated with investigating the mechanical behaviour of FpC_6 became apparent. These challenges arise primarily due to the system's sensitivity to thermal history, ageing, and measurement history. Also, the metastable nature of FpC_6 makes reproducibility challenging. These challenges must be addressed in order to continue research into FpC_6 BSP.

The addition of bulky substituents and flexible alkyl chains have been shown to suppress crystallization, improving the stability of BSP. Therefore, it is envisioned that increasing the length of the alkyl chain may reduce the tendency of the monomers to crystallize. Increasing the alkyl chain may also influence other material properties such as T_g. As a result,

FpC_x (x = 5, 8, 10) analogues were prepared to determine the influence of the alkyl chain on the bulk supramolecular polymerization.

Previous research has shown that the formation of BSP networks can be significantly influenced by thermal treatments.[74] In particular, it has been shown that annealing BSP at temperatures above T_m plays an important role in the formation of supramolecular polymer networks and the suppression of crystallization.[74] Furthermore, the thermal treatment of BSP can also modify the properties of the BSP such as T_g. These phenomena have been attributed to the reorganization of the BSP at high temperatures into more stable networks. Additionally, this research demonstrates that BSP may form under kinetic control. To understand how these factors influence FpC_6 and FpC_8, a detailed investigation was carried out to determine how the thermal history influences the BSP of FpC_6 and FpC_8. By understanding the influence of thermal history, it will become possible to establish a reproducible initial state making systematic research into the ageing process possible. Therefore, this chapter serves as an important stepping stone for future investigation into the ageing process and controlling the supramolecular polymerization of such systems. A detailed investigation into the thermal behaviour of FpC_6 and a preliminary investigation of FpC_x analogues is discussed hereafter.

4.3 Materials

Potassium rod (99.5%, stored in mineral oil), sodium rod (99.9%), 1-bromopentane (99%), 1-bromooctane (99%), 1-bromodecane (97%), cyclopentadienyl iron (II) dicarbonyl dimer (99%), benzophenone (99%) and potassium bromide (KBr) (≥ 99%) were purchased from Sigma-Aldrich. Triphenylphosphine (> 95%) was purchased from Tokyo Chemical Industries. Deuterated benzene (C_6D_6) (99.5 %) was obtained from Cambridge Isotope

Laboratories Inc. All chemicals were used as received. Tetrahydrofuran (THF) was distilled over benzophenone and sodium under a nitrogen atmosphere to remove water.

4.4 Instrumentation

A Bruker-300 (300 MHz) spectrometer was used to record ^{1}H and ^{31}P NMR spectra at ambient temperature. ^{1}H NMR chemical shifts were reported relative to the residual C_6H_6 signal and ^{31}P NMR chemical shifts were referenced to an external standard sample of 85% H_3PO_4. Thermal gravimetric analysis (TGA) was performed using a TGA Q50 by TA instruments. TGA experiments were carried out using a heating rate of 10°C/min with a nitrogen flow rate of 40 mL/min. Differential Scanning Calorimetry (DSC) was performed using a Q20 DSC equipped with a RCS 90 cooling system from TA Instruments. All experiments were carried out using T_{zero} aluminum pans. Unless otherwise specified, all DSC measurements were performed using a heating rate of 10 °C/min with a nitrogen flow rate of 50 mL/min. X-ray data was collected using Mo Kα radiation on a Bruker Kappa APEX II System with a CCD detector equipped with an OXFORD Cryosystems Cryostream 700 and an AD51 Dry air unit.

4.4 Experimental

4.4.1 Synthesis of FpC_x (x = 5, 8, 10)

All experiments were carried out under nitrogen atmosphere using Schlenk techniques. The synthesis of FpK was performed as outlined in section 2.5. The synthesis of FpC_x was performed using a one pot synthesis strategy according to the procedures outlined in section 2.6 following the generalized Scheme 3.

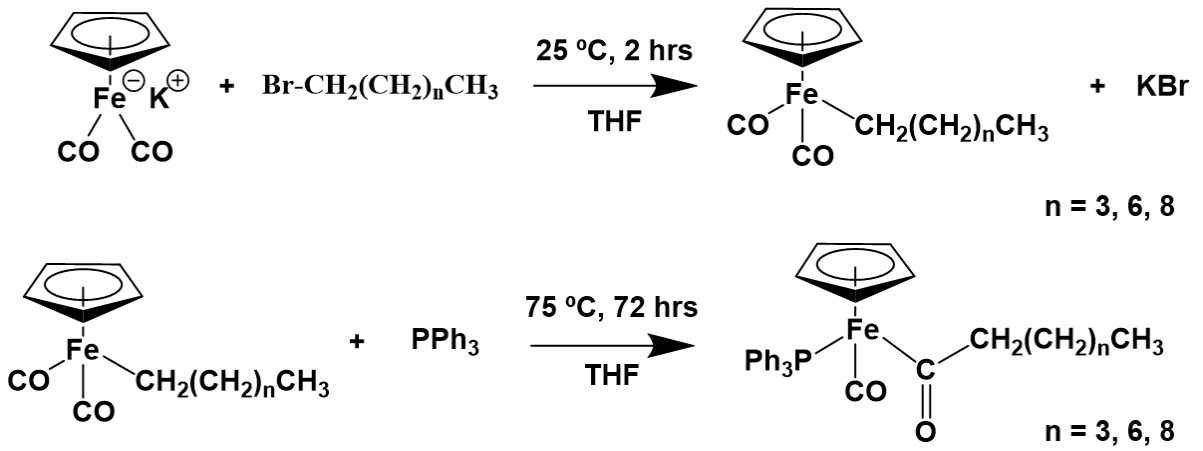

Scheme 3. Reaction scheme for the preparation of FpC_x (x = 5, 8, 10) analogues.

After synthesis THF was removed from the crude product *via* rotary evaporation. The crude product was re-dissolved in a minimum amount of hexane and loaded onto a silica gel column forming an orange band on the top of the column. The column was flushed with hexane until a yellow band was eluted. Subsequently, the column was flushed with 200 mL of 1:1 dichloromethane:hexane. Once the orange band began to move, the column was flushed with dichloromethane to collect the final product. The solvent was removed *via* rotary evaporation and the resulting sticky red solids were placed under vacuum for four hours. After purification, the analogues were characterized using ^{1}H and ^{31}P NMR with proton decoupling (Figure S4-1, Figure S4-2, Figure S4-3) and the results are summarized below:

CpFe(CO)Ph$_3$CO(CH$_2$)$_4$CH$_3$ (FpC$_5$)

^{1}H NMR (C_6D_6): 7.71 ppm (t, 6H, meta –$C_6\mathbf{H}_5$), 6.99-7.06 ppm (b, 9H, ortho, para -$C_6\mathbf{H}_5$), 4.26 ppm (s, $C_5\mathbf{H}_5$), 3.00-3.15 ppm (m, 1H ,-COC$\mathbf{H}_2$), 2.84-2.95 ppm (m, 1H, -COC$\mathbf{H}_2$), 1.48-1.60 ppm (b, 1H, -$COCH_2C\mathbf{H}_2$), 1.30-1.43 ppm (b, 1H, -$COCH_2C\mathbf{H}_2$), 1.07-1.26 ppm (b, 4H, -$COCH_2CH_2(C\mathbf{H}_2)_2CH_3$, 0.84 ppm (t, 3H, -$COCH_2CH_2(CH_2)_2C\mathbf{H}_3$). ^{31}P NMR with proton decoupling (C_6D_6): 78.8 ppm.

CpFe(CO)Ph$_3$CO(CH$_2$)$_7$CH$_3$ (FpC$_8$)

^{1}H NMR (C_6D_6): 7.72 ppm (t, 6 H, meta –C_6**H**$_5$), 6.99-7.08 ppm (b, 9H, ortho, para -C_6**H**$_5$), 4.27 ppm (s, C_5**H**$_5$), 3.05-3.16 ppm (m, 1H ,-COC**H**$_2$), 2.85-2.96 ppm (m, 1H, -COC**H**$_2$), 1.51-1.63 ppm (b, 1H, -COCH$_2$C**H**$_2$), 1.34-1.44 ppm (b, 1H, -COCH$_2$C**H**$_2$), 1.11-1.29 ppm (b, 10H, -COCH$_2$CH$_2$(C**H**$_2$)$_5$CH$_3$, 0.88 ppm (t, 3H, -COCH$_2$CH$_2$(CH$_2$)$_3$C**H**$_3$). ^{31}P NMR with proton decoupling (C_6D_6): 77.65 ppm.

CpFe(CO)Ph$_3$CO(CH$_2$)$_9$CH$_3$ (FpC$_{10}$)

^{1}H NMR (C_6D_6): 7.71 ppm (t, 6 H, meta –C_6**H**$_5$), 7.00-7.09 ppm (b, 9H, ortho, para -C_6**H**$_5$), 4.27 ppm (s, C_5**H**$_5$), 3.06-3.16 ppm (m, 1H ,-COC**H**$_2$), 2.86-2.98 ppm (m, 1H, -COC**H**$_2$), 1.53-1.61 ppm (b, 1H, -COCH$_2$C**H**$_2$), 1.33-1.41 ppm (b, 1H, -COCH$_2$C**H**$_2$), 1.25 ppm (b, 14H, -COCH$_2$CH$_2$(C**H**$_2$)$_7$CH$_3$, 0.9 ppm (t, 3H, -COCH$_2$CH$_2$(CH$_2$)$_7$C**H**$_3$). ^{31}P NMR with proton decoupling (C_6D_6): 79.04 ppm.

4.4.2 Sample Preparation for X-ray Diffraction

FpC$_x$ (x = 5, 6, 8, 10) was placed in a round bottom flask and heated in an oil bath to 110 °C for 5 minutes. The molten FpC$_x$ (x = 5, 6, 8, 10) was drawn into the tip of a Pasteur pipette, removed from heat and allowed to cool to room temperature. The pipette tip containing FpC$_x$ (x = 5, 6, 8, 10) was cut and sealed using a torch. Subsequently, the sample was mounted into the goniometer head on the Bruker Kappa APEX II System.

4.5 Thermal Behaviour and Supramolecular Polymerization of FpC$_x$ (x = 5, 8, 10)

After synthesis, the thermal behaviour FpC$_x$ analogues was investigated using TGA. TGA determined that the decomposition temperature (corresponding to a 1% weight loss) for FpC$_5$, FpC$_8$, and FpC$_{10}$, was 137 °C, 142 °C and 142 °C, respectively (Figure S4-4).

Subsequently, DSC was performed (see Figure 4-1). All samples were subjected to a heat-cool-heat cycle heating to 130 °C and cooling to −20 °C. FpC_5, FpC_6 and FpC_8 melted during the initial heating cycle (see Figure 4-1a). No melting endotherm was observed for FpC_{10} (Figure 4-1a), as it never crystallized and remained a very viscous liquid similar to molasses. As shown in Figure 4-1b, no crystallization nor cold crystallization was observed during subsequent cooling or reheating and all analogues underwent a glass transition during cooling and reheating.

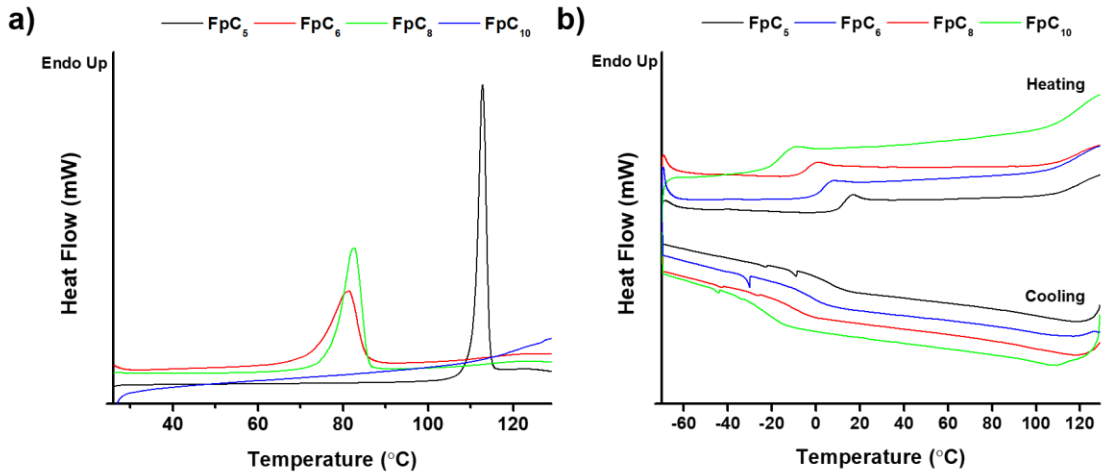

Figure 4-1 a) DSC thermograms for FpC_x (x = 5, 6, 8, 10) during the initial heating cycle. Endothermic melting peaks are observed for all analogues except FpC_{10}. b) DSC thermograms for FpC_x (x = 5, 6, 8, 10) during the subsequent cooling and reheating cycle. No recrystallization or cold crystallization is observed. In addition, all analogues undergo a glass transition.

Table 4-1 Summary of melting and glass transition temperatures of FpC_x (x = 5, 6, 8, 10)

Length of Alkyl Chain	Melting Temperature (°C)	Glass Transition Temperature (°C)
5	112.8	13.1
6	81.5	3.8
8	82.6	-3.8
10	--	-16.8

In the case of FpC_6, the suppression of crystallization and a glass transition are attributed to the presence of supramolecular polymer chains. Therefore, the similar thermal behaviour of FpC_x (x = 5, 8, 10) may be caused by the presence of supramolecular polymer chains. To investigate this possibility, PXRD was used to characterize the melts of FpC_x (x = 5, 8, 10). As shown in Figure 4-4, all FpC_x analogues show the characteristic double peak attributed to the presence of chains with structure **1**. Consequently, all FpC_x analogues appear to form BSP. As shown in Table 4-1, the T_g of FpC_x analogues decreases as the length of the alkyl chain in the monomer increases. This effect is similar to when alkyl side chain length are increased in covalent polymers.[87] The decrease in T_g is attributed to the introduction of more free volume which reduces the packing density, resulting in a lower T_g.[144] Shortening the alkyl chain length to 5 carbons resulted in a higher T_m than FpC_6. In contrast, increasing the alkyl chain length to 8 carbons, resulted in a slightly higher T_m than FpC_6. These results make it difficult to establish a clear trend on the effect of alkyl chain length on T_m. It is worthwhile to note that when the alkyl chain was increased to 10, the material did not crystallize even when stored at room temperature for over 1 year. This may be caused by the polymorphic nature of FpC_6 and potentially the analogues as well. Even after storing for over one year at room temperature FpC_{10} does not crystallize, making it an ideal candidate for future research into these systems.

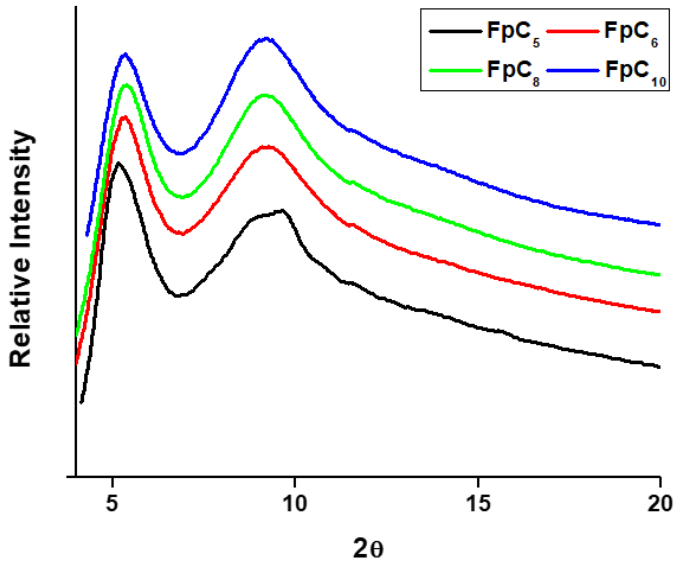

Figure 4-2 PXRD diffractograms for FpC_x (x =5, 6, 8, 10). All analogues display the characteristic double peak pattern associated with chain structure **1**. This result indicates that all analogues form BSP.

4.6 Influence of Thermal History on FpC_6 and FpC_8

4.6.1 Effect of Upper Heating Temperature and Annealing on T_g (FpC_6)

In order to create a reproducible initial state it is necessary to explore the effect of heating temperature on the supramolecular polymer chains after melting. Crystalline FpC_6 samples were heated to the specified upper heating temperature (above T_m), cooled to − 20 °C and re-heated to the specified upper heating temperature. The experiments were repeated three times to ensure reproducibility.

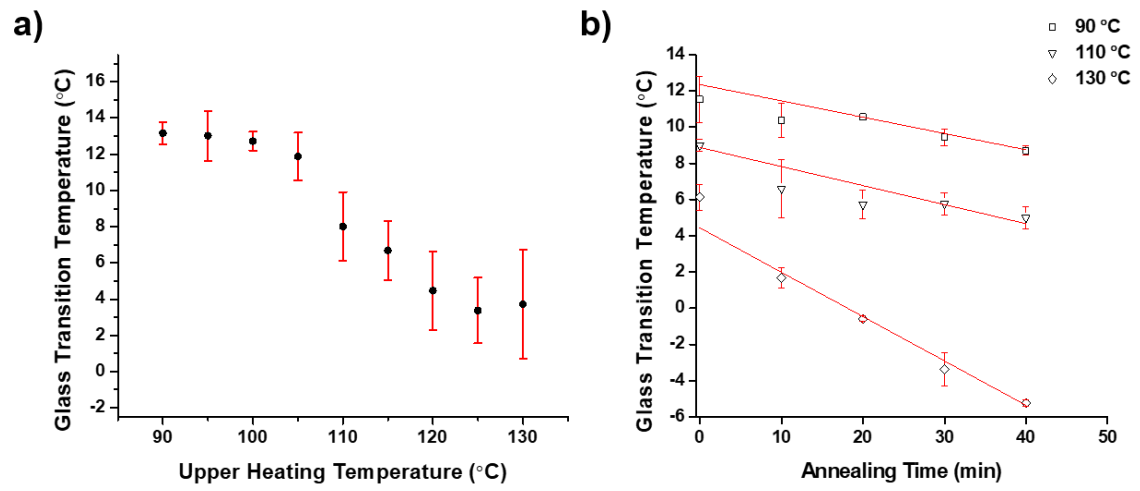

Figure 4-3 a) Glass transition temperature vs. upper heating temperature for FpC_6 during heating cycle. b) Glass transition temperature as a function of annealing at 90, 110, 130 °C for FpC_6 during heating cycle.

As previously discussed, during the first heating cycle a melting peak was observed; however, no recrystallization occurred. Subsequently, a glass transition temperature was observed during both the cooling and reheating cycles. As shown in Figure 4-3a, when FpC_6 is heated to 90-100 °C, the T_g does not change significantly. However, the T_g decreases as the samples are heated to higher temperatures. The results demonstrate that the network formed by FpC_6 supramolecular polymer chains is changing when the sample is heated to temperatures above T_m.

To determine if the networks reach an equilibrium structure at temperatures above T_m, FpC_6 was annealed at different temperatures. Samples were heated to the specified annealing temperature using a ramp rate of 10 °C/min. Once at the annealing temperature samples were annealed for 0, 10, 20, 30 or 40 minutes. After annealing, the samples were cooled to −20 °C and reheated to the annealing temperature using a temperature ramp rate of 10 °C/min. The experiments were performed twice and the results are summarized in Figure 4-3b.

At all temperatures investigated, T_g decreased linearly with increasing annealing time. This suggests that the network is changing at higher temperatures. In addition, the network structures appear to change faster at higher temperature. To see if an equilibrium structure could be reached at higher temperatures, a sample of FpC_6 was annealed at 130 °C for 60 and 90 minutes. When annealed at 130 °C for 60 and 90 minutes, the T_g decreased to −9.2 °C and −12.3 °C, respectively. These results show that the network does not reach an equilibrium structure even after annealing for 60 minutes at 130 °C.

4.6.2 Hysteresis (FpC_6)

From the results discussed in the previous section, it is clear that it takes a significant amount of time for the FpC_6 network to reorganize even at higher temperatures. Consequently, an interesting question is how significant is the reorganization upon cooling. Samples of FpC_6 were subjected to multiple heating cycles by first heating to 130 °C and then to 90 °C. As shown in Figure 4-4a, the T_g does not change. When the heat cycles were performed by first heating to 90 °C and then to 130 °C, the T_g decreased as shown in Figure 4-4b. These hysteresis experiments show that little reorganization occurs during cooling or subsequent reheating cycles. Consequently, the T_g is determined by the highest temperature reached.

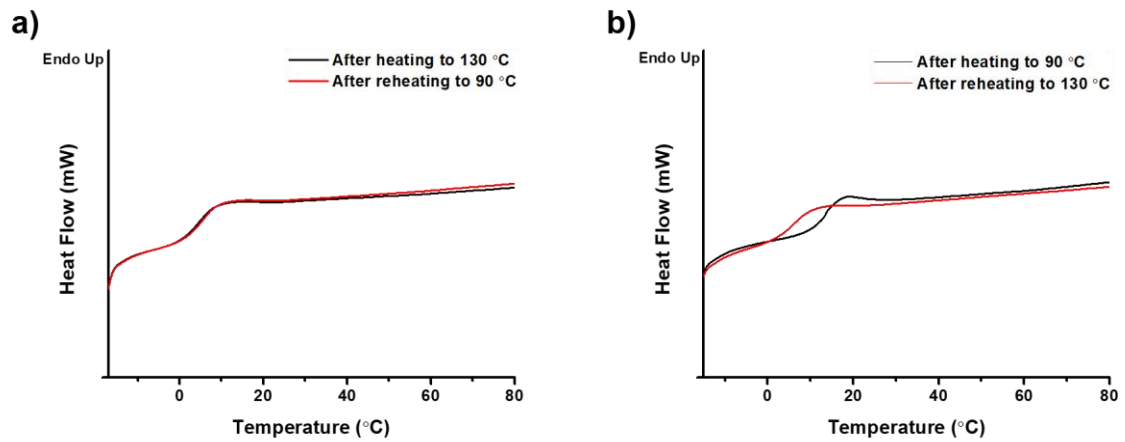

Figure 4-4 a) DSC thermogram for FpC_6 after initial heating of the sample to 130 °C and subsequent reheating to 90 °C. b) DSC thermogram for FpC_6 after initial heating of the sample to 90 °C and reheating to 130 °C.

4.6.3 Effect of Temperature on Supramolecular Chain Length (FpC_6)

To investigate how the network structure changes with annealing, ideally PXRD should be performed at the annealing temperature to see how the diffractogram changes over time. However, it was not possible to perform PXRD at temperatures above 90 °C, due to the need to protect the X-ray detector from high temperatures. Consequently, to understand the effect of temperature on the length of the supramolecular chains, PXRD of fresh and aged FpC_6 was performed at different temperatures below 90 °C (Figure 4-5). The double peak pattern of freshly melted FpC_6 did not change with increasing temperature (Figure 4-5a). In contrast, the double peak pattern of aged FpC_6 changed significantly with temperature (Figure 4-5b). For aged FpC_6, the intensity of the first and second peak decreases as the temperature increases. Additionally, the second peak broadens significantly. The decrease in intensity and broadening of the peaks indicates that the sample is becoming more disordered as the temperature increases. Since the change in double peak pattern occurs below the T_m, this behaviour can be interpreted as the disassembly of FpC_6 chains as the temperature is increased. Notably, the

double peak pattern does not significantly change between 65 °C and 85 °C. DSC indicates that the change in T_g is very slow at temperatures below 100 °C. Therefore, the double peak pattern may not change significantly because the FpC_6 chains need more time to further shorten. Interestingly, the double peak pattern of freshly melted FpC_6 does not change with temperature, because the temperatures investigated are below the temperature used to prepare the sample. As previously discussed, the length of the FpC_6 chains was determined by the highest temperature reached. Consequently, the chains in the freshly melted sample have already shortened to their length at 110 °C and they will not shorten further as the temperature is increased from 25 °C to 85 °C. Based on these results we tentatively attribute the decrease in T_g after annealing at high temperatures to the depolymerisation of the supramolecular polymer chains at higher temperatures. The combination of DSC and PXRD experiments show that re-polymerization appears to be slow and does not occur on the timescale of the experiments.

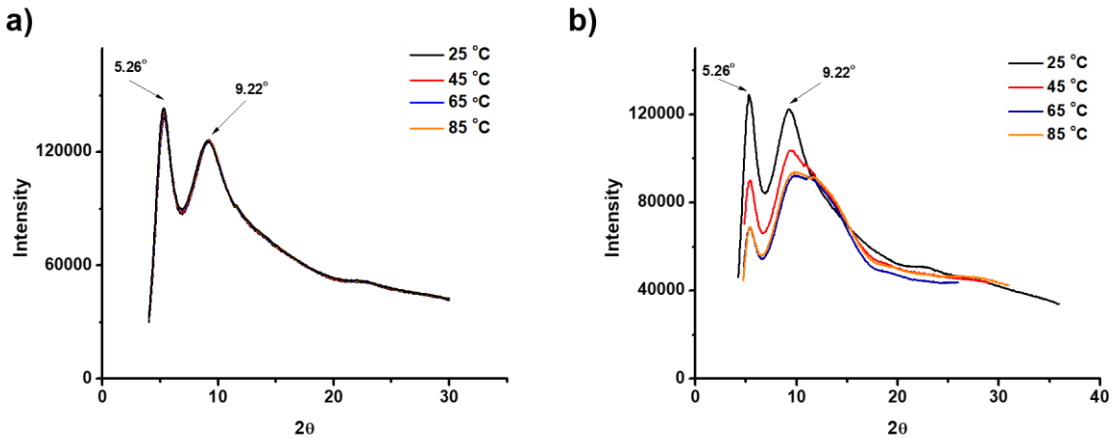

Figure 4-5 a) PXRD diffractogram for freshly melted FpC_6 at different temperatures. The double peak pattern does not change suggesting that the chains are not affected by temperature. b) PXRD diffractogram for aged FpC_6 at different temperatures. The intensity of the peaks decrease as the temperature increases, indicating that the sample is becoming more disordered. This implies the chains shorten with increasing temperature.

4.6.4 Effect of Upper Heating Temperature and Annealing on T_g (FpC_8)

To explore how the length of the alkyl chain affects the disassembly of the supramolecular polymer chains FpC_8 was heated to different temperatures above T_m and the resulting T_g was determined as shown in Figure 4-6. Compared to FpC_6, the T_g of FpC_8 decreases as the sample is heated to higher temperatures until 120 °C. Heating FpC_8 to 125 °C or 130 °C did not significantly change the T_g, suggesting that the length of FpC_8 chains do not significantly shorten when heated to these temperatures during the time of the DSC experiment. Samples of FpC_8 were annealed at 110 °C for 0-40 minutes. Like FpC_6, the T_g of FpC_8 decreases with increasing annealing time, suggesting that the chains shorten. In the case of FpC_8, after annealing for 40 minutes the T_g at 110 °C changes by approximately 5 °C. In contrast, the T_g of FpC_6 only changes by approximately 3 °C. This suggests that FpC_8 disassembles faster at 110 °C due to the increased mobility of the monomers from the longer alkyl chains.

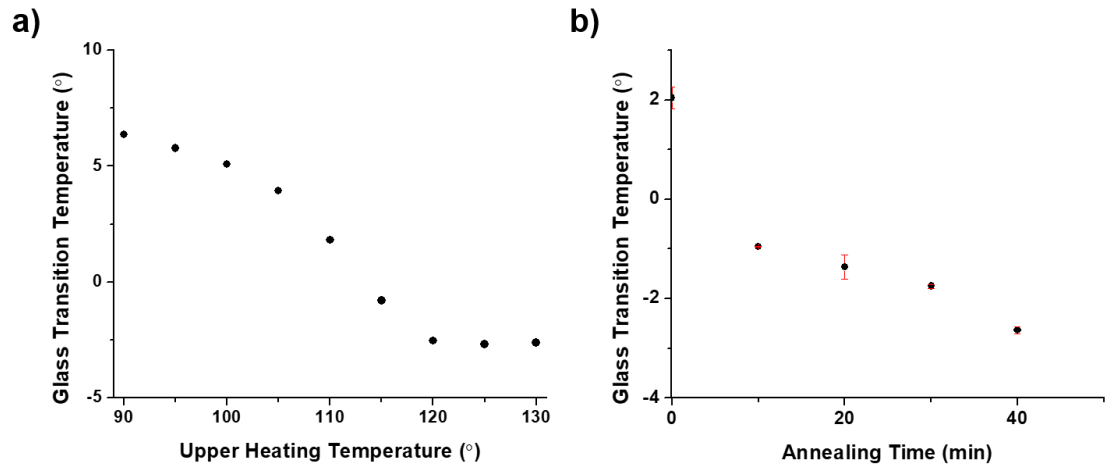

Figure 4-6 a) Glass transition temperature vs. upper heating temperature for FpC_8 during heating cycle. b) Glass transition temperature as a function of annealing at 110 °C for FpC_8 during heating cycle.

4.9 Conclusion

In summary, melts of FpC_x analogues (x = 5, 8, 10) display the characteristic double peak pattern attributed to the presence of chain structure **1**. For all analogues, crystallization is suppressed within the timescale of DSC experiments and a glass transition is observed. From the presence of the double peak pattern in the melts, this thermal behaviour is attributed to the formation of supramolecular chains. Consequently, all FpC_x analogues appear to form BSP. Despite being stored at room temperature for over a year, FpC_{10} never crystallized, suggesting that increasing the alkyl chain length to 10, can prevent crystallization completely. Therefore, FpC_{10} may be a good candidate to further explore the mechanical behaviour and ageing of these BSP, since crystallization is prevented. For FpC_6 and FpC_8, as the upper heating temperature is increased the T_g decreases. This is attributed to the shortening of the supramolecular polymer chains. No significant re-polymerization occurs during cooling, suggesting that the BSP exist under kinetic control at the temperatures investigated. Annealing FpC_6 and FpC_8 at temperatures above T_m, reveals that T_g decreases with increasing annealing time. The T_g decreases faster when annealed at higher temperatures, possibly due to the higher mobility of the monomer, which increases the rate of depolymerisation. Re-polymerization at low temperatures may be slow because of the low mobility of the monomer. Lastly, these experiments reveal that simply melting the sample is insufficient to erase the thermal history. Annealing the samples at temperatures above T_m is required to achieve a reproducible initial state and the initial length of the FpC_6 chains will depend on both the temperature and time used to anneal the sample. The experiments in this chapter represent a significant step forward in overcoming the sensitivity to thermal history associated with BSP obtained from small molecules.

Chapter 5. Summary and Future Work

5.1 Summary

As discussed in Chapter 1, despite the significant progress of solution based SP, the development of BSP has been hindered by restrictive monomer requirements. Namely, the directionality and strength of the intermolecular interactions must be carefully balanced alongside the mobility of the monomer in order to prevent crystallization. Different design strategies have been adopted to overcome this barrier. While the use of macromonomers has been successful, it does not take full advantage of having an entirely reversible backbone. The use of small molecule monomers takes full advantage of having a reversible backbone, improving processability and stimuli-responsiveness. Additionally, the anisotropy arising from the ordering of the monomers in the chain imparts additional properties such as liquid crystalline behaviour. The critical challenge with this approach, is the tendency of small molecules to crystallize.

Crystallization can be prevented by carefully designing the monomers. It has been shown that by using strong binding motifs between monomers, it is possible to sequester the monomers in the chain, preventing crystallization. Furthermore, the addition of bulky or flexible substituents can reduce crystallization and improve monomer mobility. Additionally, monomer asymmetry has also been shown to play a role in preventing crystallization. Due to the complexities of monomer design, the monomers are developed from well-established binding motifs such as the interactions between thymine and adenine or the self-association of ureido-4-pyrimidone. The innovation of monomer designs based on novel binding motifs is virtually non-existent, because of the lack of understanding on how intermolecular interactions can be used in the solid state to direct the assembly of molecules.

Crystal engineering has emerged as a powerful tool to understand how intermolecular interactions direct the packing of molecules in the solid state. In particular, weaker intermolecular interactions, such as C—H---O interactions, have been shown to play a significant role in directing the packing of molecules in the bulk state. Furthermore, aromatic embraces have been shown to form one dimensional chain structures in crystalline material; however, no examples of these chains forming polymeric material has been reported thus far. Recently, crystal engineering has been successfully used to elucidate the structure of solution SP based on weak non-covalent interactions formed *via* C—H---O and C—H---π interactions. However, no reported examples of BSP based on weak intermolecular interactions have been reported.

Organometallic small molecules are promising candidates as new monomers for BSP, thanks to their unique metal coordination geometry. Based on this, Chapter 2 discusses the synthesis and crystal engineering of an organometallic small molecule monomer FpC_6. Following successful synthesis, crystal engineering was performed to elucidate the intermolecular interactions and packing motifs available to FpC_6. By recrystallizing under a variety of conditions, five unique structural morphologies were obtained, revealing the highly polymorphic nature of FpC_6. Short contact analysis of the supramolecular structures reveals that FpC_6 is involved in different C—H---O interactions and aromatic embraces. Of the five supramolecular structures, four of them consist of repeating one dimensional chains.

When recrystallized from non-polar solvent conditions, supramolecular structures **1**, **2**, and **3** were obtained. In these crystalline solid-state structures, FpC_6 formed chains through cooperative aromatic embraces and C—H---O hydrogen bonding. In the case of supramolecular structures **1** and **2**, the same duplex ladder structure is observed which is

formed by two repeating chains EF_3 embraces linked at their edges OFF(EF_2) embraces and C—H---O hydrogen bonds. Since this structure is obtained in two unique supramolecular structures, it suggests that this packing motif is indeed a supramolecular synthon for FpC_6. In the case of supramolecular structure **3**, a zig-zag chain structure was formed by repeated EF_4 embraces and C—H---O hydrogen bonds. Supramolecular structures **4** and **5**, were obtained by recrystallizing from methanol and a 15% H_2O: 85% ethanol solution, respectively. Supramolecular structure **4** consisted of a firecracker ladder chain formed through a repeating motif of EF_4 embraces linked at their edges through an OFF(EF_2) embrace. Lastly, supramolecular structure **5** consisted of FpC_6 molecules packed so as to create alternating sequences of P4PE. These results highlight that the packing motifs of FpC_6 are governed by a balance between C—H---O interactions and aromatic embraces. Under fast recrystallization and polar solvent conditions, FpC_6 packs to maximize aromatic interactions. On the other hand, under slow non-polar solvent conditions, FpC_6 molecules pack to optimize both hydrogen bonding and aromatic interactions.

The results presented in Chapter 2 highlight FpC_6's propensity to form one dimensional chains in the supramolecular structures. Crystal engineering establishes an in-depth understanding of the binding motifs of FpC_6 and how they are governed by the interplay between hydrogen bonding and aromatic embraces. This work highlights the power of crystal engineering to elucidate weak intermolecular interactions and bonding motifs in the solid state.

Expanding upon the knowledge developed in Chapter 2, Chapter 3 explored the bulk supramolecular polymerization of FpC_6. After a cycle of heating and cooling, FpC_6 forms a sticky red solid. Fibres could be drawn from the red solid and a free-standing film could be formed by compression molding. Over time, the sticky red solid formed a resin-like brown

solid which could be molded into a variety of shapes. This physical behaviour is characteristic of polymers. PXRD was used to characterize the chain structure responsible for this behaviour. The diffractogram of amorphous FpC_6 revealed a characteristic double peak pattern attributed to chain structure **1**, which was observed in supramolecular structures **1** and **2**.

DSC revealed that after melting during an initial heating cycle, FpC_6 does not recrystallize on the time scale of the DSC experiments. Over days to weeks, however, FpC_6 eventually crystallizes depending on storage conditions. Upon cooling and reheating, a glass transition was observed. These results are characteristic of BSP formed by strong hydrogen bonding which sequester the monomers in the chains. Excitingly, this behaviour is observed in FpC_6 where the chains are formed by aromatic embraces and C—H---O hydrogen bonding, which are comparatively weaker interactions. This remarkable achievement is attributed to the cooperative nature of the weak interactions involved. Furthermore, PXRD of FpC_6 at 100 °C and of a sample quenched from 130 °C suggests the chains are present well above the crystalline melting temperature. These results highlight the thermal stability of the chain structure.

The mechanical properties of FpC_6 are influenced by a variety of factors. In particular, FpC_6 was sensitive to the ageing process. Freshly prepared FpC_6 behaved like a viscous liquid, whereas aged FpC_6 displayed viscoelastic behaviour characteristic of chain entanglement. Assuming chain entanglement, the M_e was estimated to be 5091 g/mol, or approximately 10 FpC_6 molecules. Additionally, the complex viscosity of aged FpC_6 displays shear thinning behaviour. Both freshly prepared and aged FpC_6 exhibit a tan δ peak during dynamic oscillatory experiments. This tan δ peak is attributed to relaxation *via* chain scission due to the dynamic nature of non-covalent interactions. The position of the tan δ peak shifted to lower

frequencies as the temperature decreased, suggesting that the average lifetime of the supramolecular polymer chains increases with decreasing temperature. When characterized at the same temperature the tan δ peak of aged samples occurred at lower frequencies than freshly melted FpC_6 samples. This suggests that ageing may increase the average lifetime of the supramolecular polymer chains. Furthermore, time sweeps of aged FpC_6 showed that the samples become more elastic over time, potentially due to elongation of the chains. This suggests that the mechanical response of FpC_6 is sensitive to measurement history as well. While PXRD experiments show that no sharp crystalline peaks are observed in aged FpC_6 samples, the formation and presence of microcrystallites cannot be ruled out. While the mechanical behaviour of FpC_6 is rich and promising, reproducibility is challenging, because of the sensitivity of FpC_6 to thermal history, ageing, measurement history as well as the appearance of an FpC_6 induced instrument artifact.

The results discussed in Chapter 3 demonstrate the formation of the first bulk supramolecular polymer based on aromatic embraces and weak hydrogen bonding. These intermolecular interactions have long been overlooked in the field and represent a dramatically different approach to monomer design. FpC_6 forms a glassy state and suppresses crystallization on the timescale of DSC experiments which is difficult to achieve, even for BSP formed with strong intermolecular interactions. Finally, the complex mechanical behaviour of FpC_6 highlights the promising behaviour and challenging nature of these systems.

To address the challenges encountered in Chapter 3, Chapter 4 explores FpC_x (x = 5, 8 and 10) analogues with different alkyl chain lengths to see if crystallization can be suppressed. In addition, a detailed investigation of the influence of thermal history on FpC_6 and FpC_8 was carried out. FpC_x (x = 5, 8 and 10) analogues appear to form BSP with chain structure **1**. The

FpC_x analogues do not recrystallize on the time scale of the DSC experiments and all are capable of forming a glassy state. As the alkyl chain length increases, the T_g decreases. Excitingly, when the alkyl chain length was increased to ten carbons long, no crystallization occurred even after storage at room temperature for over a year.

The T_g of FpC_6 and FpC_8 was found to decrease with increasing upper heating temperature and annealing time, suggesting that the networks are not at equilibrium and are changing over time. Based on temperature dependent PXRD experiments of aged FpC_6, the decrease in T_g is attributed to the de-polymerization of the supramolecular chains. Annealing FpC_6 at temperatures above the T_m indicates that the chains disassemble faster at higher temperatures. The T_g of FpC_8 appears to decrease at a faster rate than FpC_6 when annealed at the same temperature. This suggests that FpC_8 may disassemble faster due to the higher mobility of the monomer (from the longer alkyl chain). Hysteresis experiments show that no significant polymerization occurs during subsequent cooling or reheating cycles.

The work discussed in Chapter 4 demonstrates that FpC_x analogues are capable of forming BSP. Interestingly, the chain structure for these analogues appears to be chain structure **1**, suggesting that this binding motif can be readily applied to other analogues. FpC_{10} did not recrystallize despite being stored at room temperature for over a year. Consequently, FpC_{10} may be an ideal candidate to investigate the mechanical behaviour of these systems. The detailed investigation of the thermal history of FpC_6 and FpC_8 suggests the supramolecular polymerization process is not under equilibrium control. The results also demonstrate that the T_g can be systematically manipulated by exposing the BSP to high temperatures, possibly due to the disassembly of the chains. Having developed a strong understanding of the influence of

thermal history, it is possible to establish a reproducible initial state necessary for future investigation into the ageing process of these systems.

In conclusion, FpC_6 and its analogues are the first reported BSP formed *via* aromatic embraces and weak hydrogen bonding. These interactions have long been ignored because they lacked directionality and were considered too weak to sequester the monomers in the chains. This research demonstrates that these interactions are capable of forming BSPs which display viscoelasticity and can undergo a glass transition. This research was made possible by crystal engineering, which was used to identify new bonding motifs and understand how intermolecular interactions govern the packing of the molecules in the solid state. While this research is challenging, it opens the door for the development of new monomers to enable the progression of the field.

5.2 Future Work

Additional rheological experiments are required to understand the mechanical behaviour of FpC_6. In particular, experiments that investigate the influence of temperature and measurement history on the mechanical behaviour need to be carried out. These experiments are crucial as they might provide the temperature at which the supramolecular polymer chains elongate. Further investigation into the thermal behaviour of FpC_6 is required. The effects of annealing and hysteresis remain unexplored. By using DSC to investigate the effect of annealing at temperatures below T_m on the glass transition temperature, it may be possible to determine the temperature where polymerization becomes significant. This information would be invaluable to future investigations into FpC_x analogues.

FpC_6 and its analogues are the first series of monomers capable of forming a BSP *via* C—H---O hydrogen bonding and aromatic embraces. Consequently, they represent a unique opportunity to explore the resulting behaviour and properties of BSP formed by interactions which have been historically overlooked. While the research has been challenging, the results are quite encouraging. In particular, the large tan δ peak observed in the mechanical behaviour indicates that FpC_6 may be useful in applications involving the dissipation of kinetic energy. For example, FpC_6 could be used in the padding of sporting equipment to help mitigate impact. Also, since the dielectric constant of FpC_6 is comparable to SiO_2 and since FpC_6 can be processed slightly above room temperature, FpC_6 could be used as a dielectric in printed electronics. Before these potential applications can be realized, a number of key challenges must be addressed.

Firstly, the tendency of FpC_6 to crystallize and the metastable nature of the chains must be overcome in order to be used in applications and further research into the mechanical behaviour. It might be possible to prevent crystallization by the addition of a suitable plasticizer to the system, such as decane or dodecane. Preparing mixtures of two or more FpC_x (x = 5, 6, 8, 10) analogues may also prevent crystallization and change the mechanical behaviour of the resulting BSP. Since FpC_{10} did not crystallize, it is an ideal analogue to begin preparing different ratio mixtures with the other analogues. The introduction of branching into the alkyl chain is another route which may prevent the crystallization. Branching may also alter the mechanical behaviour and the glass transition. Bifunctional molecules could be synthesized with Fp groups at each end of an aliphatic spacer. These bifunctional molecules could potentially act as supramolecular cross-linkers which may modify the mechanical behaviour

of the BSP and prevent crystallization. It may be worthwhile to explore tritopic or tetratopic Fp molecules as they may generate network BSP rather than linear BSP.

Another key challenge that needs to be addressed is determining the molecular weight of the supramolecular polymer chains. To date, it has not been possible to directly characterize the molecular weight of FpC_6. Matrix-assisted laser desorption ionization time of flight (MALDI-TOF) mass spectrometry might be capable of characterizing the molecular weight of FpC_6 directly. However, preliminary attempts reveal that FpC_6 decomposes during MALDI-TOF measurements. In order for this technique to work a suitable matrix will need to be found.

If the concentration of the unassociated monomer and aggregated monomer can be determined, it may be possible to determine the molecular weight of the supramolecular polymer chains and potentially the mechanism (isodesmic vs. nucleation-growth) of supramolecular polymerization. Due to the embraces that form the polymer chain and the proximity of the phosphorus atoms, solid-state ^{31}P NMR may be able to distinguish between unassociated and associated monomers. If this is not possible, the addition of a chromophore, such as bithiophene or pyrene to the alkyl chain, might allow for the determination of the concentration of associated vs. unassociated monomer using uv-vis or fluorescence spectroscopy. However, the introduction of these chromophores may change the self-assembly behaviour of FpC_6, because the aforementioned chromophores can interact *via* aromatic interactions.

To help establish the role of the aromatic embraces and support the proposed chain structure it would be worthwhile to prepare an analogue with a phosphorus ligand which incorporated cyclohexane rings rather than phenyl rings. The resulting solid-state self-assembly behaviour or lack thereof, would provide valuable insight into the importance of the

aromatic embraces. The weak hydrogen bonding of the system could be further explored by using a different metal ion, such as Mo or Co, instead of Fe. The use of different metals will affect the polarity and number of CO ligands, which will change the hydrogen bonding of the system. Exploring new FpC_x analogues which incorporate different alkyl ligand and metals, will undoubtedly deepen the understanding of this newly discovered system and unlock its potential.

Appendices

Supporting Information for Chapter 3

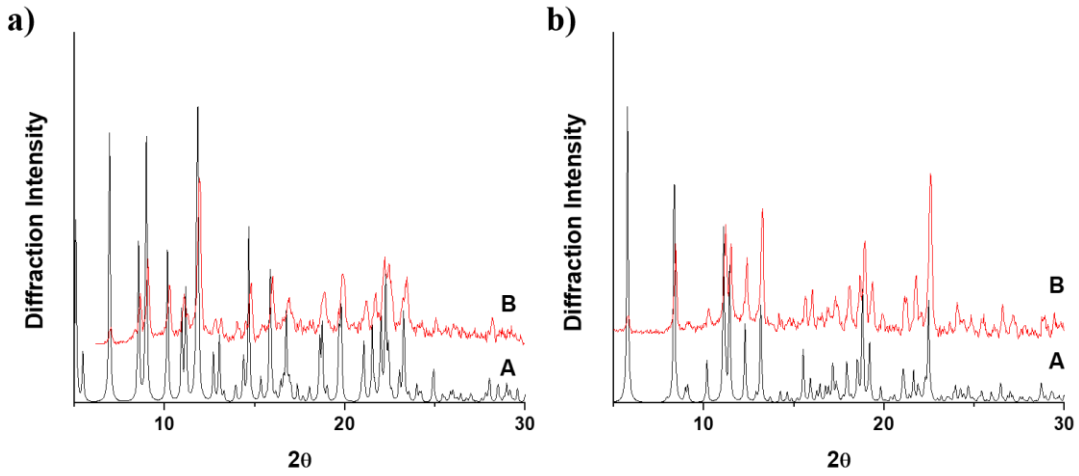

Figure S3-1 a) Comparison between the simulated powder diffractogram for supramolecular structure **1** (A) and the experimental diffraction pattern (B). b) Comparison between the simulated powder diffractogram for supramolecular structure **3** (A) and the experimental diffraction pattern (B).

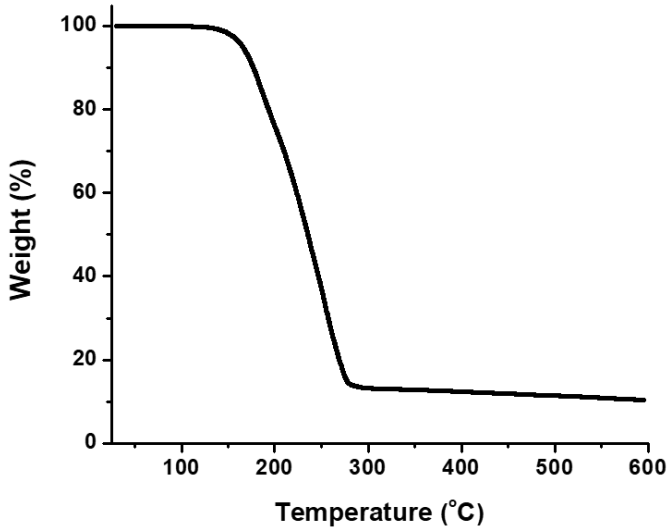

Figure S3-2 TGA analysis of FpC_6. Onset of decomposition (corresponding to 1 % weight loss) occurs at 136 °C.

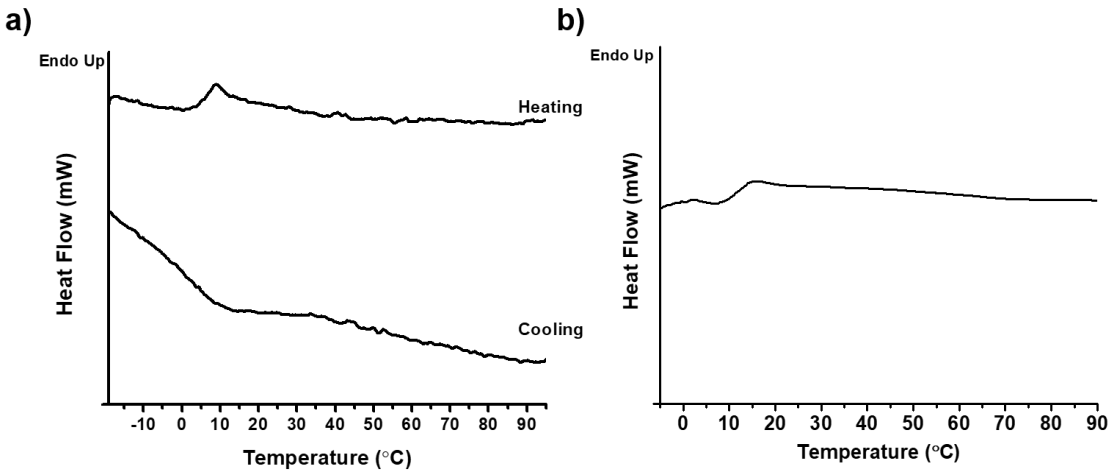

Figure S3-3 a) DSC thermogram for the cooling and reheating cycles after melting using a temperature ramp rate of 1 °C/min. No crystallization exotherm is observed. b) DSC thermogram for FpC_6 during heating cycle after annealing for two hours at 50 °C. No crystallization exotherm is observed.

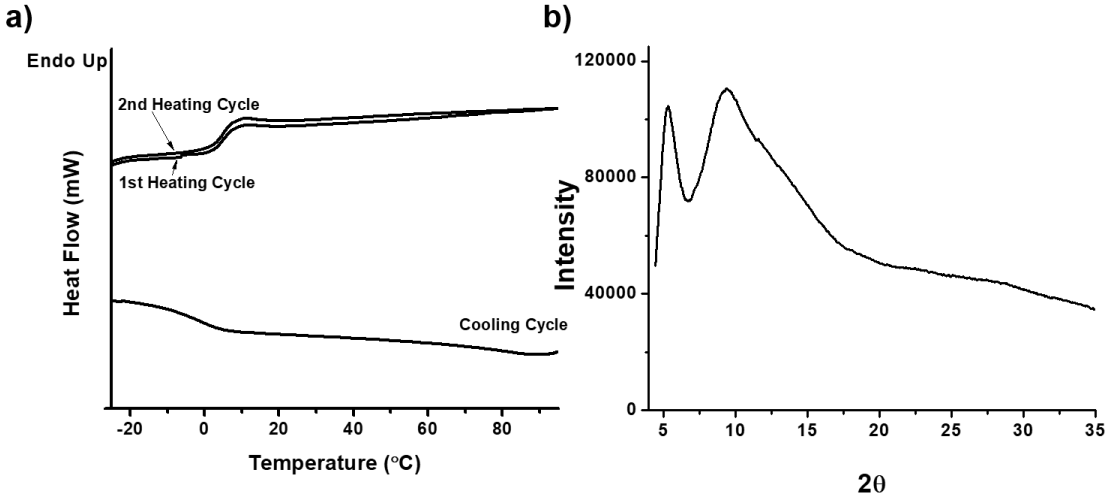

Figure S3-4 a) DSC thermogram for FpC_6 which had been aged at −50 °C for 4 months. No crystallization exotherm or melting endotherm are observed, indicating the material has not crystallized. b) PXRD for FpC_6 which had been aged at −50 °C for 4 months. Samples was heated to 50 °C for 3 hours prior to performing PXRD to soften the sample for loading. No sharp crystalline peaks are observed indicating the material remains amorphous.

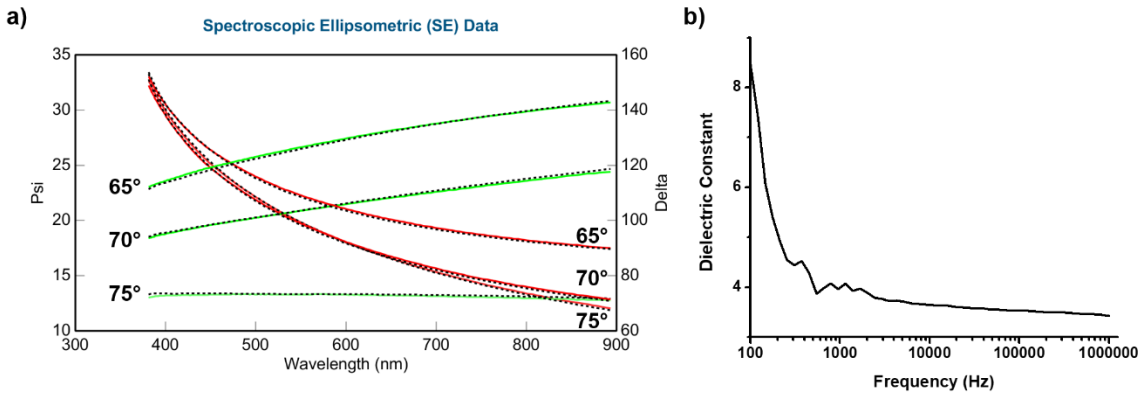

Figure S3-5 a) Ellipsometry data, Psi (green) and delta (red), fitted by model (black dotted line). b) Dielectric constant of FpC_6 as a function of frequency.

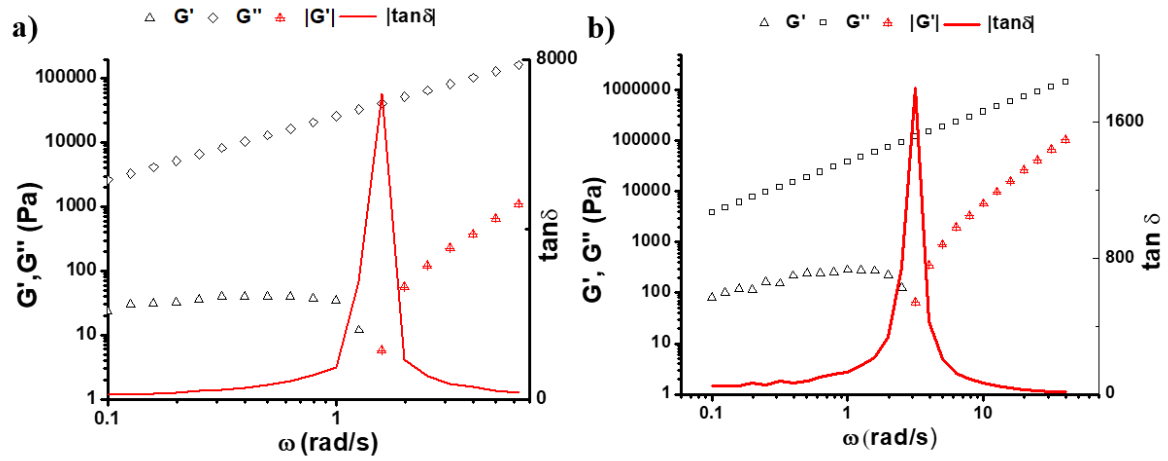

Figure S3-6 a) Results of a dynamic oscillatory experiment for freshly melted FpC_6 at 26 °C using a strain of 4%. Note: after 1.26 rad/s, the phase angle exceeds 90°. As a result, the rheometer reports negative G' and tan δ values. Consequently, the absolute values of G' and tan δ are reported. b) Results of a dynamic oscillatory experiment for aged amorphous FpC_6 at 36 °C using a strain of 2%. Note: after 2.5 rad/s, the phase angle exceeds 90°. As a result, the rheometer reports negative G' and tan δ values. Consequently, the absolute values of G' and tan δ are reported

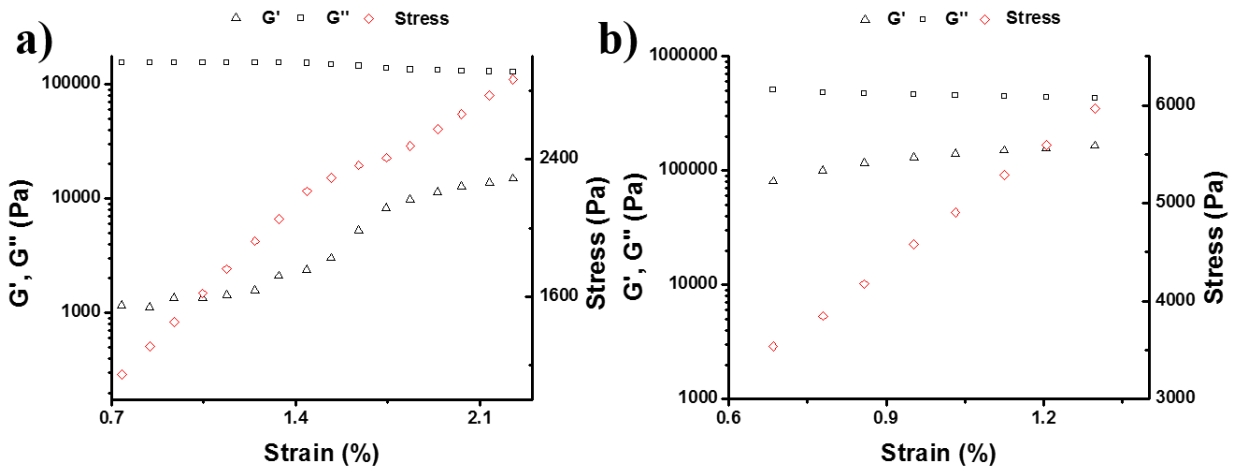

Figure S3- 7 a) Strain sweep performed on aged FpC_6 at 32 °C at a frequency of 1 rad/s. b) Strain sweep performed on aged FpC_6 at 26 °C at a frequency of 0.5 rad/s

Table S3-1 Tan δ peak positions at different temperatures, as the sample was cooled from 40 °C.

Temperature (°C)	Angular Frequency of tan δ peak (rad/s)
40	10
38	5
36	3.2
34	2
32	1
30	0.4
28	0.3
26	0.1

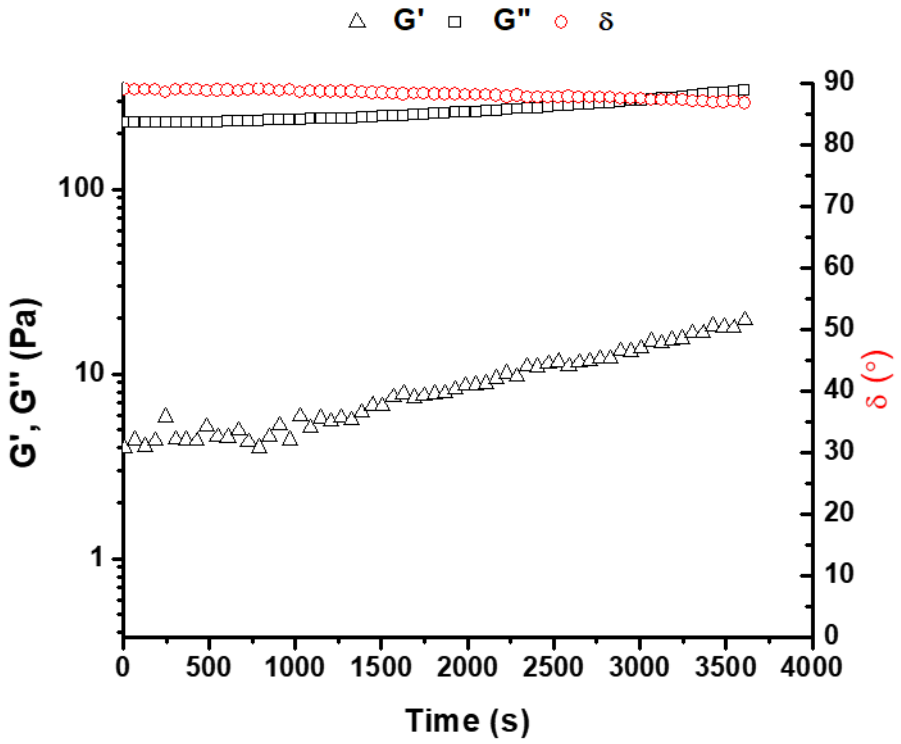

Figure S3-8 Time sweep at 50 °C of freshly melted FpC_6 using a strain of 30 % during the first hour. Measurements were made over 60 s intervals using a frequency of 1 rad/s.

Supporting Information for Chapter 4

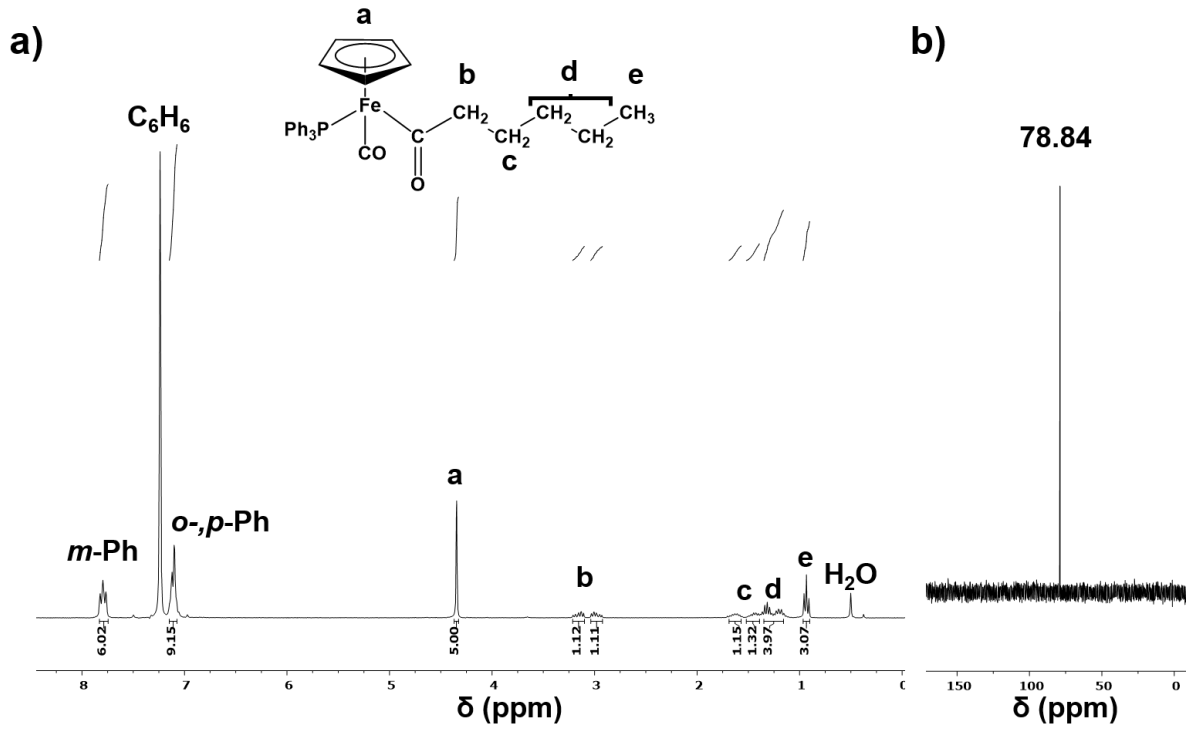

Figure S4-1 a) ^{1}H NMR and b) ^{31}P NMR spectra for FpC_5.

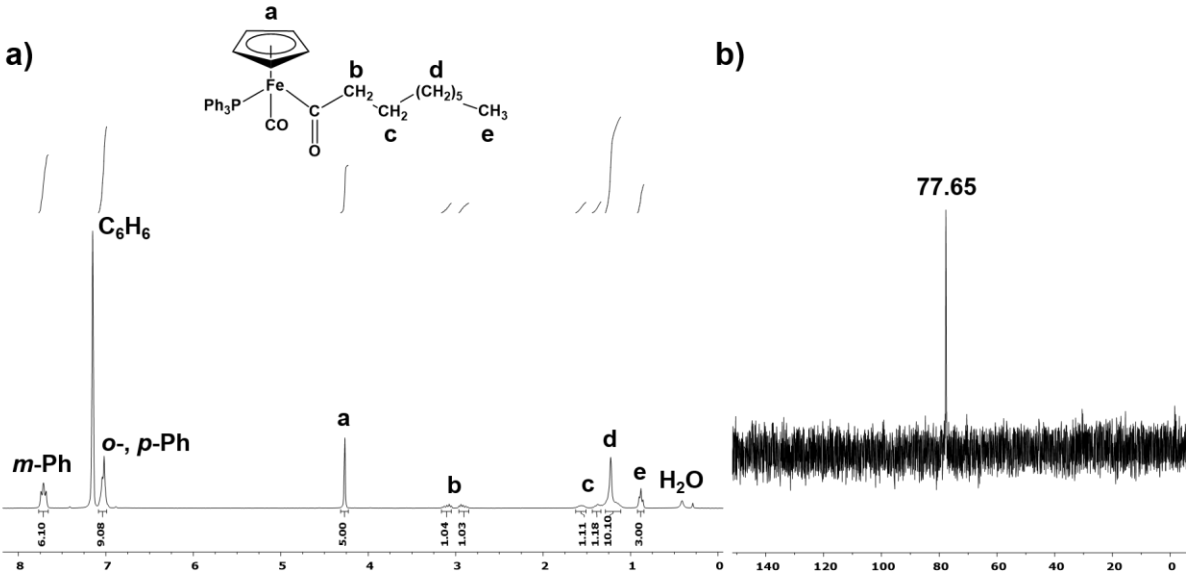

Figure S4-2 a) ^{1}H NMR and b) ^{31}P NMR spectra for FpC_8.

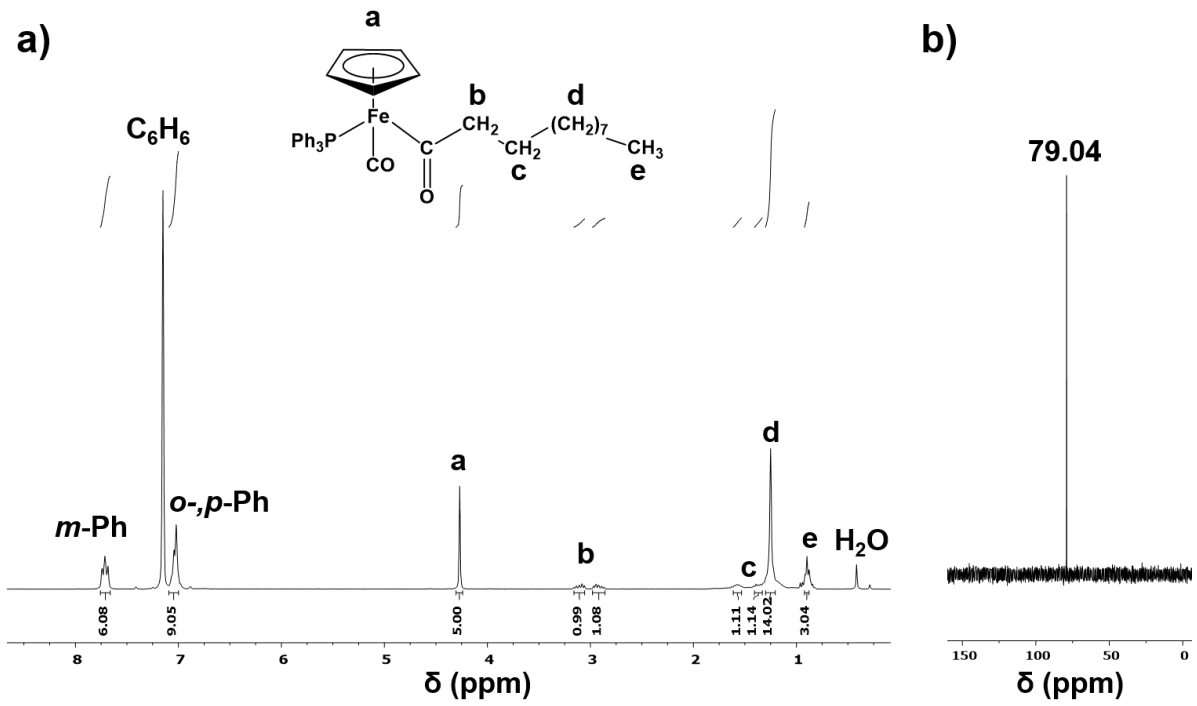

Figure S4-3 a) ^{1}H NMR and b) ^{31}P NMR spectra for FpC_{10}.

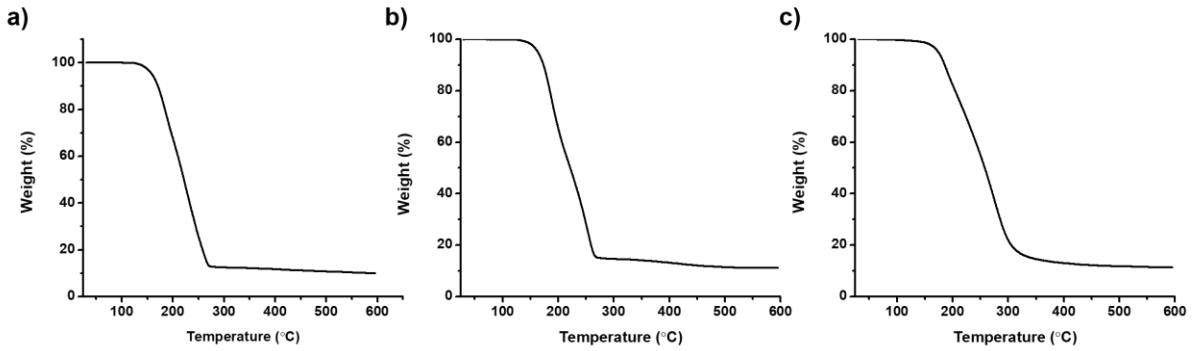

Figure S4-4 a) TGA analyses of FpC_5. Onset of decomposition (corresponding to 1 % weight loss) occurs at 137 °C. b) TGA analysis of FpC_8. Onset of decomposition (corresponding to 1 % weight loss) occurs at 142 °C. c) TGA analysis of FpC_{10}. Onset of decomposition (corresponding to 1 % weight loss) occurs at 142 °C.

References

1. Aida, T.; Meijer, E. W.; Stupp, S. I., Functional Supramolecular Polymers. *Science* **2012,** *335* (6070), 813-817.
2. Ligthart, G. B. W. L.; Scherman, O. A.; Sijbesma, R. P.; Meijer, E. W., Supramolecular Polymer Engineering. In *Macromolecular Engineering*, Wiley-VCH Verlag GmbH & Co. KGaA: 2007; pp 351-399.
3. De Greef, T. F. A.; Smulders, M. M. J.; Wolffs, M.; Schenning, A. P. H. J.; Sijbesma, R. P.; Meijer, E. W., Supramolecular Polymerization. *Chemical Reviews* **2009,** *109* (11), 5687-5754.
4. Brunsveld, L.; Folmer, B. J. B.; Meijer, E. W.; Sijbesma, R. P., Supramolecular Polymers. *Chemical Reviews* **2001,** *101* (12), 4071-4098.
5. Sijbesma, R. P.; Beijer, F. H.; Brunsveld, L.; Folmer, B. J. B.; Hirschberg, J. H. K. K.; Lange, R. F. M.; Lowe, J. K. L.; Meijer, E. W., Reversible Polymers Formed from Self-Complementary Monomers Using Quadruple Hydrogen Bonding. *Science* **1997,** *278* (5343), 1601-1604.
6. Ogi, S.; Sugiyasu, K.; Manna, S.; Samitsu, S.; Takeuchi, M., Living Supramolecular Polymerization Realized Through a Biomimetic Approach. *Nature Chemistry* **2014,** *6* (3), 188-195.
7. Kang, J.; Miyajima, D.; Mori, T.; Inoue, Y.; Itoh, Y.; Aida, T., A Rational Strategy for the Realization of Chain-Growth Supramolecular Polymerization. *Science* **2015,** *347* (6222), 646-651.
8. Ogi, S.; Stepanenko, V.; Sugiyasu, K.; Takeuchi, M.; Würthner, F., Mechanism of Self-Assembly Process and Seeded Supramolecular Polymerization of Perylene Bisimide Organogelator. *Journal of the American Chemical Society* **2015,** *137* (9), 3300-3307.
9. Lehn, J., Supramolecular Polymer Chemistry-Scope and Perspectives. In *Supramolecular Polymers*, 2nd ed.; Ciferri, A., Ed. CRC Press: Boca Raton, 2005; pp 3-28.
10. Brienne, M.-J.; Gabard, J.; Lehn, J.-M.; Stibor, I., Macroscopic Expression of Molecular Recognition. Supramolecular Liquid Crystalline Phases Induced by Association of Complementary Heterocyclic Components. *Journal of the Chemical Society, Chemical Communications* **1989,** (24), 1868-1870.
11. Kato, T.; Fréchet, J. M. J., A New Approach to Mesophase Stabilization Through Hydrogen Bonding Molecular Interactions in Binary Mixtures. *Journal of the American Chemical Society* **1989,** *111* (22), 8533-8534.
12. Beijer, F. H.; Sijbesma, R. P.; Kooijman, H.; Spek, A. L.; Meijer, E. W., Strong Dimerization of Ureidopyrimidones via Quadruple Hydrogen Bonding. *Journal of the American Chemical Society* **1998,** *120* (27), 6761-6769.

13. Söntjens, S. H. M.; Sijbesma, R. P.; van Genderen, M. H. P.; Meijer, E. W., Stability and Lifetime of Quadruply Hydrogen Bonded 2-Ureido-4[1H]-pyrimidinone Dimers. *Journal of the American Chemical Society* **2000,** *122* (31), 7487-7493.
14. Tsuda, A.; Nagamine, Y.; Watanabe, R.; Nagatani, Y.; Ishii, N.; Aida, T., Spectroscopic Visualization of Sound-Induced Liquid Vibrations Using a Supramolecular Nanofibre. *Nature Chemistry* **2010,** *2*, 977-983.
15. Schenning, A. P. H. J.; v. Herrikhuyzen, J.; Jonkheijm, P.; Chen, Z.; Würthner, F.; Meijer, E. W., Photoinduced Electron Transfer in Hydrogen-Bonded Oligo(p-phenylene vinylene)−Perylene Bisimide Chiral Assemblies. *Journal of the American Chemical Society* **2002,** *124* (35), 10252-10253.
16. Ogata, D.; Shikata, T.; Hanabusa, K., Chiral Amplification of the Structure and Viscoelasticity of a Supramolecular Polymeric System Consisting of N,N‘,N‘‘-Tris(3,7-Dimethyloctyl)Benzene-1,3,5-Tricarboxamide and n-Decane. *The Journal of Physical Chemistry B* **2004,** *108* (40), 15503-15510.
17. Wilson, A. J.; Masuda, M.; Sijbesma, R. P.; Meijer, E. W., Chiral Amplification in the Transcription of Supramolecular Helicity into a Polymer Backbone. *Angewandte Chemie International Edition* **2005,** *44* (15), 2275-2279.
18. Jonkheijm, P.; van der Schoot, P.; Schenning, A. P. H. J.; Meijer, E. W., Probing the Solvent-Assisted Nucleation Pathway in Chemical Self-Assembly. *Science* **2006,** *313* (5783), 80-83.
19. George, S. J.; Tomović, Ž.; Smulders, M. M. J.; de Greef, T. F. A.; Leclère, P. E. L. G.; Meijer, E. W.; Schenning, A. P. H. J., Helicity Induction and Amplification in an Oligo(p-phenylenevinylene) Assembly through Hydrogen-Bonded Chiral Acids. *Angewandte Chemie International Edition* **2007,** *46* (43), 8206-8211.
20. Korevaar, P. A.; George, S. J.; Markvoort, A. J.; Smulders, M. M. J.; Hilbers, P. A. J.; Schenning, A. P. H. J.; De Greef, T. F. A.; Meijer, E. W., Pathway Complexity in Supramolecular Polymerization. *Nature* **2012,** *481*, 492-496.
21. Kuwahara, R.; Fujikawa, S.; Kuroiwa, K.; Kimizuka, N., Controlled Polymerization and Self-Assembly of Halogen-Bridged Diruthenium Complexes in Organic Media and Their Dielectrophoretic Alignment. *Journal of the American Chemical Society* **2012,** *134* (2), 1192-1199.
22. Chen, Y.; Li, K.; Lloyd, H. O.; Lu, W.; Chui, S. S.-Y.; Che, C.-M., Tetrakis(arylisocyanide) Rhodium(I) Salts in Water: NIR Luminescent and Conductive Supramolecular Polymeric Nanowires with Hierarchical Organization. *Angewandte Chemie International Edition* **2010,** *49* (51), 9968-9971.

23. Lu, W.; Chen, Y.; Roy, V. A. L.; Chui, S. S.-Y.; Che, C.-M., Supramolecular Polymers and Chromonic Mesophases Self-Organized from Phosphorescent Cationic Organoplatinum(II) Complexes in Water. *Angewandte Chemie International Edition* **2009,** *48* (41), 7621-7625.
24. Zhang, J.-J.; Lu , W.; Sun, R. W.-Y.; Che, C.-M., Organogold(III) Supramolecular Polymers for Anticancer Treatment. *Angewandte Chemie International Edition* **2012,** *51* (20), 4882-4886.
25. Mayoral, M. J.; Rest, C.; Stepanenko, V.; Schellheimer, J.; Albuquerque, R. Q.; Ferna-ndez, G., Cooperative Supramolecular Polymerization Driven by Metallophilic Pd---Pd Interactions. *Journal of the American Chemical Society* **2013,** *135* (6), 2148-2151.
26. Kuroiwa, K.; Shibata, T.; Takada, A.; Nemoto, N.; Kimizuka, N., Heat-Set Gel-like Networks of Lipophilic Co(II) Triazole Complexes in Organic Media and Their Thermochromic Structural Transitions. *Journal of the American Chemical Society* **2004,** *126* (7), 2016-2021.
27. Kumpfer, J. R.; Rowan, S. J., Thermo-, Photo-, and Chemo-Responsive Shape-Memory Properties from Photo-Cross-Linked Metallo-Supramolecular Polymers. *Journal of the American Chemical Society* **2011,** *133* (32), 12866-12874.
28. Stone, M. T.; Moore, J. S., Supramolecular Chelation Based on Folding. *Journal of the American Chemical Society* **2005,** *127* (16), 5928-5935.
29. Wackerly, J. W.; Moore, J. S., Cooperative Self-Assembly of Oligo(m-phenyleneethynylenes) into Supramolecular Coordination Polymers. *Macromolecules* **2006,** *39* (21), 7269-7276.
30. Shirakawa, M.; Fujita, N.; Tani, T.; Kaneko, K.; Shinkai, S., Organogel of an 8-quinolinol Platinum(ii) Chelate Derivative and its Efficient Phosphorescence Emission Effected by Inhibition of Dioxygen Quenching. *Chemical Communications* **2005,** (33), 4149-4151.
31. Yamauchi, M.; Kubota, S.; Karatsu, T.; Kitamura, A.; Ajayaghosh, A.; Yagai, S., Guided Supramolecular Polymerization of Oligo(p-phenylenevinylene) Functionalized Bismelamines. *Chemical Communications* **2013,** *49* (43), 4941-4943.
32. Aparicio, F.; García, F.; Fernández, G.; Matesanz, E.; Sánchez, L., Mirror Helices and Helicity Switch at Surfaces Based on Chiral Triangular-Shape Oligo(phenylene ethynylenes). *Chemistry – A European Journal* **2011,** *17* (9), 2769-2776.
33. Kastler, M.; Pisula, W.; Wasserfallen, D.; Pakula, T.; Müllen, K., Influence of Alkyl Substituents on the Solution- and Surface-Organization of Hexa-peri-hexabenzocoronenes. *Journal of the American Chemical Society* **2005,** *127* (12), 4286-4296.

34. Danjo, H.; Hirata, K.; Yoshigai, S.; Azumaya, I.; Yamaguchi, K., Back to Back Twin Bowls of D3-Symmetric Tris(spiroborate)s for Supramolecular Chain Structures. *Journal of the American Chemical Society* **2009,** *131* (5), 1638-1639.
35. Zhang, Z.; Luo, Y.; Chen, J.; Dong, S.; Yu, Y.; Ma, Z.; Huang, F., Formation of Linear Supramolecular Polymers That Is Driven by C–H···π Interactions in Solution and in the Solid State. *Angewandte Chemie International Edition* **2011,** *50* (6), 1397-1401.
36. Hasegawa, Y.; Miyauchi, M.; Takashima, Y.; Yamaguchi, H.; Harada, A., Supramolecular Polymers Formed from β-Cyclodextrins Dimer Linked by Poly(ethylene glycol) and Guest Dimers. *Macromolecules* **2005,** *38* (9), 3724-3730.
37. Gibson, H. W.; Yamaguchi, N.; Jones, J. W., Supramolecular Pseudorotaxane Polymers from Complementary Pairs of Homoditopic Molecules. *Journal of the American Chemical Society* **2003,** *125* (12), 3522-3533.
38. Lanigan, N.; Wang, X., Supramolecular Chemistry of Metal Complexes in Solution. *Chemical Communications* **2013,** *49* (74), 8133-8144.
39. Rest, C.; Kandanelli, R.; Fernández, G., Strategies to Create Hierarchical Self-Assembled Structures via Cooperative Non-Covalent Interactions. *Chemical Society Reviews* **2015,** *44* (8), 2543-2572.
40. Smulders, M. M. J.; Schenning, A. P. H. J.; Meijer, E. W., Insight into the Mechanisms of Cooperative Self-Assembly: The "Sergeants-and-Soldiers" Principle of Chiral and Achiral C3-Symmetrical Discotic Triamides. *Journal of the American Chemical Society* **2008,** *130* (2), 606-611.
41. Dudowicz, J.; Freed, K. F.; Douglas, J. F., Lattice Model of Equilibrium Polymerization. IV. Influence of Activation, Chemical Initiation, Chain Scission and Fusion, and Chain Stiffness on Polymerization and Phase Separation. *The Journal of Chemical Physics* **2003,** *119* (23), 12645-12666.
42. Henderson, J. R., Physics of Isodesmic Chemical Equilibria in Solution. *Physical Review E* **1997,** *55* (5), 5731-5742.
43. van der Schoot, P., Scaling Theory of Chemically Activated Living Polymerization in a Good Solvent. *Macromolecules* **2002,** *35* (7), 2845-2850.
44. van Jaarsveld, J.; van der Schoot, P., Scaling Theory of Interacting Thermally Activated Supramolecular Polymers. *Macromolecules* **2007,** *40* (6), 2177-2185.
45. Ciferri, A., Supramolecular Polymerizations. *Macromolecular Rapid Communications* **2002,** *23* (9), 511-529.
46. Oosawa, F.; Kasai, M., A Theory of Linear and Helical Aggregations of Macromolecules. *Journal of Molecular Biology* **1962,** *4* (1), 10-21.

47. van der Schoot, P., Theory of Supramolecular Polymerization. In *Supramolecular Polymers*, 2nd ed.; Ciferri, A., Ed. CRC Press: Boca Raton, 2005.
48. Missel, P. J.; Mazer, N. A.; Benedek, G. B.; Young, C. Y.; Carey, M. C., Thermodynamic Analysis of the Growth of Sodium Dodecyl Sulfate Micelles. *The Journal of Physical Chemistry* **1980,** *84* (9), 1044-1057.
49. Cordier, P.; Tournilhac, F.; Soulie-Ziakovic, C.; Leibler, L., Self-Healing and Thermoreversible Rubber from Supramolecular Assembly. *Nature* **2008,** *451* (7181), 977-980.
50. Hirschberg, J. H. K. K.; Beijer, F. H.; van Aert, H. A.; Magusin, P. C. M. M.; Sijbesma, R. P.; Meijer, E. W., Supramolecular Polymers from Linear Telechelic Siloxanes with Quadruple-Hydrogen-Bonded Units. *Macromolecules* **1999,** *32* (8), 2696-2705.
51. Folmer, B. J. B.; Sijbesma, R. P.; Versteegen, R. M.; van der Rijt, J. A. J.; Meijer, E. W., Supramolecular Polymer Materials: Chain Extension of Telechelic Polymers Using a Reactive Hydrogen-Bonding Synthon. *Advanced Materials* **2000,** *12* (12), 874-878.
52. Lange, R. F. M.; Van Gurp, M.; Meijer, E. W., Hydrogen-Bonded Supramolecular Polymer Networks. *Journal of Polymer Science Part A: Polymer Chemistry* **2000,** *37* (19), 3657-3670.
53. Dankers, P. Y. W.; Harmsen, M. C.; Brouwer, L. A.; Van Luyn, M. J. A.; Meijer, E. W., A Modular and Supramolecular Approach to Bioactive Scaffolds for Tissue Engineering. *Nature Materials* **2005,** *4*, 568-574.
54. Guan, Z.; Roland, J. T.; Bai, J. Z.; Ma, S. X.; McIntire, T. M.; Nguyen, M., Modular Domain Structure: A Biomimetic Strategy for Advanced Polymeric Materials. *Journal of the American Chemical Society* **2004,** *126* (7), 2058-2065.
55. Rowan, S. J.; Suwanmala, P.; Sivakova, S., Nucleobase-Induced Supramolecular Polymerization in the Solid State. *Journal of Polymer Science Part A: Polymer Chemistry* **2003,** *41* (22), 3589-3596.
56. Keizer, H. M.; Sijbesma, R. P.; Jansen, J. F. G. A.; Pasternack, G.; Meijer, E. W., Polymerization-Induced Phase Separation Using Hydrogen-Bonded Supramolecular Polymers. *Macromolecules* **2003,** *36* (15), 5602-5606.
57. Keizer, H. M.; van Kessel, R.; Sijbesma, R. P.; Meijer, E. W., Scale-up of the Synthesis of Ureidopyrimidinone Functionalized Telechelic Poly(ethylenebutylene). *Polymer* **2003,** *44* (19), 5505-5511.
58. Yamauchi, K.; Kanomata, A.; Inoue, T.; Long, T. E., Thermoreversible Polyesters Consisting of Multiple Hydrogen Bonding (MHB). *Macromolecules* **2004,** *37* (10), 3519-3522.
59. Sivakova, S.; Bohnsack, D. A.; Mackay, M. E.; Suwanmala, P.; Rowan, S. J., Utilization of a Combination of Weak Hydrogen-Bonding Interactions and

Phase Segregation to Yield Highly Thermosensitive Supramolecular Polymers. *Journal of the American Chemical Society* **2005,** *127* (51), 18202-18211.
60. Balkenende, D. W. R.; Coulibaly, S.; Balog, S.; Simon, Y. C.; Fiore, G. L.; Weder, C., Mechanochemistry with Metallosupramolecular Polymers. *Journal of the American Chemical Society* **2014,** *136* (29), 10493-10498.
61. Balkenende, D. W. R.; Monnier, C. A.; Fiore, G. L.; Weder, C., Optically Responsive Supramolecular Polymer Glasses. *Nature Communications* **2016,** *7:10995*.
62. Kato, T.; Wilson, P. G.; Fujishima, A.; Fréchet, J. M. J., Hydrogen-Bonded Liquid Crystals. A Novel Mesogen Incorporating Nonmesogenic 4,4′-Bipyridine through Selective Recognition between Hydrogen Bonding Donor and Acceptor. *Chemistry Letters* **1990,** *19* (11), 2003-2006.
63. Alexander, C.; Jariwala, C. P.; Lee, C. M.; Griffin, A. C., Self-Assembly of Main Chain Liquid Crystalline Polymers via Heteromeric Hydrogen Bonding. *Macromolecular Symposia* **1994,** *77* (1), 283-294.
64. Kihara, H.; Kato, T.; Uryu, T.; Fréchet, J. M. J., Supramolecular Liquid-Crystalline Networks Built by Self-Assembly of Multifunctional Hydrogen-Bonding Molecules. *Chemistry of Materials* **1996,** *8* (4), 961-968.
65. Ciferri, A., Liquid Crystallinity in Linear, Helical, Columnar Supramolecular Polymers. *Liquid Crystals* **2004,** *31* (11), 1487-1493.
66. Fouquey, C.; Lehn, J.-M.; Levelut, A.-M., Molecular Recognition Directed Self-Assembly of Supramolecular Liquid Crystalline Polymers from Complementary Chiral Components. *Advanced Materials* **1990,** *2* (5), 254-257.
67. Lehn, J.-M., Supramolecular chemistry — Molecular Information and the Design of Supramolecular Materials. *Makromolekulare Chemie. Macromolecular Symposia* **1993,** *69* (1), 1-17.
68. Lee, C. M.; Jariwala, C. P.; Griffin, A. C., Heteromeric Liquid-Crystalline Association Chain Polymers: Structure and Properties. *Polymer* **1994,** *35* (21), 4550-4554.
69. St.Pourcain, C. B.; Griffin, A. C., Thermoreversible Supramolecular Networks with Polymeric Properties. *Macromolecules* **1995,** *28* (12), 4116-4121.
70. Lee, C.-M.; Griffin, A. C., Hydrogen Bonding as the Origin of Both Liquid Crystallinity and Polymer Formation in Some Supramolecular Materials. *Macromolecular Symposia* **1997,** *117* (1), 281-290.
71. He, C.; Donald, A. M.; Griffin, A. C.; Waigh, T.; Windle, A. H., Structure of a Self-Assembled Hydrogen-Bonded 'Living' Main Chain Liquid Crystalline Polymer. *Journal of Polymer Science Part B: Polymer Physics* **1998,** *36*, 1617-1624.

72. Lu, X.; He, C.; Terrell, C. D.; Griffin, A. C., Self-Assembly of a Hydrogen-Bonded Association Chain Liquid Crystalline Polymer (LCP). *Macromolecular Chemistry and Physics* **2002,** *203* (1), 85-88.
73. Lu, X.; He, C.; Griffin, A. C., Crystallization and Phase Behaviors of Multicomponent Supramolecular Complexes through Hydrogen-Bonding Association. *Macromolecules* **2003,** *36* (14), 5195-5200.
74. Wiegel, K. N.; Griffin, A. C.; Black, M. S.; Schiraldi, D. A., Memory Effects in Supramolecular Networks of Diacids and Polyfunctional Pyridine Derivatives. *Journal of Applied Polymer Science* **2004,** *92* (5), 3097-3106.
75. Xu, J.; He, C.; Toh, K. C.; Lu, X., Intermolecular Interaction in Multicomponent Supramolecular Complexes through Hydrogen-Bonding Association. *Macromolecules* **2002,** *35* (23), 8846-8851.
76. Rogness, D. C.; Riedel, P. J.; Sommer, J. R.; Reed, D. F.; Wiegel, K. N., Supramolecular Main Chain Liquid Crystalline Polymers Utilizing Azopyridine Derivatives. *Liquid Crystals* **2006,** *33* (5), 567-572.
77. Boileau, S.; Bouteiller, L.; Foucat, E.; Lacoudre, N., Stable Low Molecular Weight Glasses Based on Mixtures of Bisphenol-A and Bispyridines. *Journal of Materials Chemistry* **2002,** *12* (2), 195-199.
78. Sivakova, S.; Rowan, S. J., Fluorescent Supramolecular Liquid Crystalline Polymers from Nucleobase-Terminated Monomers. *Chemical Communications* **2003,** (19), 2428-2429.
79. Sivakova, S.; Wu, J.; Campo, C. J.; Mather, P. T.; Rowan, S. J., Liquid-Crystalline Supramolecular Polymers Formed through Complementary Nucleobase-Pair Interactions. *Chemistry – A European Journal* **2005,** *12* (2), 446-456.
80. Araki, K.; Takasawa, R.; Yoshikawa, I., Design, Fabrication, and Properties of Macroscalesupramolecular Fibers Consisted of Fully Hydrogen-Bonded Pseudo-Polymer chains. *Chemical Communications* **2001**, 1826-1827.
81. Takasawa, R.; Murota, K.; Yoshikawa, I.; Araki, K., Steric-Factor-Directed Alternating Supramolecular Copolymer Composed of Hydrogen-Bonded Cyclohexanetricarboxamide Units. *Macromolecular Rapid Communications* **2003,** *24* (4), 335-339.
82. Takasawa, R.; Yoshikawa, I.; Araki, K., Design, Fabrication and Properties of Triamidecyclohexane Supramolecular Fibers Consisted of Hydrogen-Bonded Pseudo-Polymer Chains. *KOBUNSHI RONBUNSHU* **2002,** *59* (10), 616-622.
83. Kihara, H.; Kato, T.; Uryu, T.; Fréchet, J. M. J., Induction of a Cholesteric Phase via Self-Assembly in Supramolecular Networks Built of Non-Mesomorphic Molecular Components. *Liquid Crystals* **1998,** *24* (3), 413-418.

84. Brunet, P.; Demers, E.; Maris, T.; Enright, G. D.; Wuest, J. D., Designing Permeable Molecular Crystals that React with External Agents to Give Crystalline Products. *Angewandte Chemie International Edition* **2003,** *42* (43), 5303-5306.
85. Le Fur, E.; Demers, E.; Maris, T.; Wuest, J. D., Excavations in Molecular Crystals. *Chemical Communications* **2003,** (24), 2966-2967.
86. Brunet, P.; Simard, M.; Wuest, J. D., Molecular Tectonics. Porous Hydrogen-Bonded Networks with Unprecedented Structural Integrity. *Journal of the American Chemical Society* **1997,** *119* (11), 2737-2738.
87. Boils, D.; Perron, M.-È.; Monchamp, F.; Duval, H.; Maris, T.; Wuest, J. D., Molecular Tectonics. Disruption of Self-Association in Melts Derived from Hydrogen-Bonded Solids. *Macromolecules* **2004,** *37* (19), 7351-7357.
88. Lehn, J.-M., Toward Complex Matter: Supramolecular Chemistry and Self-Organization. *Proceedings of the National Academy of Sciences* **2002,** *99* (8), 4763-4768.
89. Steed, J. W.; Atwood, J. L., Crystal Engineering. In *Supramolecular Chemistry*, Wiley: 2009.
90. Dunitz, J., Phase Transitions in Molecular Crystals from Chemical Viewpoint. *Pure and Applied Chemistry* **1991,** *63*, 177-185.
91. Dunitz Jack, D., Thoughts on Crystals as Supermolecules. In *Perspectives in Supramolecular Chemistry: The Crystal as a Supramolecular Entity*, Desiraju Gautam, R., Ed. John Wiley & Sons Ltd: Chichester, 1996; Vol. 2, pp 1-30.
92. Desiraju Gautam, R., Supramolecular Synthons in Crystal Engineering—A New Organic Synthesis. *Angewandte Chemie International Edition in English* **1995,** *34* (21), 2311-2327.
93. Braga, D.; Grepioni, F.; Desiraju, G. R., Crystal Engineering and Organometallic Architecture. *Chemical Reviews* **1998,** *98* (4), 1375-1406.
94. Braga, D.; Brammer, L.; Champness, N. R., New Trends in Crystal Engineering. *Crystal Engineering Communications* **2005,** *7* (1), 1-19.
95. Desiraju, G. R., Crystal Engineering: A Holistic View. *Angewandte Chemie International Edition* **2007,** *46* (44), 8342-8356.
96. Desiraju, G. R.; Steiner, T., *The Weak Hydrogen Bond in Structural Chemistry and Biology*. Oxford University Press: New York, 1999.
97. Steed, J. W.; Atwood, J. L., The Supramolecular Chemistry of Life. *Supramolecular Chemistry* **2009**.
98. Desiraju, G. R.; Sharma, C. V. K., Crystal Engineering and Molecular Recognition—Twin Facets of Supramolecular Chemistry. In *Perspectives in Supramolecular Chemistry: The Crystal as a Supramolecular Entity*, Desiraju Gautam, R., Ed. John Wiley & Sons Ltd: Chichester, 1996; Vol. 2, pp 31-62.

99. Steiner, T.; Saenger, W., Role of C--H---O Hydrogen Bonds in the Coordination of Water Molecules. Analysis of Neutron Diffraction Data. *Journal of the American Chemical Society* **1993,** *115* (11), 4540-4547.
100. Steiner, T., The Hydrogen Bond in the Solid State. *Angewandte Chemie International Edition* **2002,** *41* (1), 48-76.
101. Desiraju, G. R., A Bond by Any Other Name. *Angewandte Chemie International Edition* **2010,** *50* (1), 52-59.
102. Steiner, T., C–H···O Hydrogen Bonding in Crystals. *Crystallography Reviews* **2003,** *9* (2-3), 177-228.
103. Desiraju, G. R., The C–H---O Hydrogen Bond in Crystals: What Is It? *Accounts of Chemical Research* **1991,** *24* (10), 290-296.
104. Taylor, R.; Kennard, O., Crystallographic Evidence for the Existence of CH---O, CH---N and CH---Cl Hydrogen Bonds. *Journal of the American Chemical Society* **1982,** *104* (19), 5063-5070.
105. Steiner, T., Unrolling the Hydrogen Bond Properties of C–H···O Interactions. *Chemical Communications* **1997,** (8), 727-734.
106. Braga, D.; Grepioni, F.; Biradha, K.; Pedireddi, V. R.; Desiraju, G. R., Hydrogen Bonding in Organometallic Crystals. 2. C-H---O Hydrogen Bonds in Bridged and Terminal First-Row Metal Carbonyls. *Journal of the American Chemical Society* **1995,** *117* (11), 3156-3166.
107. Desiraju, G. R., C–H---O Hydrogen Bonding and the Deliberate Design of Organic Crystal Structures. *Molecular Crystals and Liquid Crystals Science and Technology. Section A. Molecular Crystals and Liquid Crystals* **1992,** *211* (1), 63-74.
108. Desiraju, G. R., Distance Dependence of C–H ··· O Interactions in Some Chloroalkyl Compounds. *Journal of the Chemical Society, Chemical Communications* **1989,** (3), 179-180.
109. Desiraju, G. R., Strength and Linearity of C–H ··· O Bonds in Molecular Crystals: A Database Study of Some Terminal Alkynes. *Journal of the Chemical Society, Chemical Communications* **1990,** (6), 454-455.
110. Steiner, T.; R. Desiraju, G., Distinction Between the Weak Hydrogen Bond and the Van der Waals Interaction. *Chemical Communications* **1998,** (8), 891-892.
111. Rest, C.; Martin, A.; Stepanenko, V.; Allampally, N. K.; Schmidt, D.; Fernandez, G., Multiple CH---O Interactions Involving Glycol Chains as Driving Force for the Self-Assembly of Amphiphilic Pd(ii) Complexes. *Chemical Communications* **2014,** *50* (87), 13366-13369.
112. Rest, C.; Mayoral María, J.; Fucke, K.; Schellheimer, J.; Stepanenko, V.; Fernández, G., Self-Assembly and (Hydro)gelation Triggered by Cooperative π–

π and Unconventional C–H···X Hydrogen Bonding Interactions. *Angewandte Chemie International Edition* **2013,** *53* (3), 700-705.
113. Singh, J.; Thornton, J. M., The Interaction Between Phenylalanine Rings in Proteins. *FEBS Letters* **1985,** *191* (1), 1-6.
114. Hunter, C. A.; Sanders, J. K. M., The Nature of π-π Interactions. *Journal of the American Chemical Society* **1990,** *112* (14), 5525-5534.
115. Hunter, C. A.; Singh, J.; Thornton, J. M., π-π Interactions: The Geometry and Energetics of Phenylalanine-Phenylalanine Interactions in Proteins. *Journal of Molecular Biology* **1991,** *218* (4), 837-846.
116. Hunter, C. A.; Lawson, K. R.; Perkins, J.; Urch, C. J., Aromatic Interactions. *Journal of the Chemical Society, Perkin Transactions 2* **2001,** (5), 651-669.
117. Kim, E.-i.; Paliwal, S.; Wilcox, C. S., Measurements of Molecular Electrostatic Field Effects in Edge-to-Face Aromatic Interactions and CH-π Interactions with Implications for Protein Folding and Molecular Recognition. *Journal of the American Chemical Society* **1998,** *120* (43), 11192-11193.
118. Janiak, C., A Critical Account on π-π Stacking in Metal Complexes with Aromatic Nitrogen-Containing Ligands. *Journal of the Chemical Society, Dalton Transactions* **2000,** (21), 3885-3896.
119. Hunter, C. A., Meldola Lecture. The Role of Aromatic Interactions in Molecular Recognition. *Chemical Society Reviews* **1994,** *23* (2), 101-109.
120. Scudder, M.; Dance, I., Crystal Supramolecular Motifs. Ladders, Layers and Labyrinths of Ph_4P^+ Cations Engaged in Fourfold Phenyl Embraces. *Journal of the Chemical Society, Dalton Transactions* **1998,** (19), 3155-3166.
121. Dance, I.; Scudder, M., Molecules Embracing in Crystals. *Crystal Engineering Communications* **2009,** *11* (11), 2233-2247.
122. Dance, I.; Scudder, M., The Sextuple Phenyl Embrace, a Ubiquitous Concerted Supramolecular Motif. *Journal of the Chemical Society, Chemical Communications* **1995,** (10), 1039-1040.
123. Mueller, U.; Klingelhoefer, P.; Eicher, J.; Bohrer, R., Crystal Structures of Bis(tetraphenylarsonium) Hexachlorotitanate(IV)-2 Dichloromethane and Bis(tetraphenylarsonium) Hexachlorouranate(IV)-2 Dichloromethane. *Zeitschrift für Kristallographie* **1984,** *168*, 121-131.
124. Dance, I.; Scudder, M., Supramolecular Motifs: Concerted Multiple Phenyl Embraces between Ph_4P^+ Cations Are Attractive and Ubiquitous. *Chemistry – A European Journal* **1996,** *2* (5), 481-486.
125. Dance, I., Inorganic Intermolecular Motifs, and Their Energies. *Crystal Engineering Communications* **2003,** *5* (37), 208-221.
126. Mueller, U.; Mronga, N.; Schumacher, C.; Dehnicke, K., The Crystal Structures of Tetraphenylphosphonium Trichlorostannate and Tribromostannate.

Zeitschrift fuer Naturforschung, Teil B: Anorganische Chemie, Organische Chemie **1982,** *37B* (9), 1122-1126.
127. Dance, I.; Scudder, M., Supramolecular Motifs: Sextuple Aryl Embraces in Crystalline [M(2,2′-bipy)$_3$] and Related Complexes *Journal of the Chemical Society, Dalton Transactions* **1998,** (8), 1341-1350.
128. Wubbenhorst, M.; Turnhout, J. v.; Folmer, B. J. B.; Sijbesma, R. P.; Meijer, E. W., Complex Dynamics of Hydrogen Bonded Self-Assembling Polymers. *IEEE Transactions on Dielectrics and Electrical Insulation* **2001,** *8* (3), 365-372.
129. Dong, S.; Leng, J.; Feng, Y.; Liu, M.; Stackhouse, C. J.; Schönhals, A.; Chiappisi, L.; Gao, L.; Chen, W.; Shang, J.; Jin, L.; Qi, Z.; Schalley, C. A., Structural Water as an Essential Comonomer in Supramolecular Polymerization. *Science Advances* **2017,** *3* (11).
130. Ciferri, A., Growth of Supramolecular Structures. In *Supramolecular Polymers*, 2nd ed.; Ciferri, A., Ed. CRC Press: Boca Raton, 2005; pp 29-75.
131. Plotkin, J. S.; Shore, S. G., Convenient Preparation and Isolation of Pure Potassium Cyclopentadienyldicarbonylferrate, K[(η^5-C_5H_5)Fe(CO)$_2$]. *Inorganic Chemistry* **1981,** *20*, 284-285.
132. Spek, A., Structure Validation in Chemical Crystallography. *Acta Crystallographica Section D* **2009,** *65* (2), 148-155.
133. Macrae, C. F.; Edgington, P. R.; McCabe, P.; Pidcock, E.; Shields, G. P.; Taylor, R.; Towler, M.; van de Streek, J., Mercury: Visualization and Analysis of Crystal Structures. *Journal of Applied Crystallography* **2006,** *39* (3), 453-457.
134. Macrae, C. F.; Bruno, I. J.; Chisholm, J. A.; Edgington, P. R.; McCabe, P.; Pidcock, E.; Rodriguez-Monge, L.; Taylor, R.; van de Streek, J.; Wood, P. A., Mercury CSD 2.0 - New Features for the Visualization and Investigation of Crystal Structures. *Journal of Applied Crystallography* **2008,** *41* (2), 466-470.
135. McGaughey, G. B.; Gagné, M.; Rappé, A. K., π-Stacking Interactions: Alive and Well in Proteins. *Journal of Biological Chemistry* **1998,** *273* (25), 15458-15463.
136. Lanigan, N.; Assoud, A.; Wang, X., Intermolecular Interactions of CpFePPh3(CO)CO(CH2)5CH3: From a Crystalline Solid to a Supramolecular "Iron-Truss" Polymer. *ACS Macro Letters* **2014,** *3* (12), 1281-1285.
137. Andrianov, K. A.; Slonimsky, G. L.; Zhdanov, A. A.; Tsvankin, D. Y.; Levin, V. Y.; Papkov, V. S.; Kvachev, Y. P.; Belavtseva, E. M., Morphology of Organosilicon Ladder Polymers. *Journal of Polymer Science: Polymer Chemistry Edition* **1976,** *14* (5), 1205-1212.
138. Liu, C.; Liu, Y.; Shen, Z.; Xie, P.; Zhang, R.; Yang, J.; Bai, F., Study of the Steric Tacticity of Novel Soluble Ladderlike Poly(phenylsilsesquioxane)

Prepared by Stepwise Coupling Polymerization. *Macromolecular Chemistry and Physics* **2001,** *202* (9), 1581-1585.
139. Tang, H.; Sun, J.; Jiang, J.; Zhou, X.; Hu, T.; Xie, P.; Zhang, R., A Novel Aryl Amide-Bridged Ladderlike Polymethylsiloxane Synthesized by an Amido H-Bonding Self-Assembled Template. *Journal of the American Chemical Society* **2002,** *124* (35), 10482-10488.
140. Zhang, Z.-X.; Hao, J.; Xie, P.; Zhang, X.; Han, C. C.; Zhang, R., A Well-Defined Ladder Polyphenylsilsesquioxane (Ph-LPSQ) Synthesized via a New Three-Step Approach: Monomer Self-Organization−Lyophilization—Surface-Confined Polycondensation. *Chemistry of Materials* **2008,** *20* (4), 1322-1330.
141. Sivakova, S.; Wu, J.; Campo, C. J.; Mather, P. T.; Rowan, S. J., Liquid-Crystalline Supramolecular Polymers Formed through Complementary Nucleobase-Pair Interactions. *Chemistry – A European Journal* **2006,** *12* (2), 446-456.
142. Ian, M., Polyferrocenylsilanes: Metallopolymers for Electronic and Photonic Applications. *Journal of Optics A: Pure and Applied Optics* **2002,** *4* (6), S221.
143. Eckstein, A.; Suhm, J.; Friedrich, C.; Maier, R. D.; Sassmannshausen, J.; Bochmann, M.; Mülhaupt, R., Determination of Plateau Moduli and Entanglement Molecular Weights of Isotactic, Syndiotactic, and Atactic Polypropylenes Synthesized with Metallocene Catalysts. *Macromolecules* **1998,** *31* (4), 1335-1340.
144. Reimschuessel, H. K., On the Glass Transition Temperature of Comblike Polymers: Effects of Side Chain Length and Backbone Chain Structure. *Journal of Polymer Science: Polymer Chemistry Edition* **1979,** *17* (8), 2447-2457.